Smart Polymers & Hydrogels

Path to Greatness: Discipline, Persistence, & Professionalism

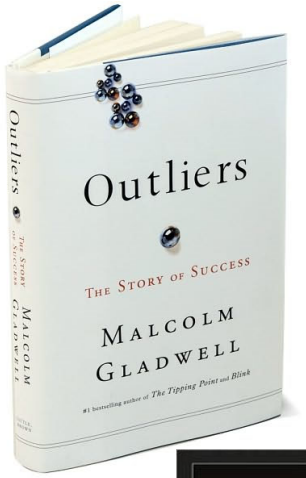

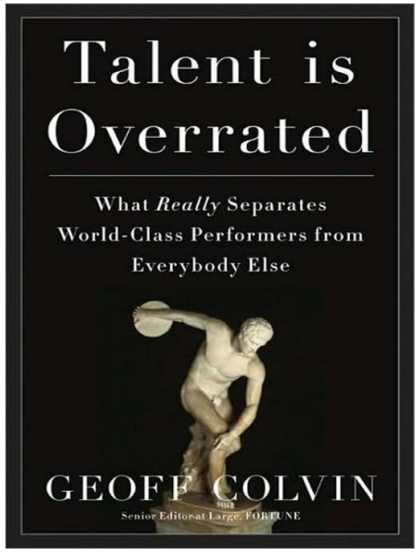

10,000 Hours of Practice

Smart and Ordinary ~ Dumb and Dumber

Dumb Dumber

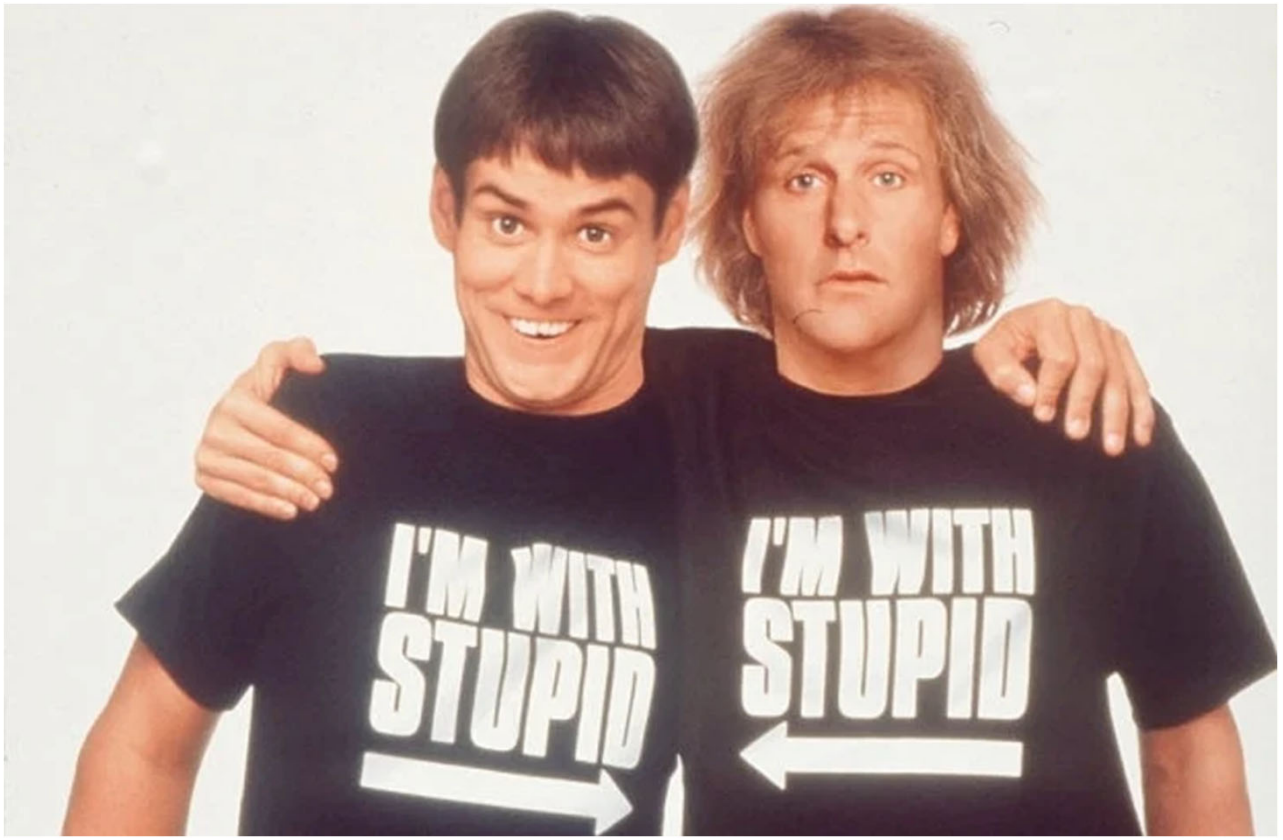

Smart Ordinary

Ordinary Polymers & Hydrogels

Polymers

Precipitation ⟷ Dissolution

Contraction ⟷ Expansion

Hydrogels

Shrinking ⟷ Swelling

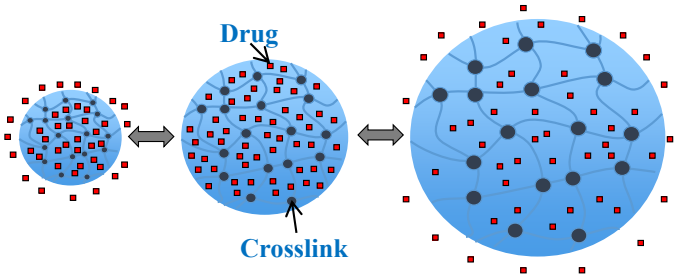

Precipitation

Shrunken state
- Squeezing
- Trapping

Dilution

Swollen state
- Opening
- Absorbing

Smart Polymers & Hydrogels

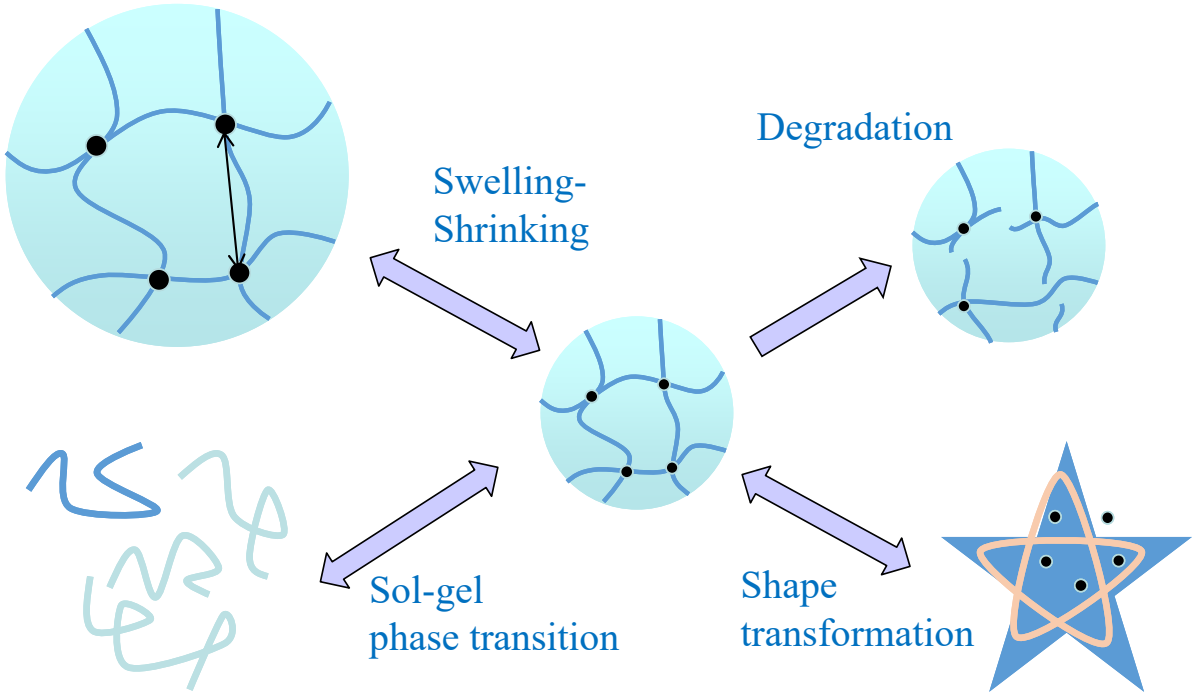

Respond to minute changes in environmental conditions by large and sharp changes in physicochemical properties

(Intelligent, Environment-sensitive, Stimulus-responsive)

Ordinary Polymers & Hydrogels

Polymers

Precipitation ⟷ Dissolution

Contraction ⟷ Expansion

Hydrogels

Shrinking ⟷ Swelling

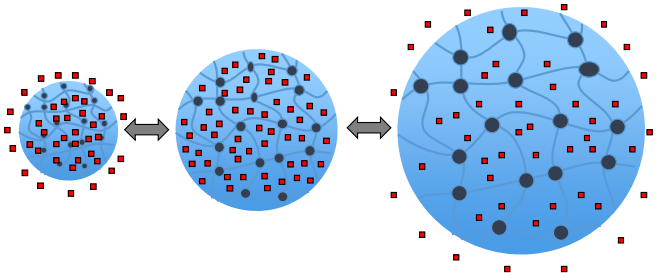

Polymers and hydrogels that undergo changes in physicochemical properties without external factors.

PopMech May 2014

Adjunctive Hemostats

https://www.jnjmedtech.com/en-US/product/surgicel-original-absorbable-hemostat

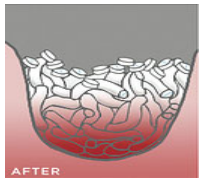

Wound Care

Severe puncture wounds can be life-threatening if first aid is delayed. Oregon-based company RevMedx has developed a new medical product that can staunch bleeding, and is particularly useful for wounds to the shoulder and pelvis, where tourniquets are ineffective. The XStat injects compressed sponges that have been treated with blood clotting and antimicrobial agents. The pellets expand to 10 times their original size and exert pressure to stop the bleeding. In animal studies, the XSTAT reduced blood loss and increased survival rates. The company hopes the device will become FDA-approved this year for military and medical applications.

https://www.revmedx.com/xstat/

Smart Polymers & Hydrogels

Polymers and hydrogels that undergo changes in physicochemical properties by external factors, commonly known as environmental stimuli.

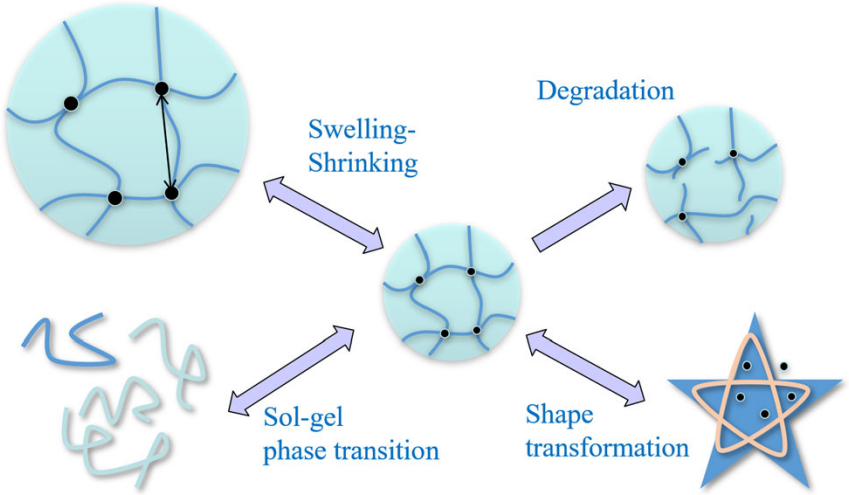

Respond to minute changes in environmental conditions by large and sharp changes in physicochemical properties

(Intelligent, Environment-sensitive, Stimulus-responsive)

Environmental Stimuli

Physical

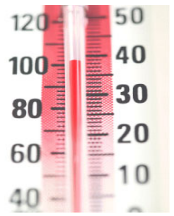
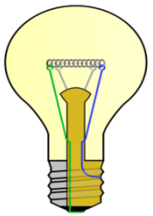

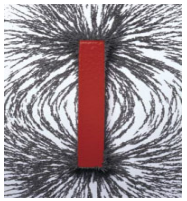

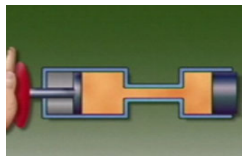

Stimuli

Biological

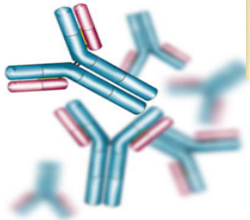
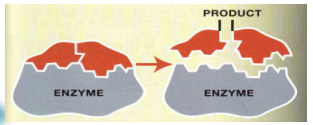

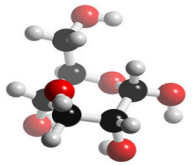

Chemical

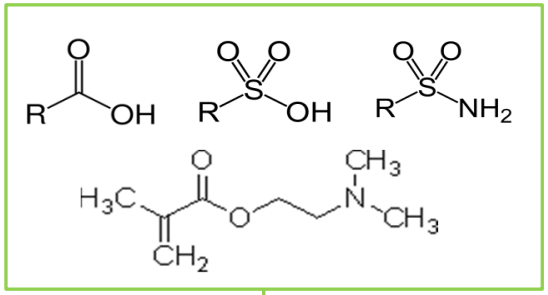

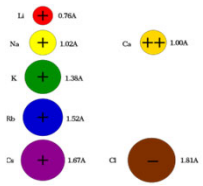
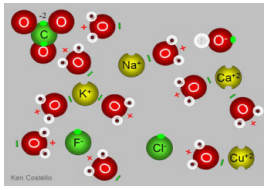
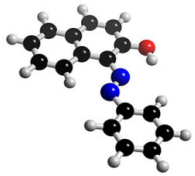
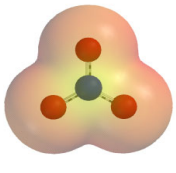

Smart Polymers & Hydrogel

Prof. You Han Bae, University of Utah

Drug Delivery

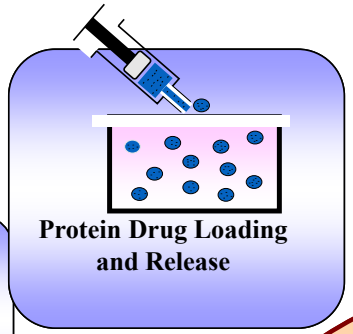

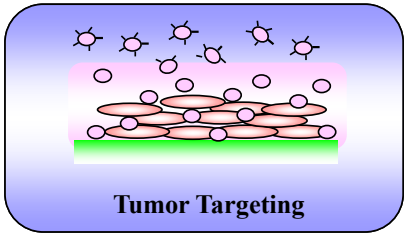

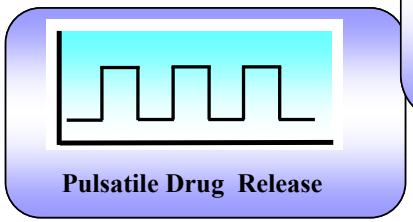

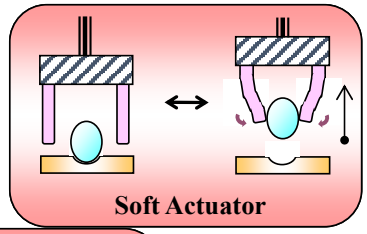

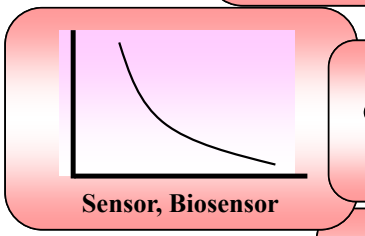

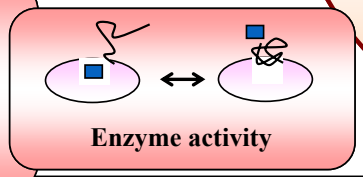

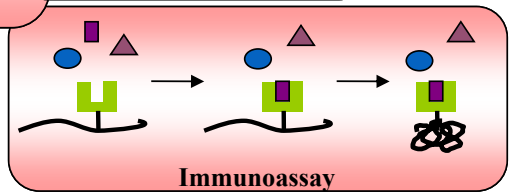

Biosensor

Bioseparation

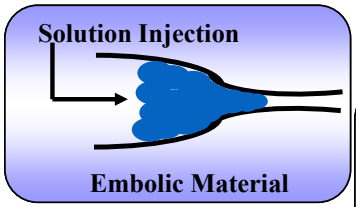

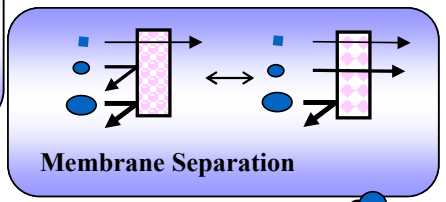

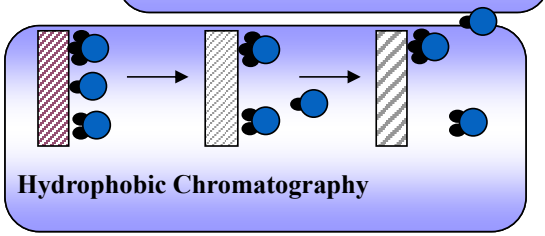

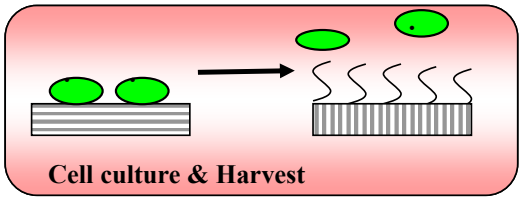

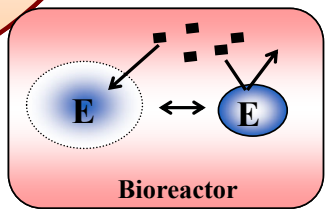

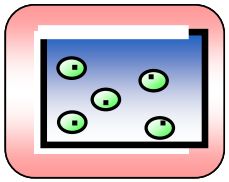

Tissue Engineering

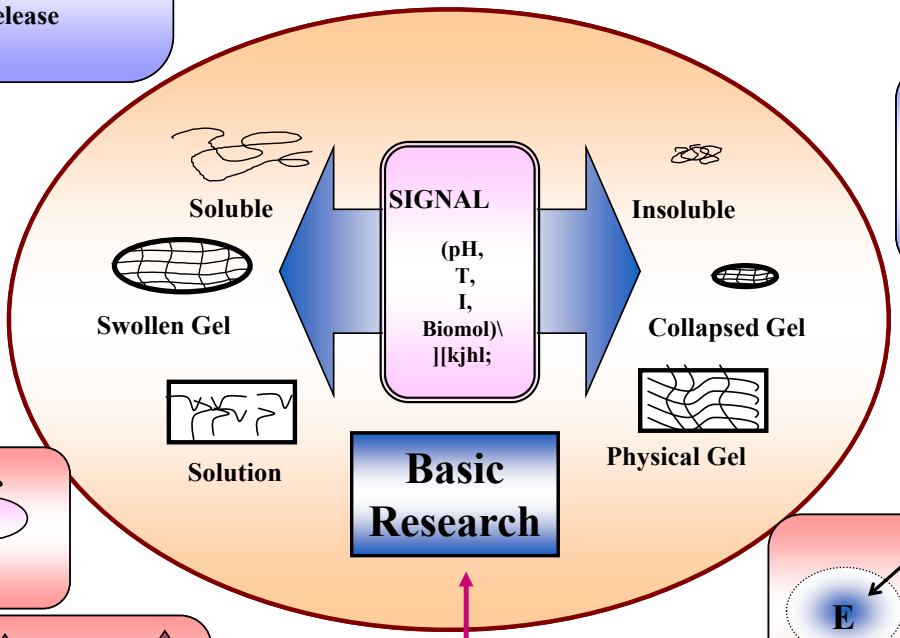

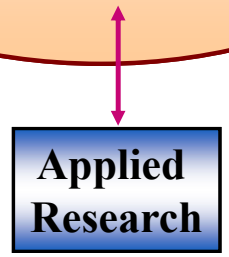

Pressure- & Temperature-Sensitive Materials

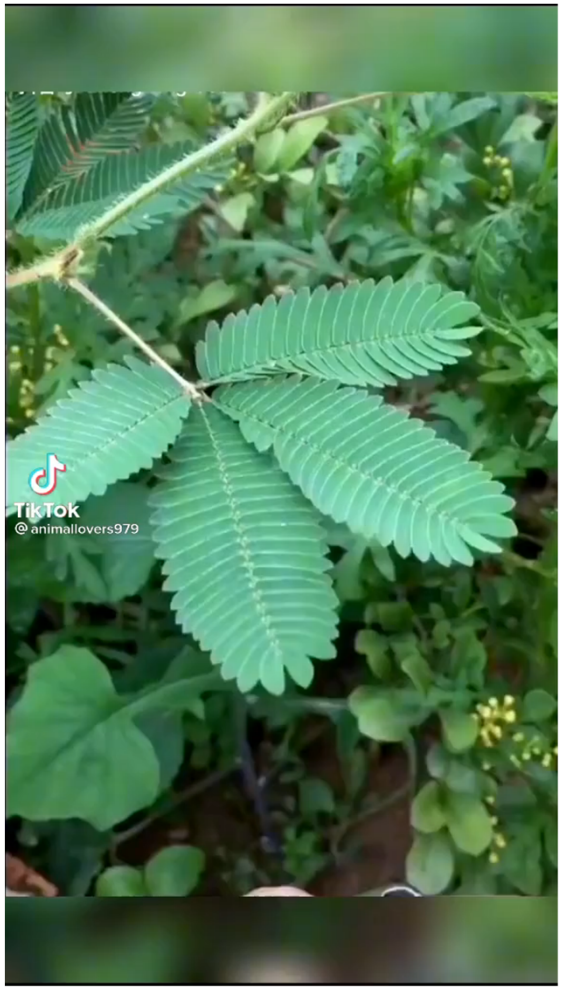

https://www.youtube.com/watch?v=ULa60DWu66U

Phase Separation

Role of Water in Some Biological Processes

MICROBIOLOGICAL REVIEWS, Dec. 1990, p. 432–449
0146-0749/90/040432-18$02.00/0

Vol. 54, No. 4

Role of Water in Some Biological Processes

PHILIPPA M. WIGGINS

Department of Medicine, University of Auckland School of Medicine, Private Bag, Auckland, New Zealand

Philippa Wiggins, 1925-2017
https://philippawiggins.com/

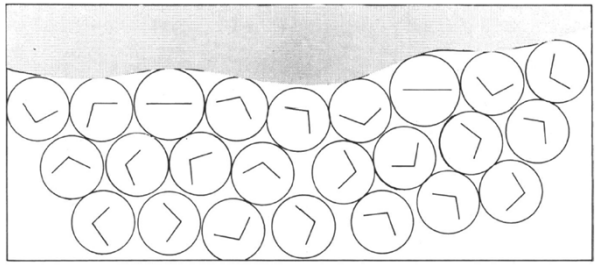

FIG. 1. Two-dimensional arrangement of water molecules round two negatively charged sites on a surface. Four molecules are shown in contact with each charge, the majority of them with a positive hydrogen atom directed toward the negative charge. Outside those four molecules is a layer of randomly oriented molecules.

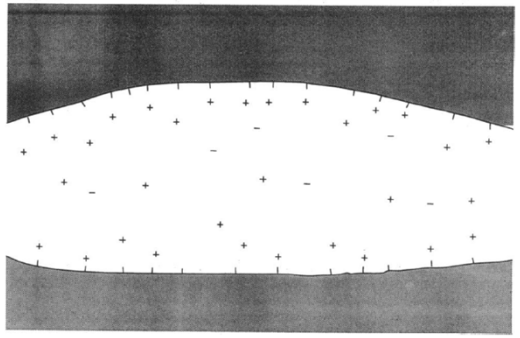

FIG. 3. Distribution of ions inside an aqueous compartment of a negatively charged gel. Counter cations are concentrated in a region of solution close to the surfaces. Away from the surfaces ions are relatively sparse.

Hoffmeister Series

Kosmotropes

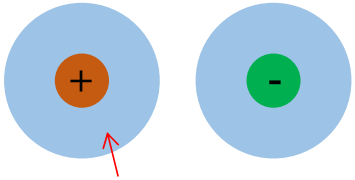

Chaotropes

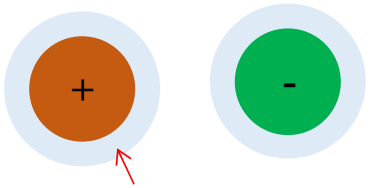

Kosmotropes	Chaotropes
Tightly bound water layer	Weakly bound water layers
Difficult to remove the water layer	Easy to remove the water layer
Stabilizing (order) the structure of hydrogen-bonded water network and/or solutes (proteins/polymers)	Destabilizing (disorder or disruption) of the structure of hydrogen-bonded water network and solutes. Since water-water interaction is higher than chaotrope-water interactions, more water molecules are available for interaction with the solute, leading to expansion of the solute.
Increased hydrophobic interaction to make a compact polymer structure	Decreased hydrophobic interaction to make an expanded (denatured) polymer structure
Salting out at high salt concentrations (Ions keep water molecules, and so less water molecules are available for a large solute.)	Salting in
	Easy to interact with the weakly hydrated portions of a large solute.
Decreased surface tension (as water is attracted more to solute than to water molecules).	Increased surface tension

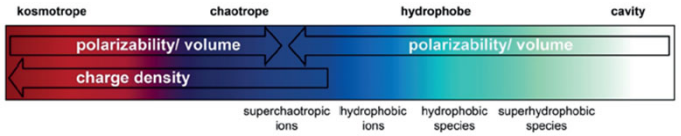

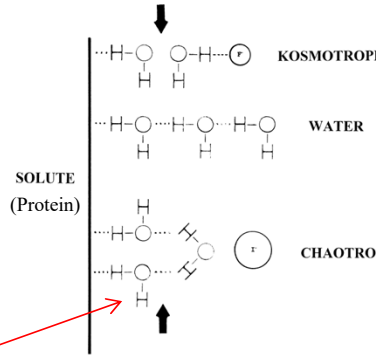

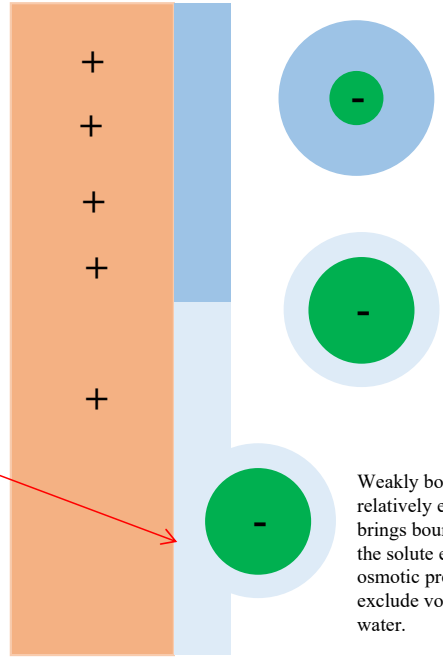

Tightly bound water molecules are difficult to remove. They are outside of the excluded volume, increasing the osmotic pressure of the bulk water. This results in compacted form of proteins or polymers.

Weakly bound water molecules are relatively easily removed. The ion brings bound water molecules making the solute expanded by minimizing the osmotic pressure difference between exclude volume area and the bulk water.

See Romero-Perez 2023, When phased without water-Biophysics of cellular desiccation, from biomolecules to condensates

Hoffmeister Series

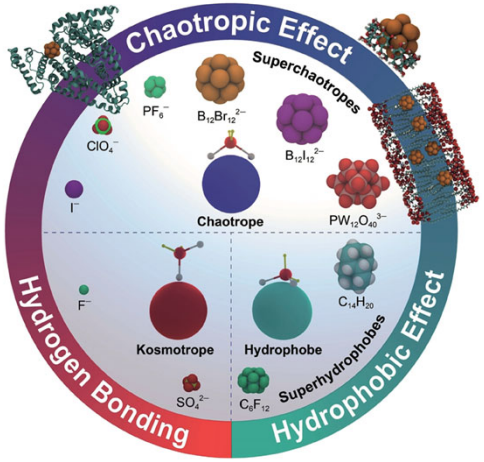

Figure 1. Principal aqueous solvation patterns for anions. a) Presumed favorable orientations of water molecules around a cavity and at the surface of different solutes: kosmotropic and chaotropic ions, hydrophobic molecules, and void space. Electron lone pairs are visualized in yellow. b) Extended Hofmeister scale with specification of the superchaotropic, hydrophobic ionic, and superhydrophobic regions.

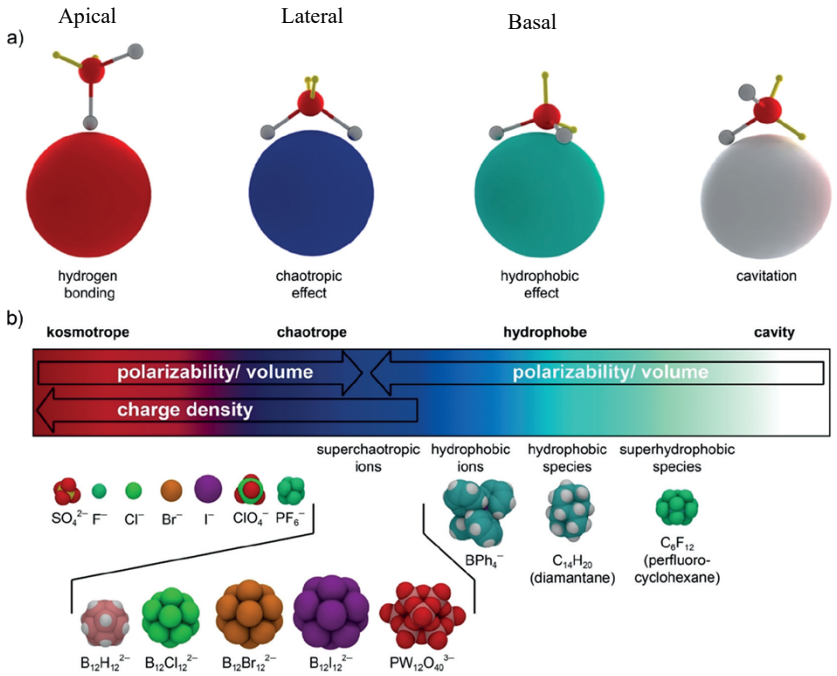

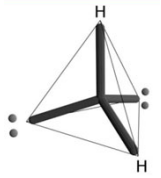

Figure 3 Representation of a single water molecule. Water's two hydrogen atoms and two electron pairs are oriented tetrahedrally. (Herzfeld 2001, Hydrophobic effect)

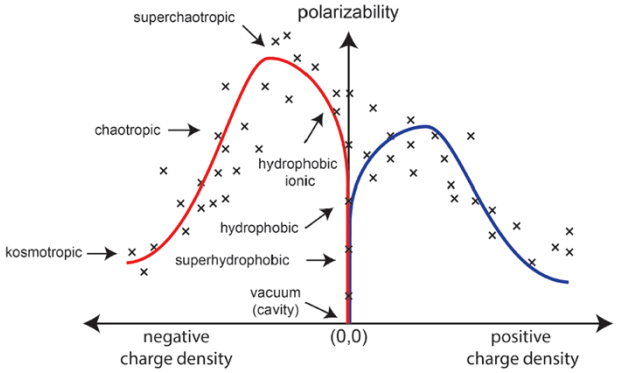

Figure S1: Two-dimensional, purely schematic illustration of the extended Hofmeister scale with specification of the superchaotropic, hydrophobic ionic, and superhydrophobic regions and reflecting the on average higher polarizability of anions (left) versus cations (right). The red line would correspond to the one-dimensional, linearized solvation scale depicted in Figure 1b of the main text.

Common kosmotropic ions are characterized by a small size and large charge density. The positioning of a kosmotropic anion in the cavity results in highly directional hydrogen-bonding or coordinative interaction, which leads to a strong apical orientation of the water molecules (Figure 1a, left). **Chaotropic ions are typically large and charge-delocalized**. The positioning of a chaotropic ion in the cavity causes less directional ion–dipole interactions to predominate, which results in a lateral orientation of the water molecules under alignment of their dipole moment (Figure 1a, second from the left). The positioning of a hydrophobic solute in the cavity activates predominantly distance-dependent dispersion interactions, which lead to a preferred basal orientation of the water molecules, maximizing the proximity to bonding electrons, lone pairs, and the oxygen atom (Figure 1a, second from the right). For cations instead of anions, the principle orientations of the water molecules (apical versus lateral) remain the same except that the interactions occur through the lone pairs instead of the hydrogens, with only the latter variant shown in Figure 1a. The pictorial representations of the different aqueous solvation modes allow us to advance a continuum model for solvation, which not only spans from kosmotropes to chaotropes but extends further to hydrophobes and, ultimately, an empty cavity (Figure 1b). This continuum view of solvation corresponds to a gradual change of the preferred orientation of the inner-sphere water molecules from apical (left) to lateral to basal. The continuum includes as prominent cases the established effects of hydrogen bonding (coordinative bonding) and the hydrophobic effect. As an additional effect, the chaotropic effect emerges in the transition region beyond the classical Hofmeister scale (kosmotrope–chaotrope) and the recognized hydrophobic domain, which spans from hydrophobic ions to neutral species. Others and we have recently introduced the term "superchaotropic", akin to superhydrophobic, for those ions that exceed common chaotropic properties. Superchaotropic ions do not display hydrophobic properties by the common definitions. It is consequential that the water orientations induced by the different types of dominant intermolecular interactions in the first hydration shell (Figure 1a) have characteristic consequences for the hydrogen-bonding network in the entire solvation shell. This accounts for many of the physicochemical and thermochemical properties of the associated solvation processes, including the entropic signature of the hydrophobic effect, the hydrogen-bond-forming or disrupting effect of kosmotropes and chaotropes.

Assaf 2018, The chaotropic effect as an assembly motif in chemistry, Assaf 2018, The chaotropic effect - Supporting Info

Solubilities of Polyethers in Water

The solubilities of polyethers are surprisingly counter-intuitive. The best-known example is the difference between polyethylene glycol ($[-CH_2-CH_2-O-]_n$) which is infinitely soluble, and polyoxymethylene ($[-CH_2-O-]_n$) which is completely insoluble in water, exactly the opposite of what one expects from the C/O ratios of these molecules. Similar anomalies exist for oligomeric and cyclic polyethers. To solve this apparent mystery, we use femtosecond vibrational and GHz dielectric spectroscopy with complementary *ab initio* calculations and molecular dynamics simulations. We find that the dynamics of water molecules solvating polyethers is fundamentally different depending on their C/O composition. The *ab initio* calculations and simulations show that this is not because of steric effects (as is commonly believed), but because the partial charge on the O atoms depends on the number of C atoms by which they are separated. Our results thus show that inductive effects can have a major impact on aqueous solubilities.

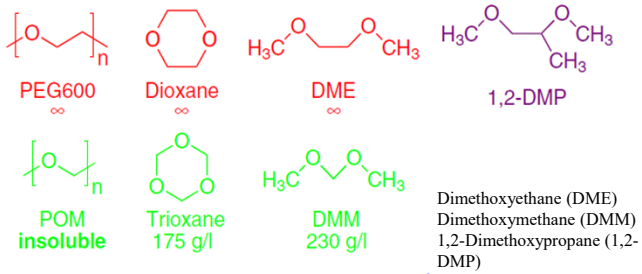

Dimethoxyethane (DME)
Dimethoxymethane (DMM)
1,2-Dimethoxypropane (1,2-DMP)

Fig. 1 Investigated polyethers and their solubilities[4].

The origin of the different solubilities is not well understood[5]. It is commonly explained by assuming that the distances between the O atoms in different polyethers have consequences for their solubility in water. As early as 1969, Blandamer et al.[6] suggested that water molecules solvating PEG can form a hydrogen-bond network similar to that of bulk water on the basis of the distances between O atoms in the trans-gauche-trans conformation of the OCCO backbone. The resulting good fit of the solvation hydrogen-bond network into that of the surrounding water would then explain the high solubility of PEG. Previous studies[7–22] have shown evidence for this intuitively appealing idea, but to date no systematic experimental investigation of the origin of the different solubilities of polyethers exists. Here, we investigate this issue using spectroscopic experiments in combination with *ab initio* calculations and molecular dynamics simulations. We find evidence that the solubility difference is not due to a difference in hydrogen-bond geometry but has a completely different origin: our results indicate that it is mainly the difference in partial charges on the oxygen atoms that determines the difference in solubility, a result that may be relevant for understanding the solubilities of many other compounds.

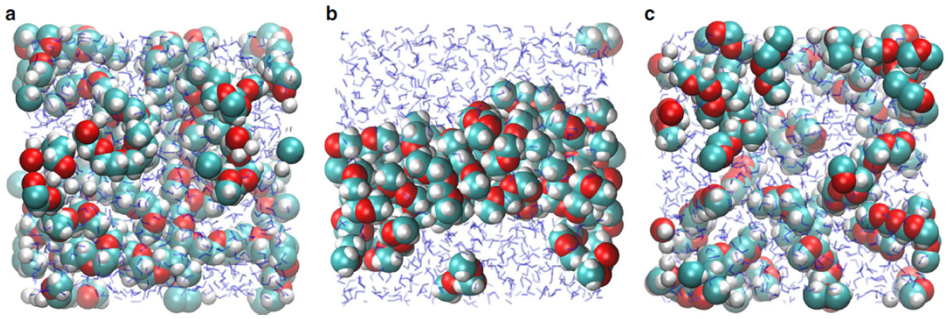

Fig. 6 Snapshots after 1 ns of FF-MD simulation. **a** PEG3, **b** POM3, and **c** fictitious POM3 molecules with modified atomic charges. Water molecules are indicated in blue. Time series of snapshots are provided in Supplementary Fig. 8, together with a clustering analysis obtained from a 50 ns simulation

Discussion

Our experimental and computational results suggest a new explanation for the different solubilities of polyethers: water interacts more strongly with PEG-like polyethers than with POM-like polyethers (Fig. 5) as a consequence of the larger partial charge on the O atoms in the former (Fig. 4). The larger partial charges of PEG-like polyethers would also result in a larger enthalpy of hydration as compared to POM-like polyethers, and this could partly explain the larger negative enthalpy of solution[2,3], and hence the better solubility. It should be noted that in general, solubility is determined not only by the hydration strength. Dissolving a substance can be regarded energetically as a process involving two steps, each of which is accompanied by an enthalpy change: (1) removing the molecules (or ions, in the case of a salt) from their pure solid or liquid phase, and (2) subsequent hydration of these free molecules (or ions). The net enthalpy change when dissolving a substance in water is the sum of these two contributions. In the case of polyethers, the enthalpy change of the first step (removing a molecule from its pure liquid phase) is very similar for PEG- and POM-like polyethers of similar size: for $CH_3OCH_2CH_2OCH_3$ and $CH_3OCH_2OCH_3$ the vaporization enthalpies at room temperature are $+36.6$ and $+31.2\,kJ\,mol^{-1}$ respectively[75,76], a difference of only $+5.4\,kJ\,mol^{-1}$. On the other hand, the heats ΔH_{sol}. released upon dissolving these substances are -59.1 and $-10.5\,kJ\,mol^{-1}$ for $CH_3OCH_2CH_2OCH_3$ and $CH_3OCH_2OCH_3$ respectively[3], a difference of $-48.9\,kJ\,mol^{-1}$. Using Hess' law we can therefore conclude that the hydration enthalpies of these two ethers differ $-54.3\,kJ\,mol^{-1}$ in favor of the PEG-like polyether. The difference in polyether solubility is thus predominantly due to the hydration interaction, i.e. to the difference in hydration enthalpies (the much smaller difference in the enthalpies required to remove the ethers from their pure liquid state actually works in the opposite direction); and the simulations indicate that this stronger hydration interaction is mostly due to the higher partial O charges (as observed in the simulations). The anchoring of the hydrating water molecules due to the presence of the neighboring hydrophobic groups (the excluded-volume effect[42]) probably further enhances the solubility.

Ensing 2019, On the origin of the extremely different solubilities of polyethers in water

Stretchable Sponge-like Hydrogels with a Unique Colloidal Network

ABSTRACT: We report a series of sponge-like hydrogels prepared by polymerizing an aqueous solution of methacrylic acid (MAAc) in the presence of *N*,*N*,*N*′,*N*′-tetramethylethylenediamine (TMEDA), which results in hydrogen bond complexation, microphase separation, and formation of a unique colloidal network. The microstructure of the gels is determined by the coupling of microphase separation and gelation, which are influenced by the feeding concentrations of MAAc and TMEDA. Colloidal gels are only obtained at a relatively low concentration of MAAc in the presence of a certain amount of TMEDA. The structural evolution during the polymerization and the formation mechanism for the colloidal network are revealed by a combination of dynamic light scattering measurements and optical microscopy. It reveals that hydrogen bond complexes are formed between poly(methacrylic acid) (PMAAc) and TMEDA, leading to the formation of colloidal particles that assemble into clusters and then the interconnected colloidal network. The physical hydrogels with a colloidal network are stable in water and possess high stretchability and good self-recovery ability due to the robustness of colloidal particles joined by adhesive PMAAc chains. These sponge-like hydrogels are applied to remove dye molecules for water purification and devised into a solar vapor generation device to produce clean water. The strategy by harnessing reaction-induced phase separation should be applicable for other systems to engineering the microstructure and properties of functional materials toward specific applications.

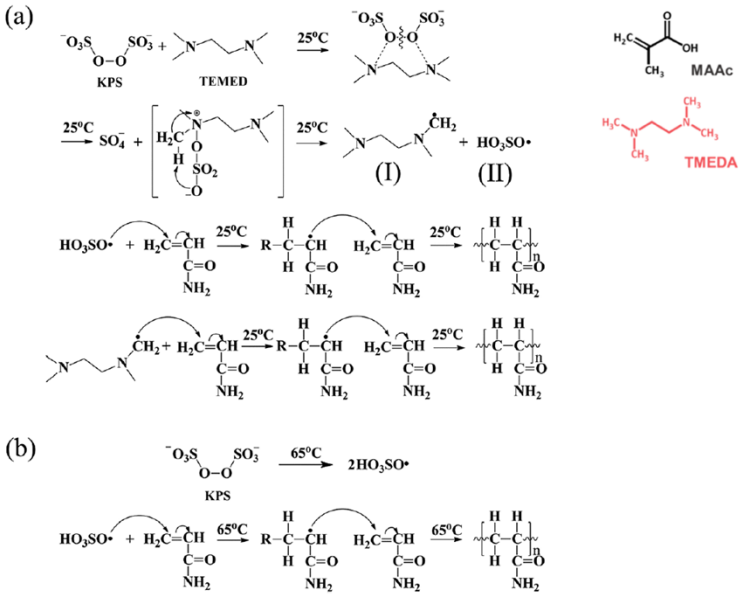

Fig. 2 Mechanism of polymerization reaction the synthesis of different initiation systems: (a) redox initial mechanism; (b) thermal initial mechanism.

Huang 2017, Enhancing the self-recovery and mechanical property of hydrogels by macromolecular microspheres with thermal and redox initiation systems

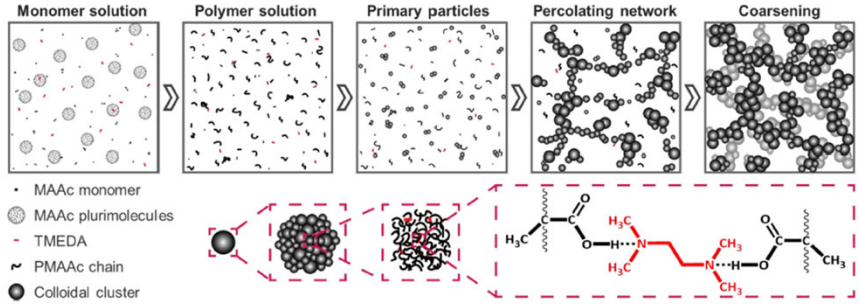

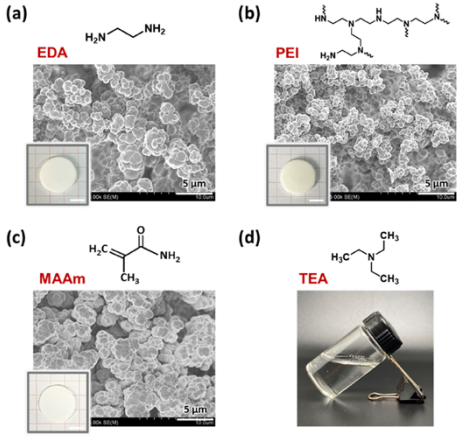

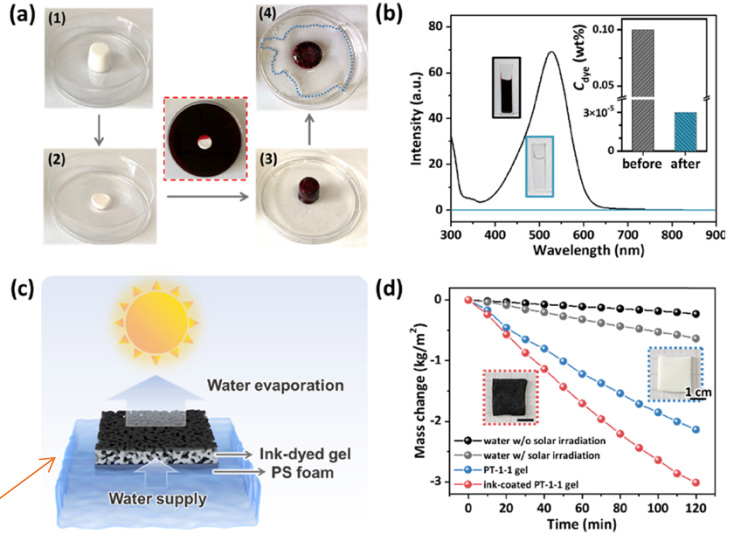

The colloidal gel was also devised into a solar vapor generator (SVG) (Figure 5c), which is useful for seawater desalination and clean water generation. The unique porous structure of the colloidal gel with micron-sized channels should facilitate the rapid transportation of water.25,64 The upper surface of the PT-1-1 gel was dyed with black ink to improve the light-to-heat conversion efficiency; the gel was placed atop a polystyrene (PS) foam as the floating support.

Figure 5. (a) Removing of dye molecules using the colloidal gel. The PT-1-1 gel was compressed to squeeze out the water and then placed in the solution of a neutral red dye to absorb the dye solution. After compression, clean water was squeezed out of the gel. (b) UV−vis spectra of the original dye solution and the squeezed solution after gel absorption. (c) Schematic for the hydrogel-based solar vapor generator (SVG). (d) Mass change of different solar vapor generators during simulated solar irradiation at room temperature and relative humidity of 50%.

Zhang 2021, Stretchable Sponge-like Hydrogels with a Unique Colloidal Network

Touch and Recyclable Phase-Separated Supramolecular Gels

INTRODUCTION

Hydrogels are soft and elastic materials consisting of flexible polymer chains solvated in water. The unique combination of softness and hydration enables their impact on fields including, personal hygiene (e.g., diapers, personal healthcare products, etc.),[1,2] agriculture (e.g., carriers of agrochemicals),[3,4] environmental remediation (e.g., adsorbents and evaporators for water purification),[5,6] and food packaging systems.[7] Hydrogels can be functionalized and are also biocompatible, which are attractive features for applications at the interface of medicine and electronics, including drug delivery,[8,9] soft actuators,[10−12] strain sensors,[13−15] touch panels,[16] and artificial muscles.[17,18] Despite their tremendous potential and societal benefit, the growing consumption of hydrogels could contribute to environmental pollution as they are generally non-biodegradable under natural conditions.[19−21] Moreover, conventional hydrogels are covalently cross-linked, thus challenging to recycle and reprocess after use or damage.[22,23] One of the most effective approaches to resolve these shortcomings is to replace conventional covalent cross-linked gels with supramolecular hydrogels (SGs) cross-linked by dynamic hydrogen bonds.[24] Supramolecular hydrogels, however, are prone to overswelling and disintegration in aqueous environments because the presence of water molecules disrupts hydrogen bonds,[25,26] thus further weakening their mechanical strength. Such instability and poor mechanical properties inhibit the long-term use and implementation of SGs. Therefore, constructing mechanically robust, yet recyclable gels that resist overswelling in a wide variety of aqueous environments is particularly attractive, but remains a significant materials challenge.

In another approach, phase separation has been exploited to improve the stiffness and restrict the overswelling of hydrogels by increasing the physical cross-linking density and reducing the flexibility of chain segments.[27,28] Recently, researchers have embarked on efforts to design phase-separated hydrogels that include a mechanism for energy dissipation, such as hydrogen bonding,[29] ionic bonding,[30,31] hydrophobic association,[31−33] or crystallization,[34] to increase strength and toughness. The most widely employed approaches to induce phase separation in hydrogels include the use of solvent exchange[35−37] or the addition of salt, i.e., the salting out effect.[33,38] However, the use of organic solvents and other chemicals is not environmentally benign nor are the gels reprocessable, which may further negatively impact the environment at the end of service life.

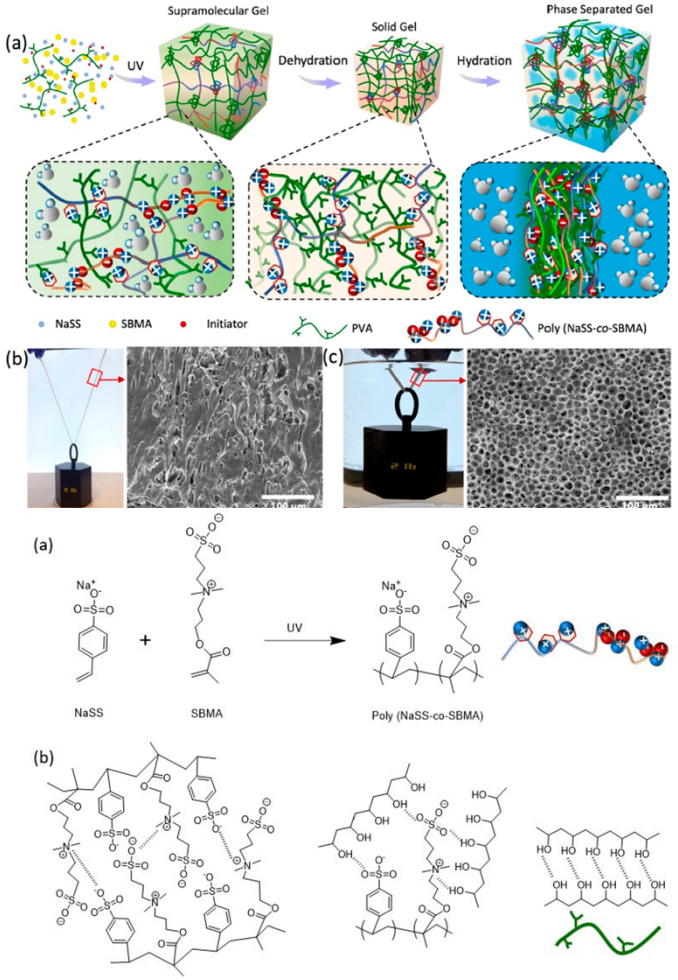

Fig. S1. (a) The chemical structures of the monomers and the poly(NaSS-co-SMBA) copolymer. (b) The polymer-polymer interactions in the PSG include the electrostatic interactions between the poly(NaSS-co-SMBA) copolymers, the hydrogen bonding between the copolymer and PVA, and the hydrogen bonding between PVA chains. The hydrophobic interactions between polymer backbones are not shown.

A dehydration−rehydration method to create tough and recyclable, phase-separated supramolecular hydrogels (PSGs): The PSG was prepared by copolymerization of sodium styrenesulfonate (NaSS) and sulfobetaine methacrylate (SBMA) in an aqueous PVA solution, followed by dehydration via air drying and rehydration via swelling in water (Figure 1a). The approach is facile, sustainable, and low-energy: all synthesis occurred in water, and the dehydration-rehydration process required no energy input. Upon dehydration, strong polymer-polymer interactions between PVA and poly(NaSS-co-SMBA) copolymer were activated, as illustrated in Figure S1. Subsequent, rehydration weakened hydrogen-bonding interactions between polymer chains while simultaneously promoting the aggregation of the hydrophobic polymer segments, leading to a PSG composed of water-rich and polymer-rich domains (Figure 1a). The polymer-rich domains acted as robust physical cross-links, which endowed the PSG with an unusual combination of material properties, including toughness, restricted swelling, and recyclability. The PSG exhibited stability in various environments, including mixed solvents containing ethanol, isopropyl alcohol (IPA), dimethyl sulfoxide (DMSO), and even extremely acidic/alkaline conditions with pH 1 and 14. We demonstrate PSG's performance as a flexible and recyclable strain sensor in both air and underwater.

Figure 1. Fabrication and porous structures of the hydrogel. (a) Schematic of the fabrication route for PSGs. Lifting performance and microstructures of (b) SGs and (c) PSGs after dehydration-hydration treatment

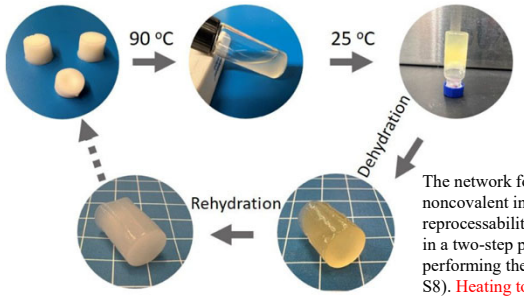

Fig. S8. Recycling and reprocessing of PSG.

The network formation of PSGs is enabled by noncovalent interactions, which enable recyclability and reprocessability of the gel. Reprocessing is accomplished in a two-step process: (1) heating the PSG and (2) performing the dehydration-hydration process (Figure S8). Heating to ~80 °C disrupts the hydrogen bonds and hydrophobic interactions within the PSG and enhances polymer mobility. The first step results in a translucent liquid, which upon cooling can be reformed into various shapes via the second step, i.e., the dehydration-hydration process.

Xu 2023, Tough and recyclable phase-separated supramolecular gels via a dehydration–hydration cycle

Environmental Stimuli

Physical

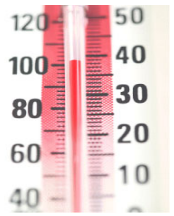
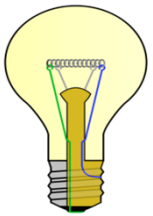

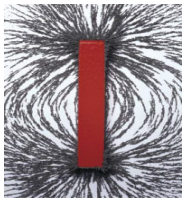

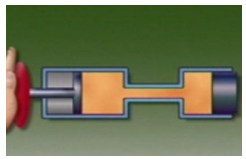

Stimuli

Biological

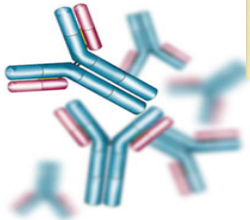
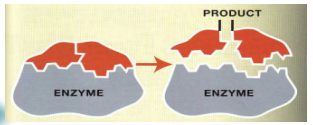

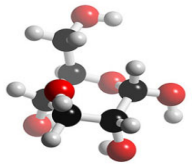

Chemical

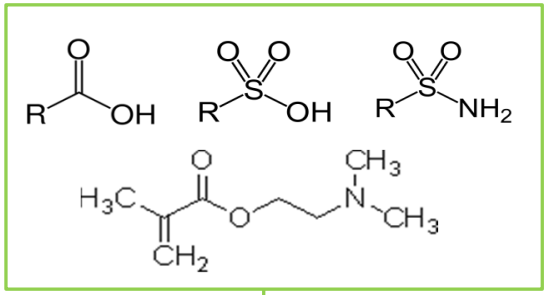

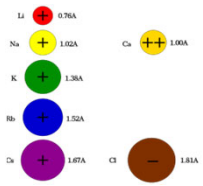
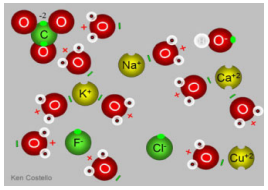
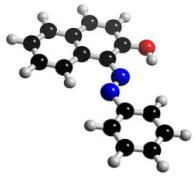
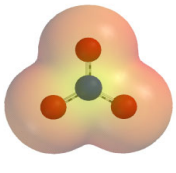

Temperature-Sensitive Systems

Temperature-Sensitive Polymers & Hydrogels

Positive Thermosensitivity

as T ↑ Solubility/Swelling ↑

Negative Thermosensitivity

as T ↑ Solubility/Swelling ↓

Covalent bond: ~ 5 eV ($\approx 0.8 \times 10^{-18}$ J)

Secondary interaction forces: ~ 0.1 eV

Thermal fluctuation energy: ~ 0.03 eV ($\approx$ 1 kT)

Competition between the two forces
(H-bonding & Hydrophobic interaction)

Temperature dependent interactions

as T ↑ Hydrogen-bonding ↓

as T ↑ Hydrophobic interaction ↑

Hydrophobic interactions

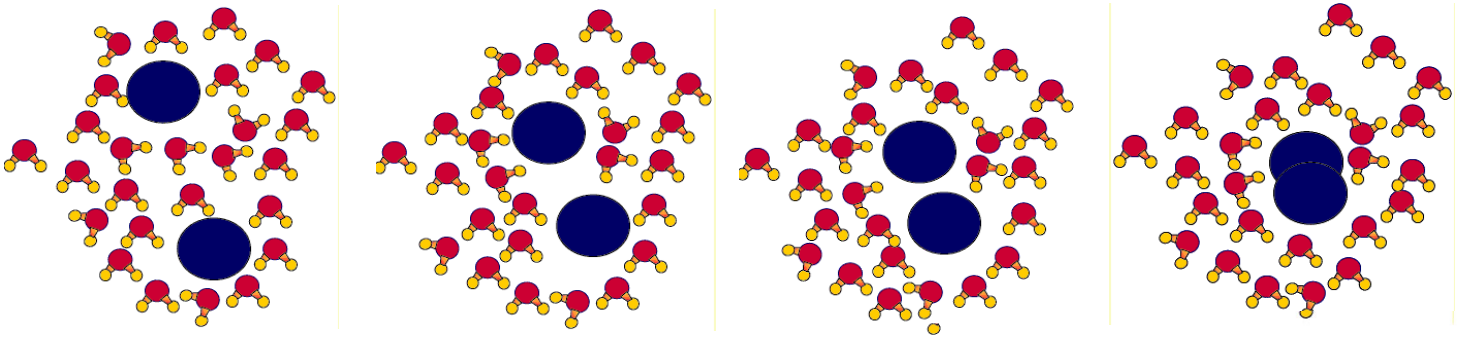

The chemical structure of PNIPAAm.

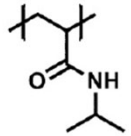

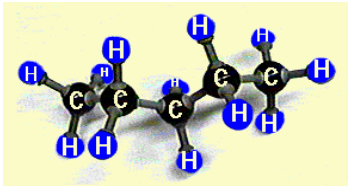

Hydrocarbons: Lipophilic hydrocarbon-like groups in solutes.

A droplet of water forms a spherical shape to minimize contact with the hydrophobic leaf.
http://en.wikipedia.org/wiki/Hydrophobic_effect

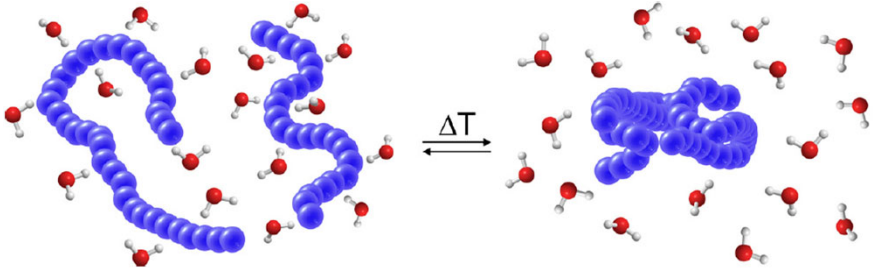

Fig. 1. Schematic representation of a polymer phase transition in aqueous solution from a completely dissolved homogeneous state to a two-phase demixed system comprising a high polymer concentration phase and a low polymer concentration aqueous phase. Even though the collapsed polymer chains in the high concentrated phase are still partially hydrated, these water molecules are not shown in the picture for simplicity. The scheme shows an LCST transition if $\Delta T > 0$ and an UCST if $\Delta T < 0$.

http://academic.brooklyn.cuny.edu/biology/bio4fv/page/hydropho.htm

Vancoillie 2014, Thermoresponsive poly(oligo ethylene glycol acrylates)

Temperature-Sensitive Polymers

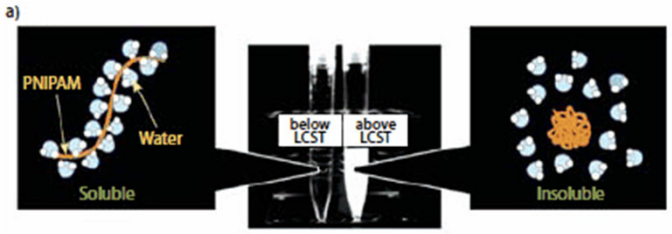

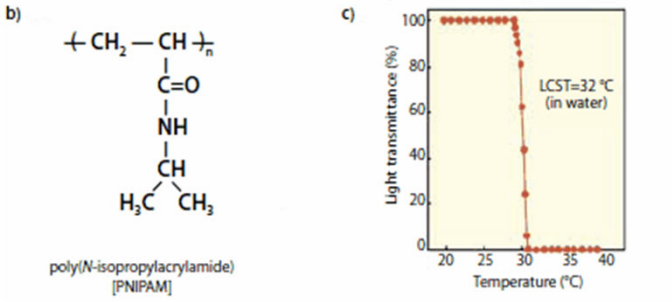

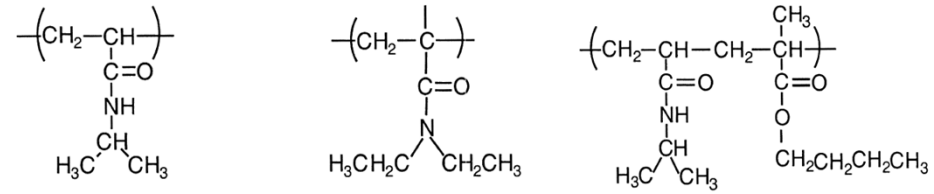

Fig. 1. Structures of some temperature-sensitive polymers.

Qiu 2001, Environment-sensitive hydrogels for drug delivery

Temperature-dependent polymers: The first smart polymers.
Lower critical solution temperature: lowest temperature at which all components are soluble.

Solution:	Soluble	→	Insoluble
Hydrogel:	Swollen	→	Collapsed
Surface:	Hydrophilic	→	Hydrophobic

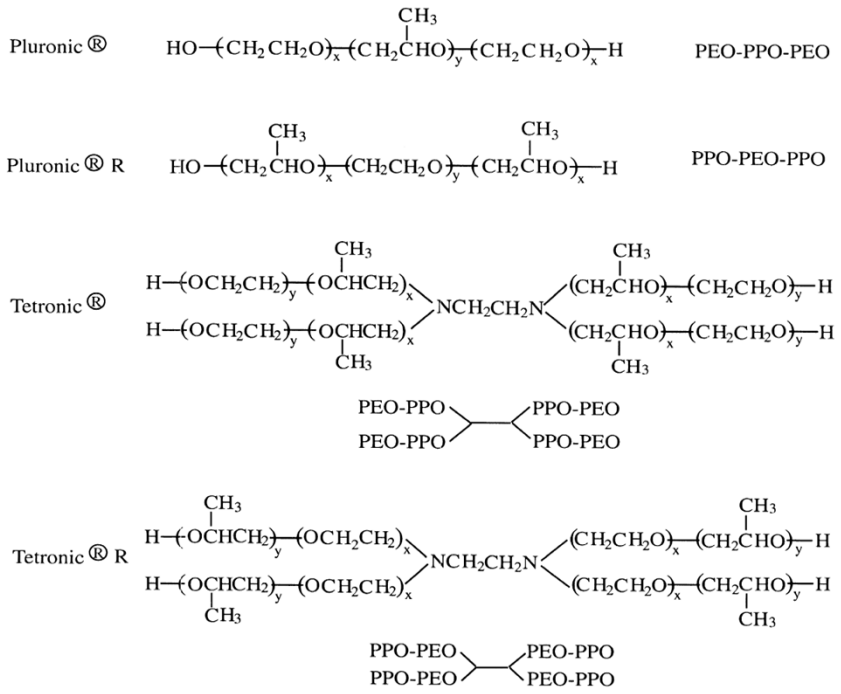

Fig. 2. Polymer structures of Pluronic®, Pluronic® R, Tetronic® and Tetronic® R.

Temperature-Sensitive Polymers & Hydrogels

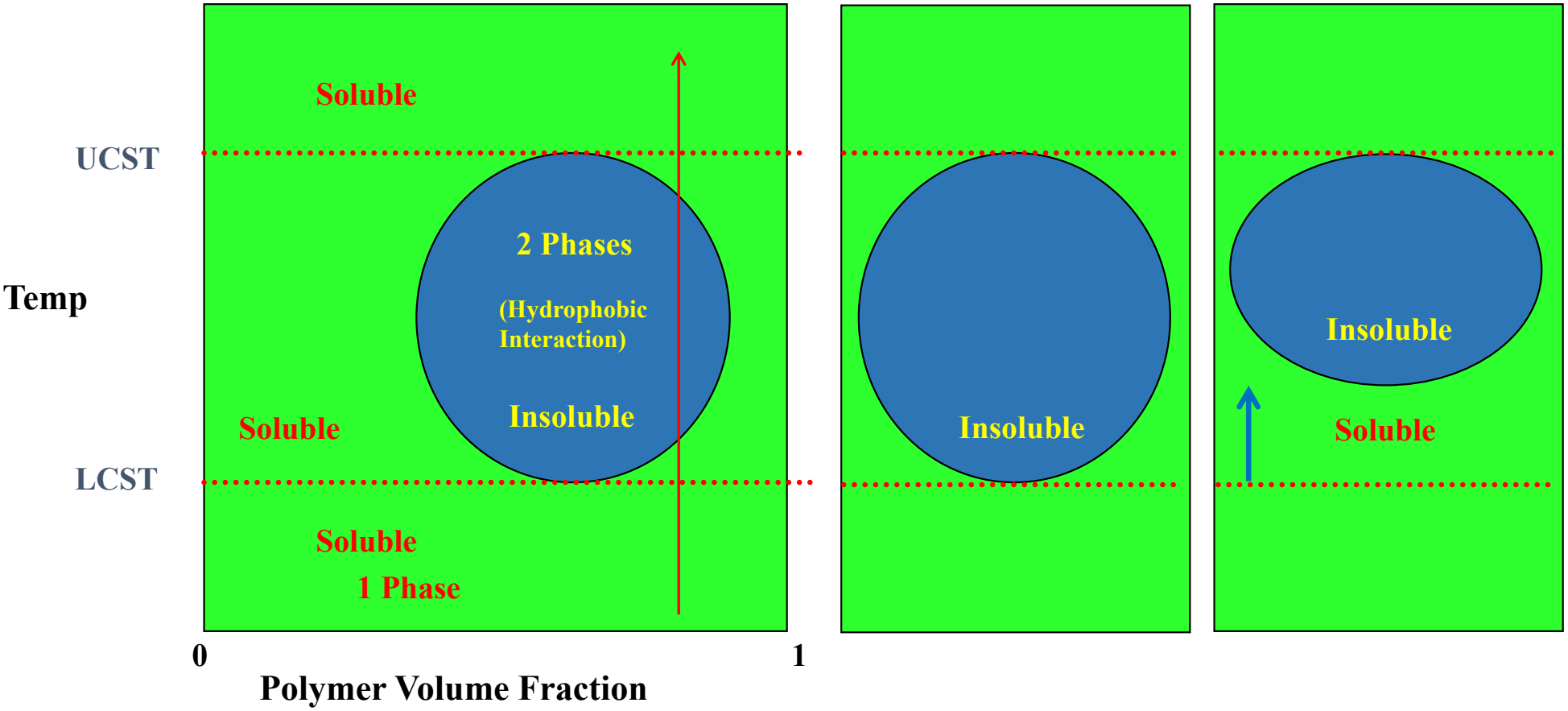

Thermosensitive Polymers

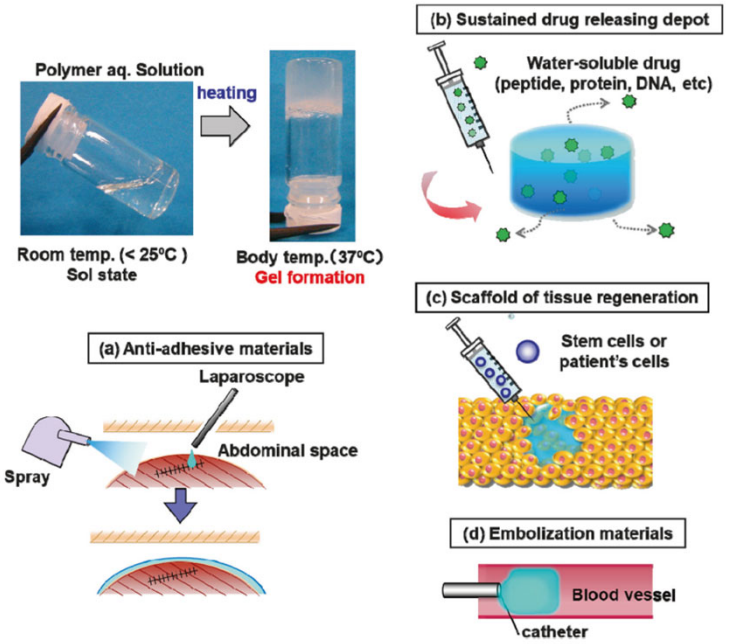

Fig. 1 Photographs of sol–gel transition and expected applications for biodegradable injectable polymer systems. (a) Antiadhesive materials for laparoscopic surgery, (b) sustained drug release system, (c) cellular scaffold for tissue regeneration, (d) vascular embolization materials.

Ohya 2019, Temperature-responsive biodegradable injectable polymer systems with conveniently controllable properties

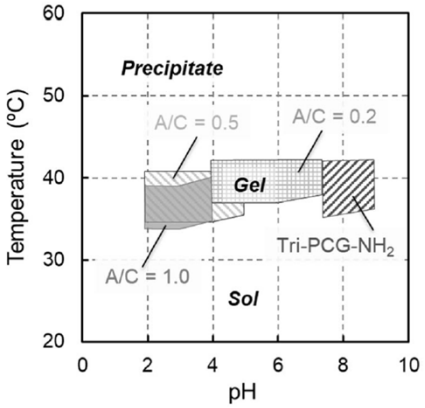

Fig. 3. Phase diagrams for the temperature and pH-dependent sol–gel transition of mixtures of tri-PCG-COOH and tri-PCG-NH_2 with various A/C ratios (1.0, 0.5, 0.2, and 0) in PBS. A/C =[tri-PCG-COOH]/[tri-PCG-NH_2].

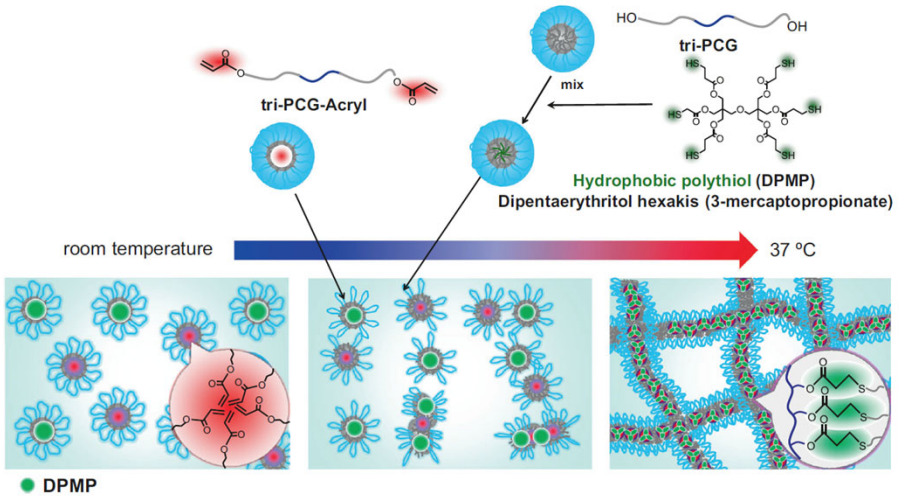

Fig. 6 Schematic illustration of the temperature-responsive irreversible sol-to-gel transition mechanism of the tri-PCG-Acryl + tri-PCG/ DPMP system with increasing temperature from room temperature to body temperature.

Thermo-Sensitive Polymers

Kim 2012, Injectable in situ-forming hydrogels for a suppression of drug burst from drug-loaded microcapsules

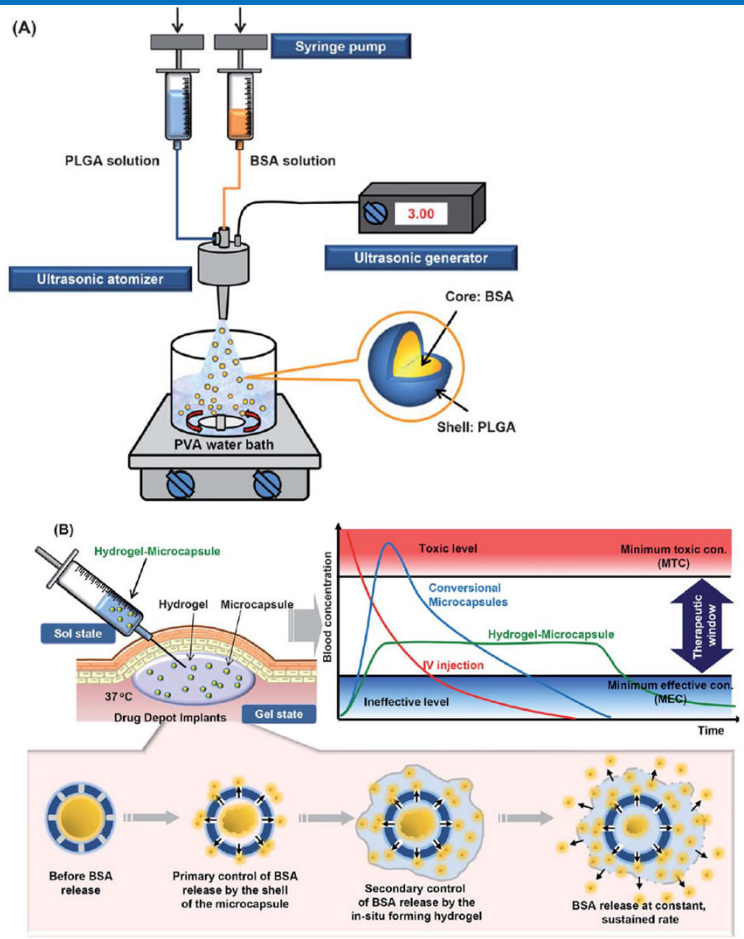

Fig. 1 Schematic representation of (A) the microencapsulation method using a mono-axial ultrasonic atomizer and (B) controlled BSA release from drug depot implants

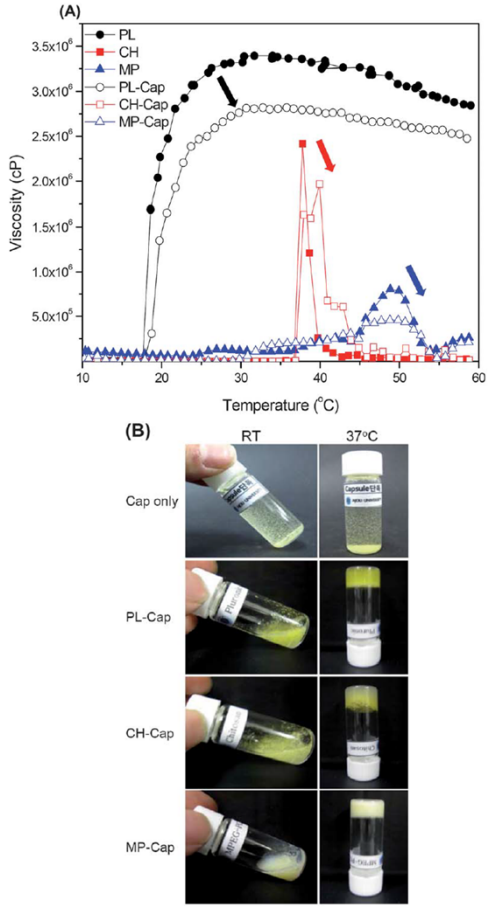

Fig. 2 (A) Viscosity versus temperature curves for PL, PL-Cap, CH, CH-Cap, MP, and MP-Cap solutions and (B) the images of each formulation.

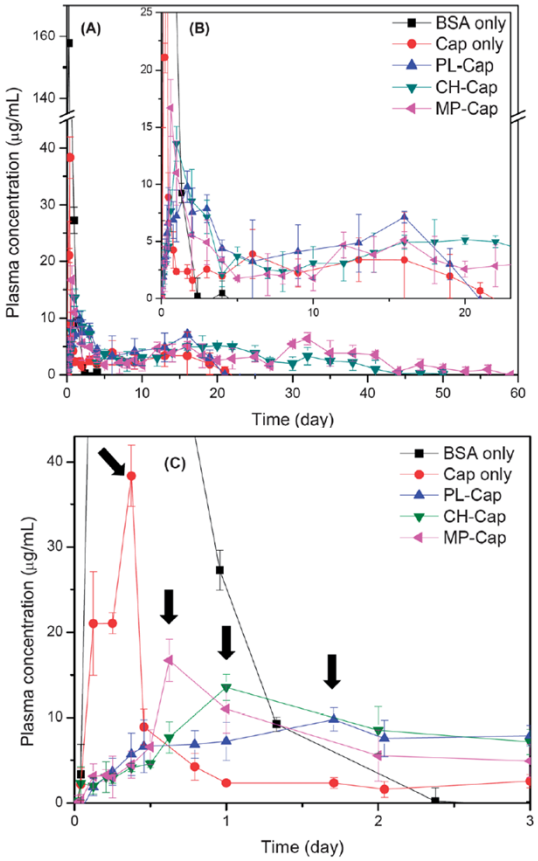

Fig. 4 Time course of BSA-FITC concentration in plasma over (A) 60 days, enlarged graph for (B) 23 days, and (C) 5 days after injection of hydrogel-BSA-FITC-loaded microcapsules. The arrows indicate the Tmax of each formulation.

Temperature-Sensitive Block Copolymers and Crosslinked Micelles

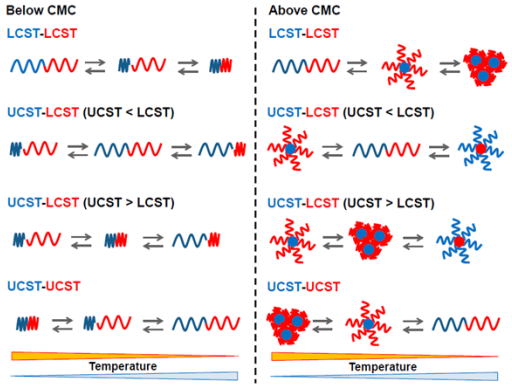

Figure 1. Conformation changes of dual thermoresponsive block copolymers at below or above the critical micelle concentration (CMC).

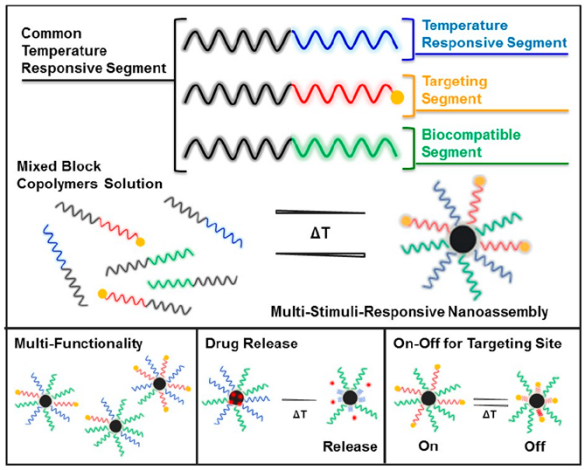

Figure 12. Multi-stimuli-responsive nanoassembly by mixing of selected block copolymers with a common temperature-responsive segment.

Kotsuchibashi 2016, Recent advances in dual temperature responsive block copolymers and their potential as biomedical applications

LCST: the lower critical solution temperature UCST: the upper critical solution temperature

The LCST types of thermo-responsive polymers can dissolve in aqueous solution at temperatures lower than the LCST and the polymers can become hydrophobic above the LCST, which is caused by accelerated polymeric intra- and inter-molecular hydrogen bonding/hydrophobic interactions resulting in disrupted hydrogen bonding interactions with surrounding water molecules. This reversible solubility change has been applied for a wide range of applications such as in the development of model proteins, triggers for self-assemblies, "on-off" switch of protein activities, cell sheet technologies, drug carriers, column chromatography, and sensors.

In contrast, UCST copolymers can dissolve in solvent above the UCST and are insoluble below the UCST. The phenomenon can occur via specific interactions such as hydrogen-bonding and electrostatic interaction. UCST copolymers are also applied in various fields such as assembled nanomaterials, sensors, and protein separations. Poly(sulfobetaine methacrylate (SBMA)) is one of the most studied UCST type temperature responsive polymers, which has a zwitterionic betaine group ($CH_2CH_2N^+(CH_3)_2CH_2CH_2CH_2SO_3^-$) in the structure. The UCST of poly(SBMA) is triggered by the charge-charge and dipole-dipole interactions of the betaine groups.

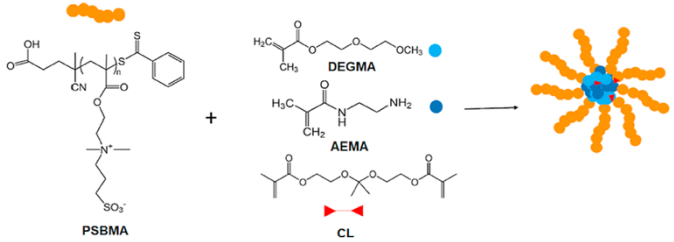

Scheme 2. CCMs Synthesis by RAFT Polymerization

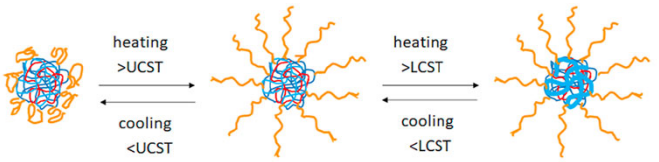

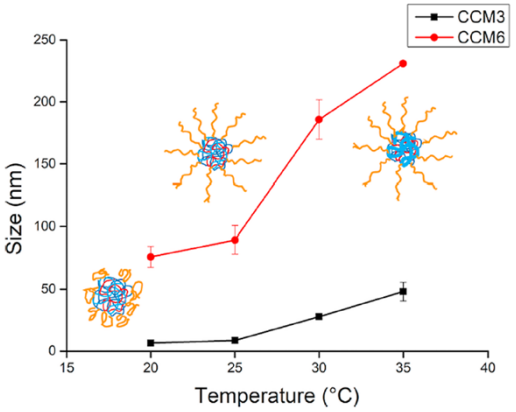

Figure 8. Change in the micelle size depending on the temperature for CCM3 and CCM6 with 1 mg/mL concentration.

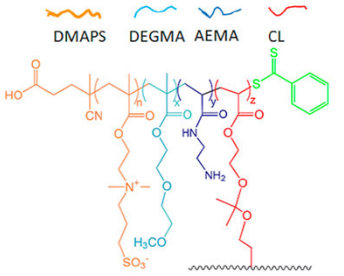

Scheme 3. Structure of CCM and Molecular Changes During UCST and LCST Transitions

Gürdap 2022, Sulfobetaine-based homo- and copolymers by RAFT: Cross-linked micelles and aqueous solution properties

Applications as a Bio-Conjugate

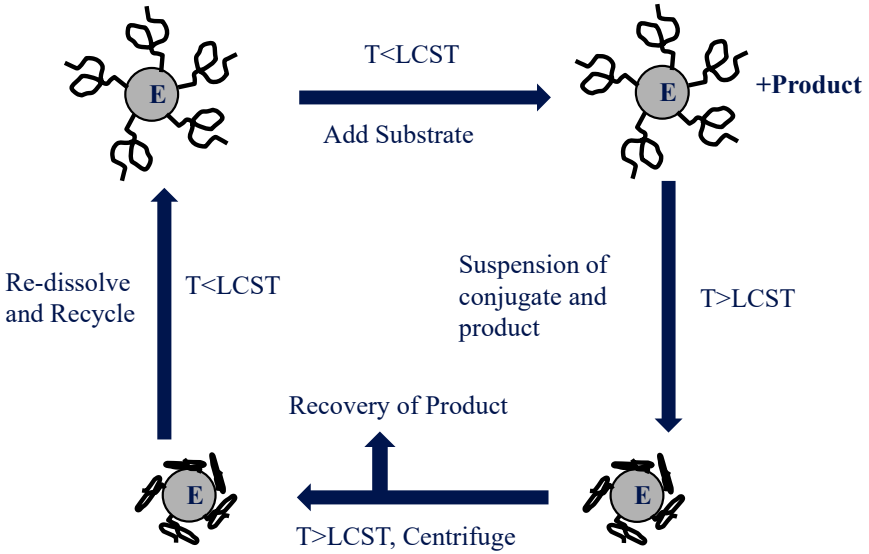

Protein is conjugated to the polymer.
Bioactivity normally decreases.
Can add to a site specific location, but difficult to do.

Ding, 1998 J Biomed Mater Res

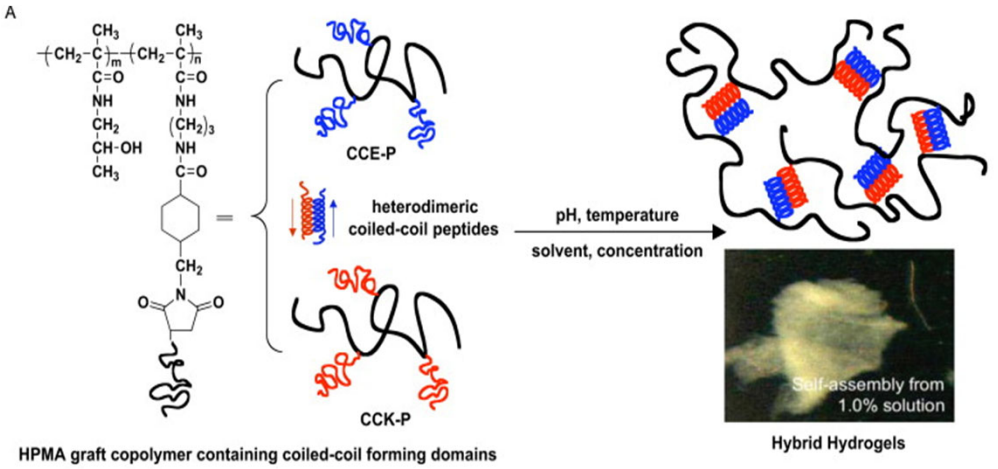

HPMA graft copolymer containing coiled-coil forming domains

Wang et. Al. *Nature* 1999

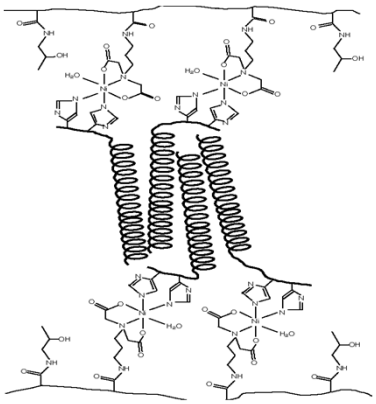

Kopeček J *Biomaterials* 2007

Applications in Tissue Engineering

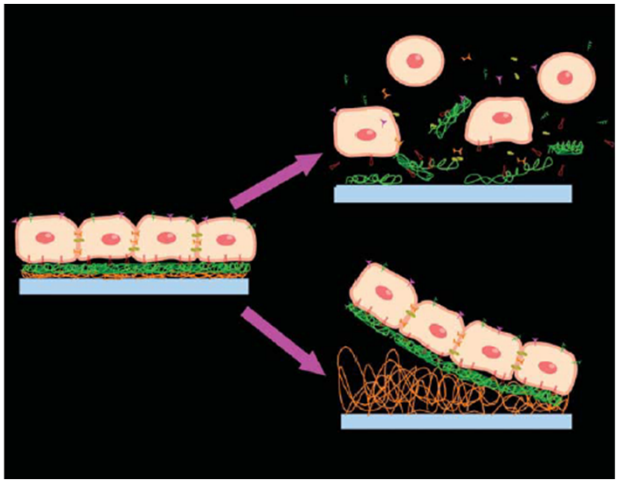

Fig. 2 Cell sheet harvest. Trypsin degrades deposited ECM (green), as well as membrane proteins, so that confluent, monolayer cells are harvested as single cells (upper right). The temperature-responsive polymer (orange) covalently immobilized on the dish surface hydrates when the temperature is reduced, decreasing the interaction with deposited ECM. All the cells connected via cell-cell junction proteins are harvested as a single, contiguous cell sheet without the need for proteolytic enzymes (lower right).

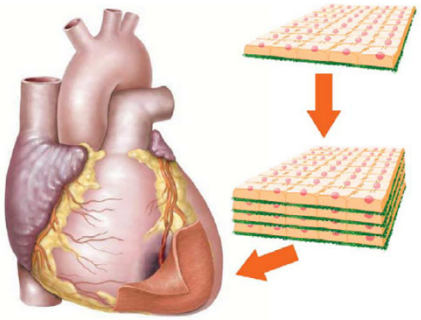

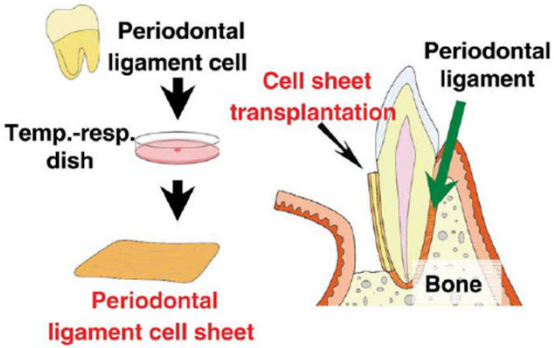

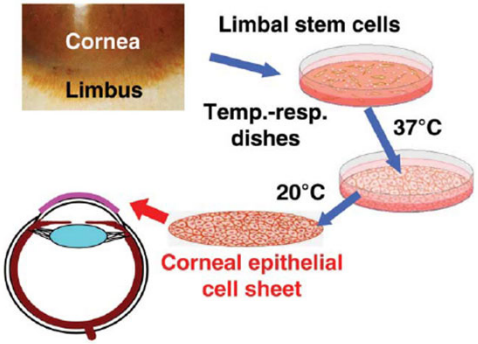

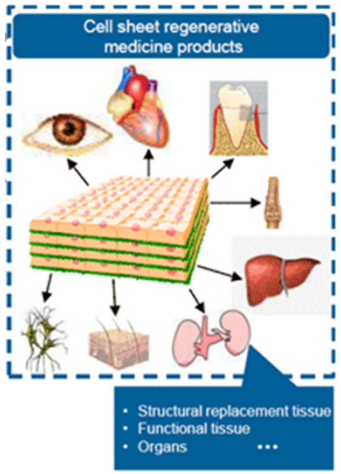

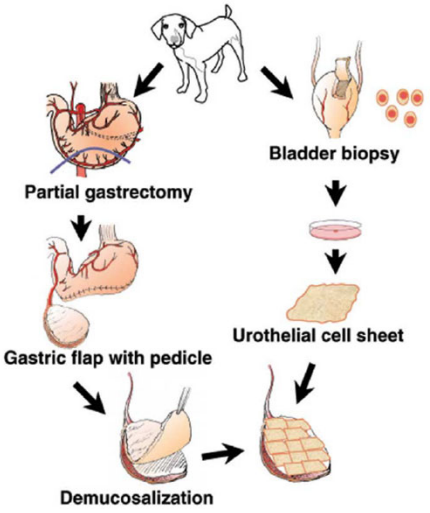

Yamato 2004, Cell sheet engineering
Teruo Okano (Professor, Tokyo Women's Medical University)

Thermo-Responsiveness

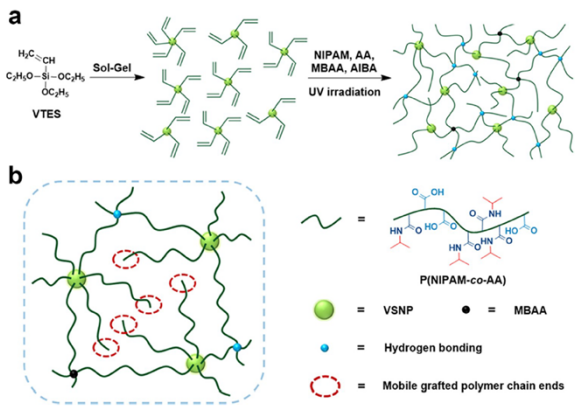

Figure 1. Thermo-responsive VSNPs-P(NIPAM-co-AA) hydrogels. (a) Synthesis and network structure of the hydrogels. The polymer network is constructed through the multivalent VSNPs (green balls), noncovalent hydrogen bonding (blue balls), and covalent cross-links by MBAA (black balls). AA monomer has carboxylic acid groups (in light blue), while NIPAM has both hydrophilic amide groups (in dark blue) and hydrophobic isopropyl groups (in red). (b) Schematic illustration of the mobile grafted polymer chain ends.

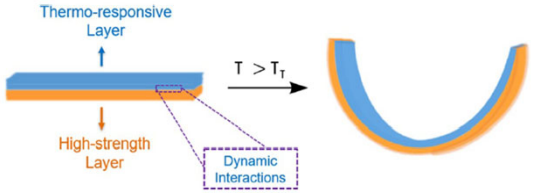

Figure 4. Design and actuating mechanism of the gradient thermo-responsive hydrogel actuators.

Li 2022, Biomimetic gradient hydrogel actuators with ultrafast thermo-responsiveness and high strength

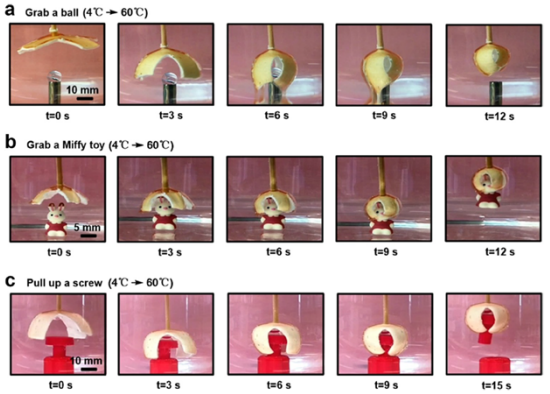

Figure 6. Schematic illustrations of the integrated gradient hydrogels as thermo-responsive grippers. (a) Grab a ball, (b) grab a Miffy toy, and (c) pull up a screw.

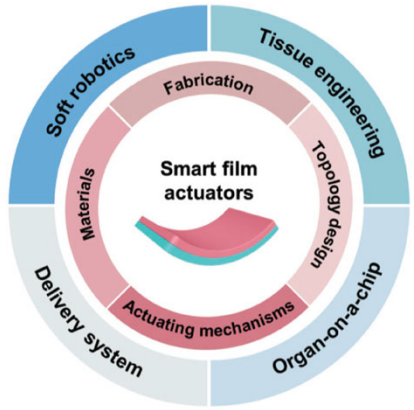

Figure 1. Overview of smart film actuators for biomedical applications.

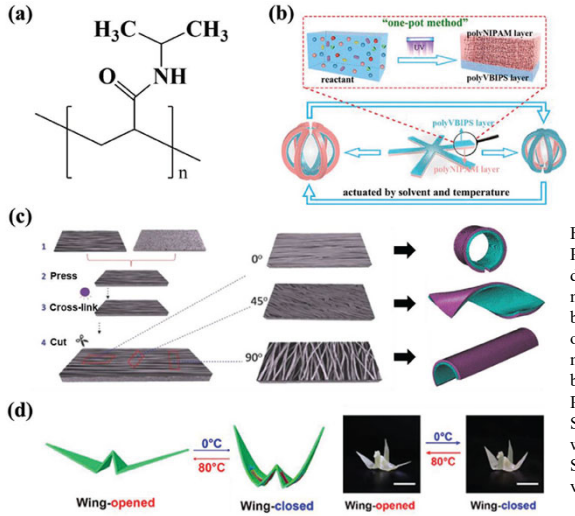

Figure 4. a) Chemical structure of the PNIPAM monomer. b) Schematic diagram of the preparation and working mechanism of the PNIPAM-PVBIPS bilayer hydrogel. c) Schematic diagram of the preparation and working mechanism of the anisotropic PNIPAM bilayer hydrogel with different internal PNIPAM fiber orientations. d) Schematic and images of the reversible wing-flapping of a crane-shaped 3D SMPs actuator triggered by temperature variation (Scale bar = 1 cm).

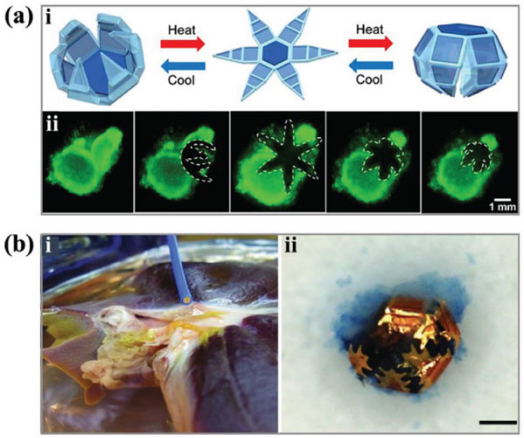

Figure 8. SFA-based soft medical robotics. a-i) Schematic diagram of the thermal-actuated soft robotics; a-ii) fluorescent images of the star-shaped microgripper capturing and excising cells from a living fibroblast clump. b-i) Photograph image of the control of the soft biopsy robotic using a magnetic catheter; b-ii) photograph image of the retrieved robotic with a piece of excised tissue, which was stained in blue (Scale bar = 100 μm).

Zhang 2022, Smart film activators for biomedical applications

Temperature-Sensitive Polymers & Hydrogels

Case study:

A veterinary company asks you to design a drug delivery platform that can be injected as a solution but converted to a gel for long-term drug release.
You are asked to make a formulation for reptiles and another one for rodents.

You decide to make it using NIPAAm, how would you have to modify the system to work for both reptiles and rodents?

Temperature-Sensitive Polymers & Hydrogels

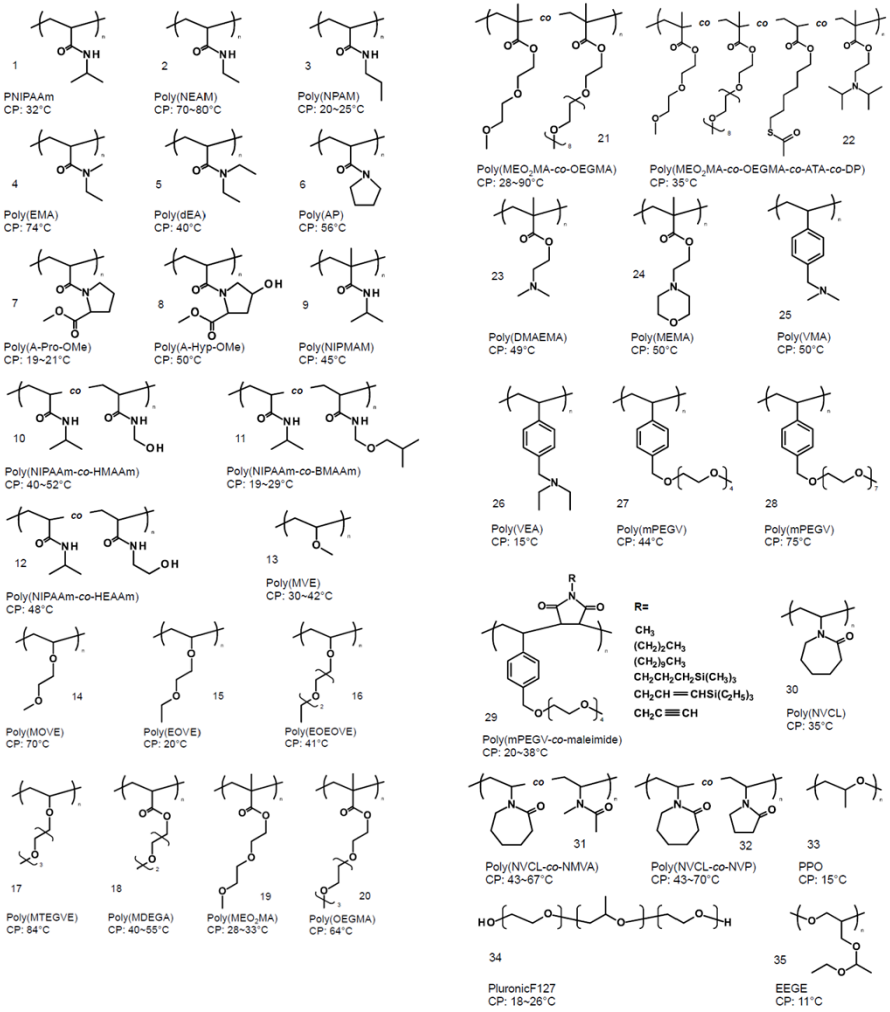

Figure 2. Structures of lower critical solution temperature (LCST) type of thermo-responsive copolymers for dual thermo-responsive block copolymers: CP: cloud point.
1. NIPAAm: N-isopropylacrylamide;
2. NEAM: N-ethylacrylamide;
3. NPAM: N-n-propylacrylamide;
4. EMA: N,N-ethylmethylacrylamide;
5. dEA: N,N-diethylacrylamide;
6. AP: N-acryloylpyrrolidine;
7. A-Pro-OMe: N-acryloyl-L-proline methylester;
8. A-Hyp-OMe: N-acryloyl-4-hydroxy-L-proline methylester;
9. NIPMAM: N-isopropyl methacrylamide;
10. HMAAm: N-hydroxymethyl acrylamide;
11. BMAAm: N-(isobutoxymethyl) acrylamide;
12. HEAAm: N-hydroxyethylacrylamide;
13. MVE: methyl vinyl ether;
14. MOVE: 2- methoxyethyl vinyl ether;
15. EOVE: 2-ethoxyethyl vinyl ether;
16. EOEOVE: 2-(2-ethoxy)ethoxyethyl vinyl ether;
17. MTEGVE: methyltriethylene glycol vinyl ether;
18. MDEGA: methoxydiethylene glycol acrylate;
19. MEO2MA: 2-(2-methoxyethoxy) ethyl methacrylate;
20–21. OEGMA: oligo(ethylethylene glycol)methyl ether methacrylate;
22. ATA: 6-acethylthiohexylacrylate, DP: 2- (diisopropylamino)ethyl methacrylate;
23. DMAEMA: 2-(dimethylamino)ethyl methacrylate;
24. 2-(N-morpholino)ethyl methacrylate;
25. VMA: N-(4-vinylbenzyl)-N,N-dimethylamine;
26. VEA: N-(4-vinylbenzyl)-N,N-diethylamine;
27–29. mPEGV: poly(ethyleneglycol)methyl ether vinyl phenyl;
30. NVCL: N-vinylcaprolactam;
31. NMVA: N-methyl-N-vinylacetamide;
32. NVP: Nvinylpyrrolidone;
33. PPO: poly(propylene oxide);
34. PluronicF127: poly(oxyethylene)- poly(oxypropylene)-poly(oxyethylene);
35. EEGE: ethoxyethylglycidyl ether.

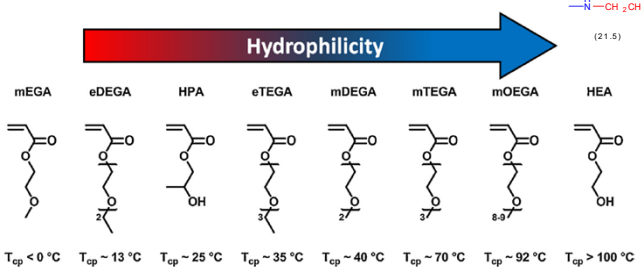

Fig. 4. Overview of the selected OEGA monomers arranged according to increased hydrophilicity, with average cloud point temperatures (T_{cp}) of the corresponding homopolymer.

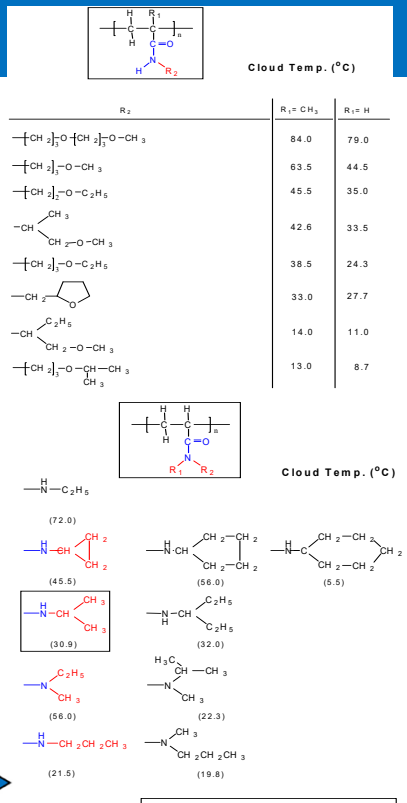

Kotsuchibashi 2016, Recent advances in dual temperature responsive block copolymers and their potential as biomedical applications

Vancoillie 2014, Thermoresponsive poly(oligo ethylene glycol acrylates)

Adjusting the LCST of Thermosensitive Polymers

Copolymer of acrylamide and n-tertbutylacrylamide
= Poly(acrylamide-co-n-tertbutylacrylamide)

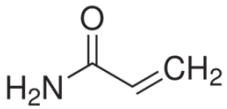

AAm: acrylamide

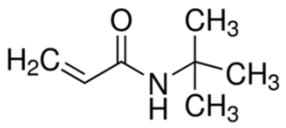

N-tBAAm: n-tertbutylacrylamide

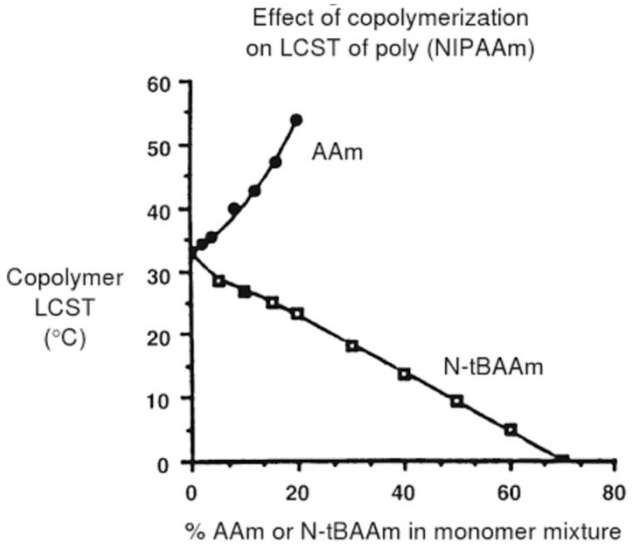

FIG. 3. Copolymerization of a thermally sensitive polymer, PNIPAAm, with a more hydrophilic comonomer, AAm, raises the LCST of the copolymer, whereas copolymerization with a more hydrophobic comonomer, N-tBAAm, lowers the LCST (Hoffman *et al.*, *Journal of Biomedical Materials Research* © 2000).

PLGA-PEG-PLGA Thermo-responsive Copolymers

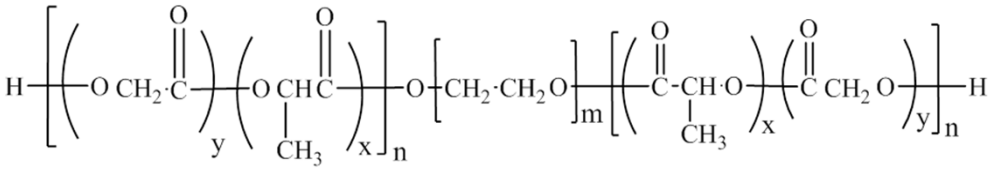

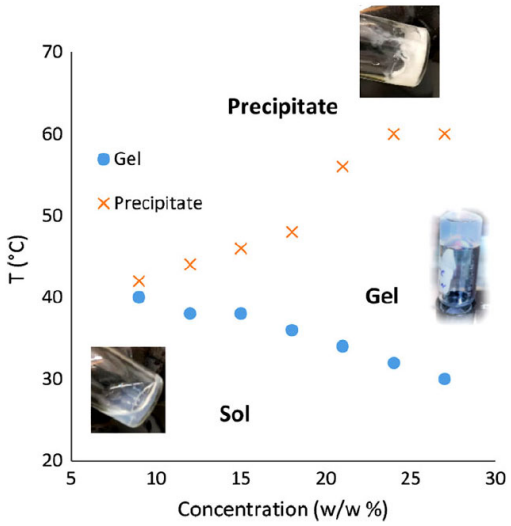

FIGURE 6. Representative phase diagram of PLGA-PEG-PLGA aqueous solutions. As temperature increases the solution turns to gel, and upon further heating a precipitate is formed.

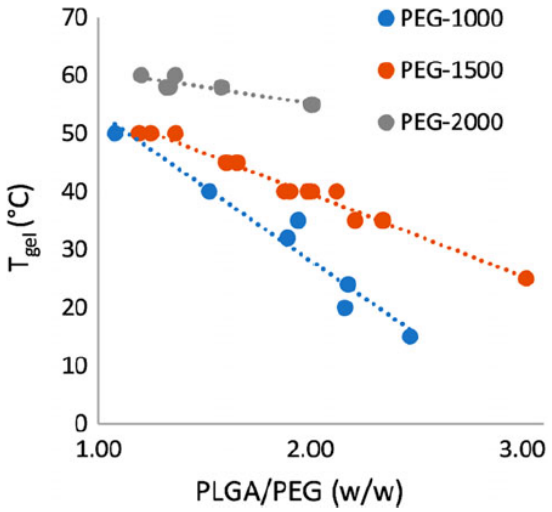

FIGURE 7. Dependence of T_{gel} on PLGA/PEG ratio. For each set of polymers based on a particular PEG MW, a linear relationship has been defined between the polymer's aqueous gelling temperature in a 20% solution and the polymer structure's PLGA/PEG ratio.

Steinman 2019, Effect of PLGA block molecular weight on gelling temperature of PLGA-PEG-PLGA thermoresponsive copolymers

PEG-PLGA-PEG Triblock Copolymer

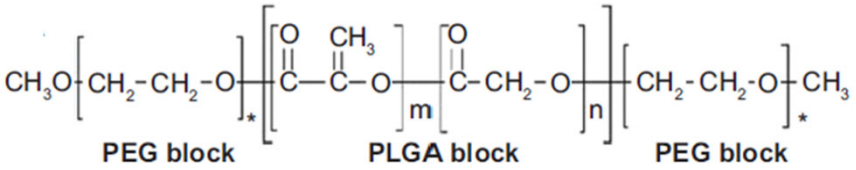

Poly(lactic-co-glycolic acid) (PLGA)
Poly(lactide-co-glycolide)

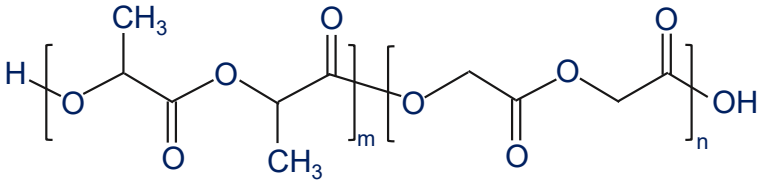

PLGA is biodegradable
PLGA is a biocompatible hydrophobic polymer commonly used in controlled release devices
PEG is a biocompatible hydrophilic polymer used for a number of applications

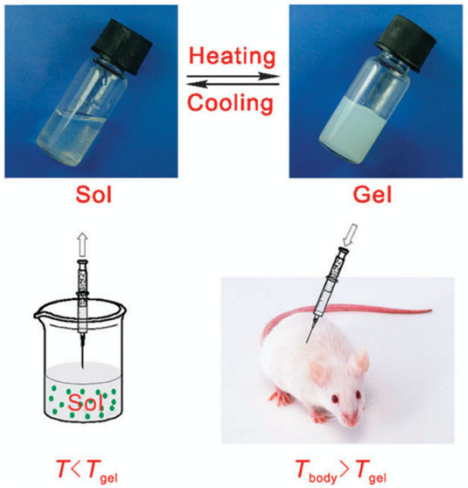

Jeong 1999, Thermoreversible gelation of PEG-PLGA-PEG triblock copolymer aqueous solutions

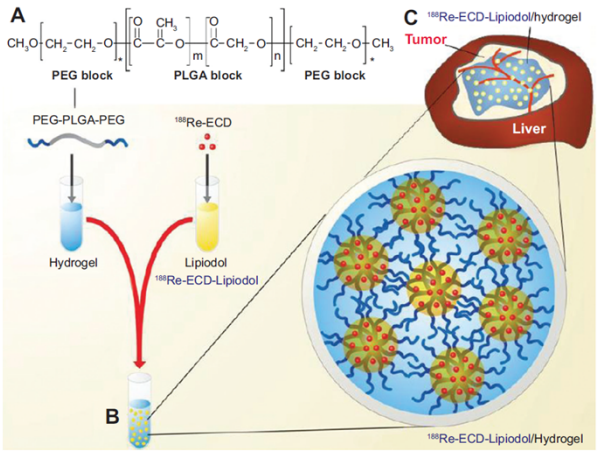

Shih 2014, Preparation and therapeutic evaluation of 188Re-thermogelling emulsion in rat model of hepatocellular carcinoma

PEG-PLGA-PEG Triblock Copolymer

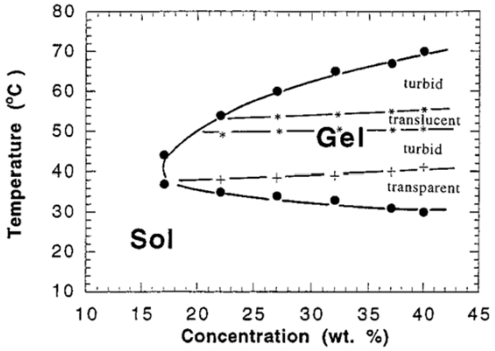

Figure 2. Phase diagram of $EG_{12}-(L_{31}G_9)-EG_{12}$ triblock copolymer aqueous solutions. Filled circles indicate sol–gel transition temperature, and the cross-bar is the temperature at which the transparent gels become turbid. The gel passes through a translucent region (*) and finally becomes turbid again with increasing temperature.

Effect of PLGA Molecular Weight

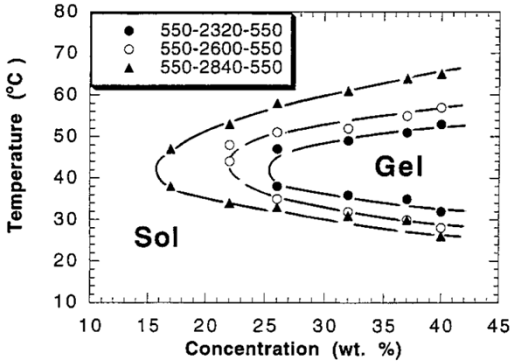

Figure 7. Phase diagram of PEG–PLGA–PEG triblock copolymers with various PLGA lengths: (●) $EG_{12}-(L_{26}G_7)-EG_{12}$; (○) $EG_{12}-(L_{29}G_8)-EG_{12}$; (▲) $EG_{12}-(L_{31}G_9)-EG_{12}$. The legend in the graph indicates molecular weight of constituting block.

Effect of L:G Ratio

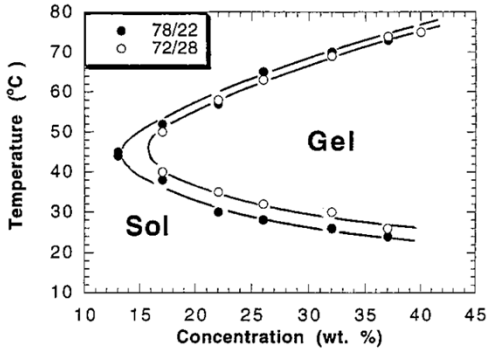

Figure 8. PLGA composition effect on the phase diagram of PEG–PLGA–PEG (550–2900–550) triblock copolymers: (●) $EG_{12}-(L_{32}G_9)-EG_{12}$; (○) $EG_{12}-(L_{31}G_{12})-EG_{12}$. The legend in the graph indicates the mole ratio of DLLA to GA.

Effect of PEG Molecular Weight

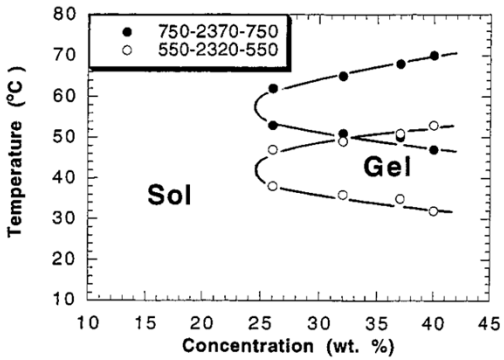

Figure 9. PEG length effect on the phase diagram of PEG–PLGA–PEG triblock copolymer aqueous solutions: (●) $EG_{17}-(L_{26}G_7)-EG_{17}$; (○) $EG_{12}-(L_{26}G_7)-EG_{12}$. The legend in the graph indicates molecular weight of constituting block.

Effect of the Solvent

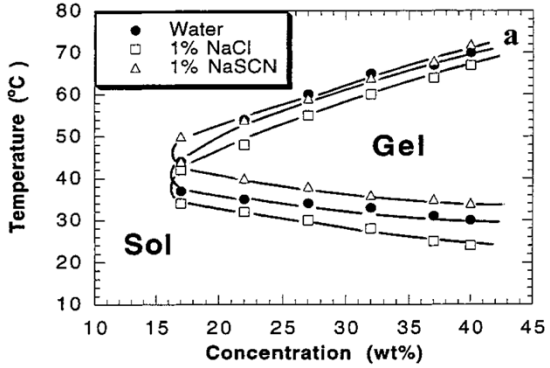

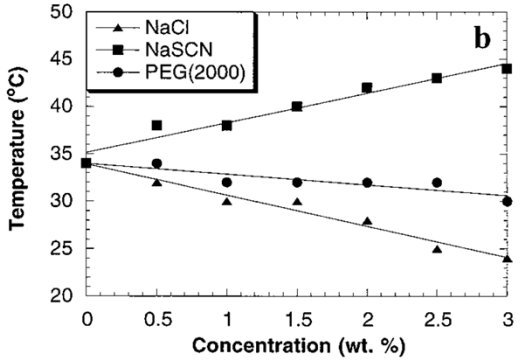

Figure 10. Additive effects on the phase transition of 27 wt % $EG_{12}-(L_{31}G_9)-EG_{12}$ triblock copolymer aqueous solutions: (a) salt effect; (b) concentration effects of NaCl, NaSCN, and PEG 2000.

Jeong 1999, Thermoreversible gelation of PEG-PLGA-PEG triblock copolymer aqueous solutions

Hofmeister Series

$CO_3^{2-} > SO_4^{2-} > S_2O_3^{2-} > H_2PO_4^- > F^- > Cl^- > Br^- > NO_3^- > I^- > ClO_4^- > SCN^-$

$N(CH_3)_4^+ > NH_4^+ > Cs^+ > Rb^+ > K^+ > Na^+ > Li^+ > Ca^{2+} > Mg^{2+} > Zn^{2+} > Ba^{2+}$

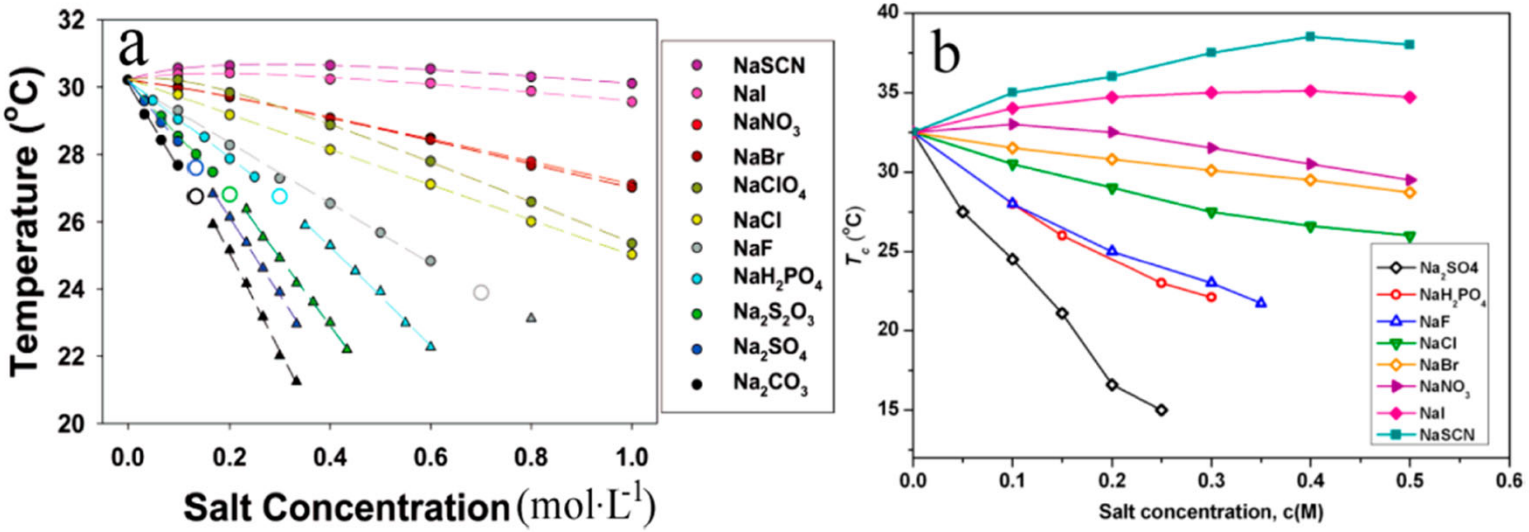

Figure 3. (a) **LCST** values of PNIPAM determined in the presence of sodium salts at different concentrations (0 to 1.0 M). The dashed lines are curve fits to the data calculated from eq 1.

(b) Change of the cloud point (T_c) of 10 g·L^{-1} HIPS solutions with the concentration of different sodium salts.

As shown in Figure 3, the ability of anions to decrease the LCST agrees with the HS sequence. The salting-out anions present a linear relationship at low salt concentration. When the concentration reaches a certain value, a two-step transition is observed, and the phase transition point is plotted. While for the chaotropic species such as $ClO4^-$ and SCN^-, the effect of anions on the LCST is nonlinear. In Figure 3a, the data calculated from eq 1 are shown with dashed lines. The experimental data coincide with the theoretical calculation. The values of c, B_{max}, and KA also fit the experimental data. Zhang et al. synthesized a novel thermoresponsive polymer, 2-hydroxy-3-isopropoxypropyl starches (HIPS), and studied the influence of sodium salts on its clou point (T_c). In the presence of kosmotropic salts, the hydrogen bonding between polymer and water would be destroyed; meanwhile, some water molecules released from the polymer chains, resulting in a reduction of polymer solubility and a dropping of T_c. On the contrary, chaotropic anions would increase the solubility of polymer and elevate the T_c with concentration, owing to the direct binding to polymer chains. At larger chaotrope concentrations, the T_c goes over a peak and then drops, due to the main driving force of hydrogen bonding between polymer and water, as shown in Figure 3b.

Kang 2020, Hofmeister Series- Insights of ion specificity from amphiphilic assembly and interface property

Thermo-Sensitive Hydrogels Induced by Divalent Counterions

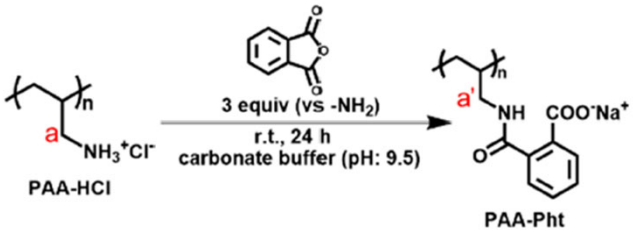

Scheme 1. Thermoresponsiveness of Carboxylated Polyallylamine (PAA) Induced by Divalent Counterions

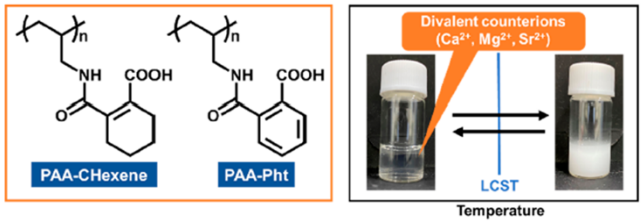

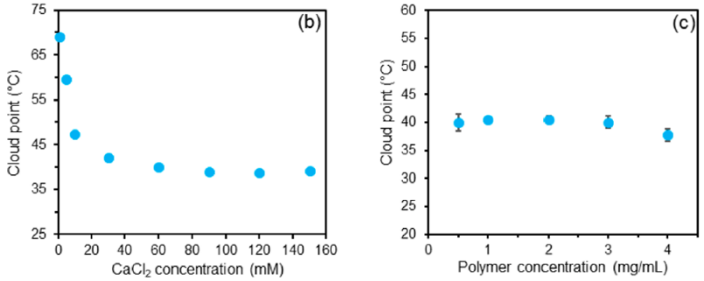

Figure 2. Plots of cloud points against $CaCl_2$ concentration (b) and polymer concentration (c) (pH 5.2, 150 mM $CaCl_2$ aq).

PAA-HCl was dissolved in carbonate buffer (pH 9.5) (2.5 mg/mL), and the pH was adjusted to 9.5 by using a 1 M sodium hydroxide aqueous solution.

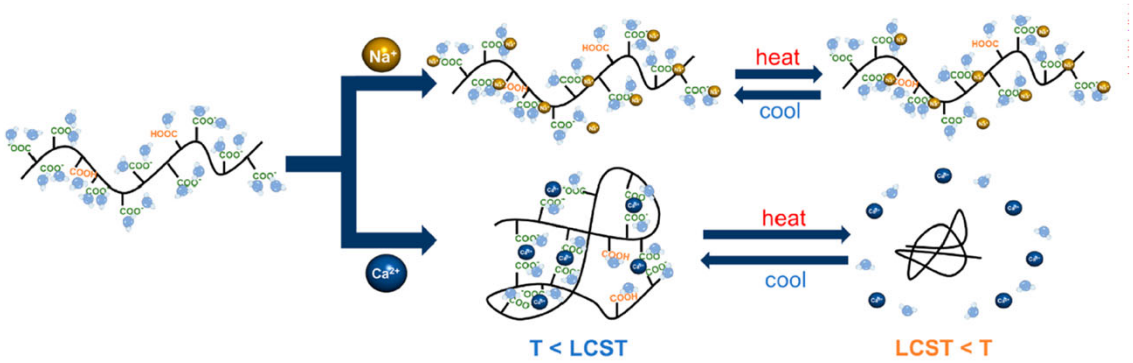

Figure 3. Schematic image of the thermoresponsive mechanism of PAA-Pht with divalent counterions.

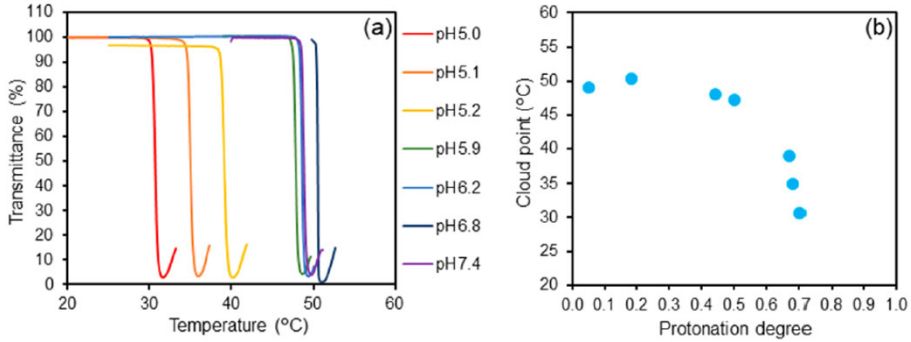

Figure 4. Changes in the transmittance of PAA-Pht in an acidic solution with $CaCl_2$ (150 mM) (pH 5.0, 5.1, 5.2, 5.9, 6.2, 6.8, and 7.4; 4.0 mg/mL) (a). Plots of cloud points against protonation degrees (b). The protonation degrees were determined by acid-base titration (Figure S1).

Emoto 2022, Thermoresponsiveness of carboxylated polyallylamines induced by divalent counterions as ionic effectors

Thermo-Sensitive Hydrogels for Batteries

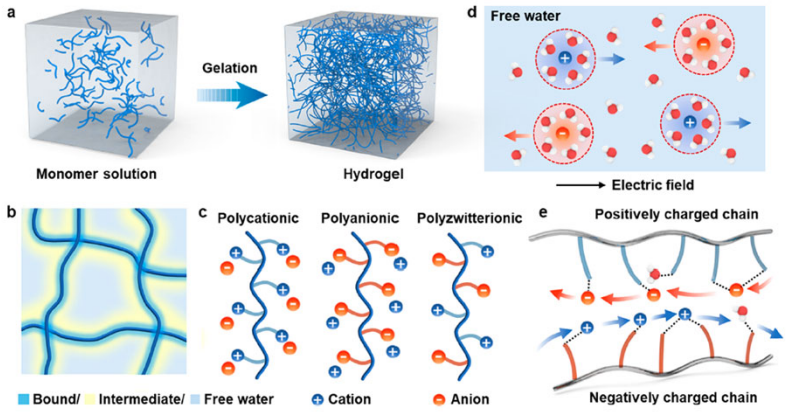

Figure 1. Hydrogel formation and basic properties. (a) Polymer networks cross-linking from monomers. (b) Water states in the hydrogel. (c) Polyionic hydrogel chains. (d) Diffusion of solvated ions in free water. (e) Interaction of ions with polyionic polymer chains.

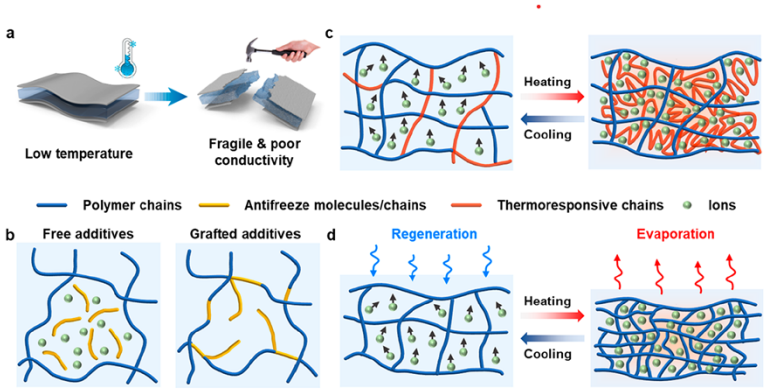

Figure 3. Temperature adaptability of aqueous batteries enabled by hydrogels. (a) Performance deterioration due to freezing of aqueous electrolyte at low temperatures. (b) Antifreezing by introducing additives to hydrogel. (c) Phase transition of hydrogel electrolyte that regulates the migration of ions. (d) Reversible water evaporation and regeneration in hygroscopic hydrogel electrolyte.

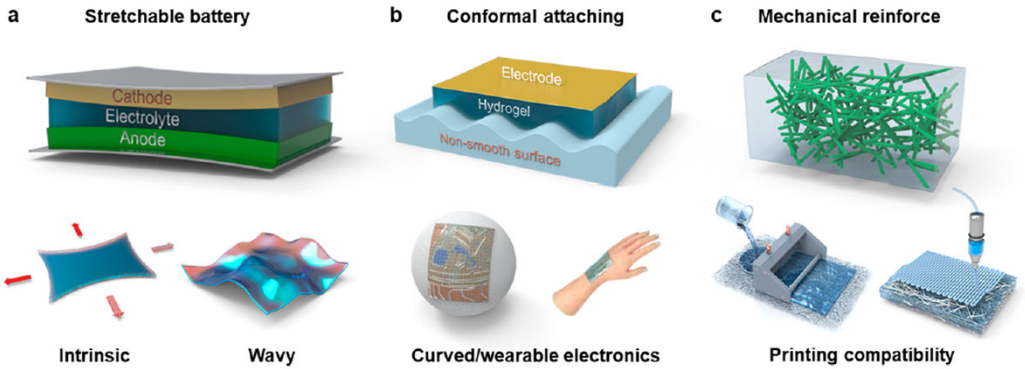

Figure 4. Mechanical regulation of batteries with hydrogel electrolytes. (a) Stretchable battery enabled by wavy structures. (b) Conformal design for structural batteries and wearable electronics. (c) Schematic of framework-reinforced hydrogel electrolyte

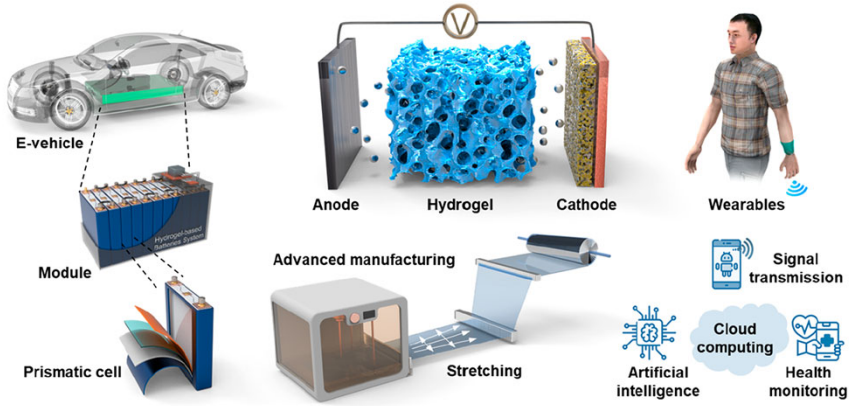

Figure 5. Perspective of hydrogels for future smart batteries

Yang 2022, Hydrogels enable future smart batteries

pH-Sensitive Systems

Intelligent Gels

Soft aggregations of long-chain molecules can shrink or swell in response to stimuli. They may form the basis of a new kind of machine. Yoshihito Osada and Simon B. Ross-Murphy. Scientific American. May 1993, p. 83)

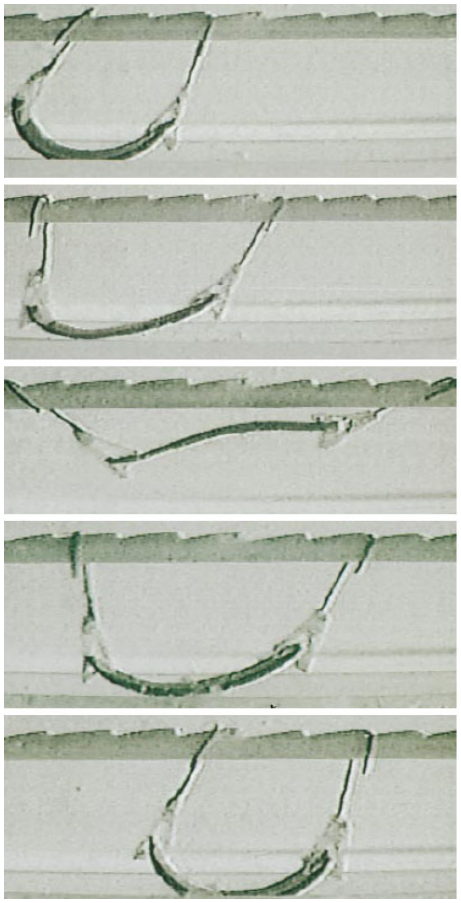

Gel Looper, and inchwormlike device that moves by repeatedly curling and straightening itself, was developed by Osada. Surfactant molecules in the liquid surrounding the looper collect on the gel's top surface under the influence of an electric field, causing the gel to shrink. When the polarity of the electric field is changed, the surfactant goes back into the solution.

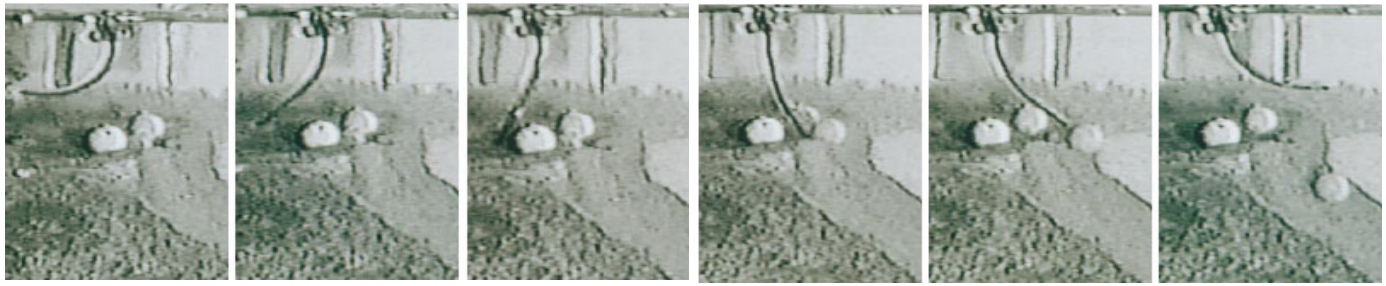

Gel Golf demonstrates the ability of an intelligent gel to act on its surroundings. A strip of gel made of the same material as the gel looper curls first one way and then the other under the influence of an electric field. During this transition, it strikes a gold ball, propelling it down a slope. Although the "club" material is sturdy enough to strike a ball directly, it must be submerged in liquid and so an actual use would probably be encases in a protective container.

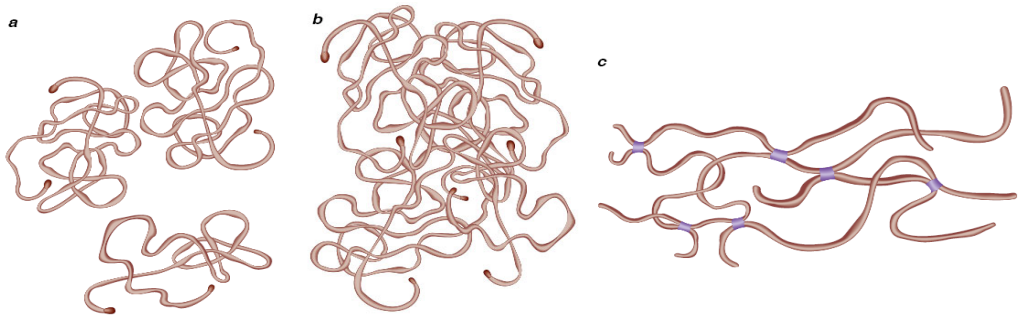

Long-chain molecules cause a solution to become viscous (a) because they interfere with one another as the solution flows. As their concentration increases, the molecules become entangled, yielding viscoelastic behavior that partakes of both solid and liquid traits (b). If the intertwined molecules bond with one another, the result is a gel (c)

pH-Sensitive Polymers (Polyelectrolytes)

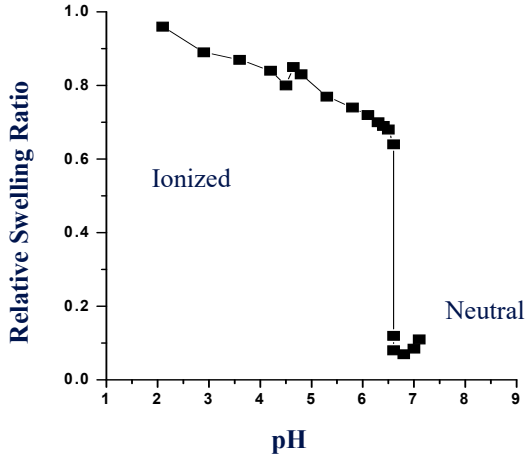

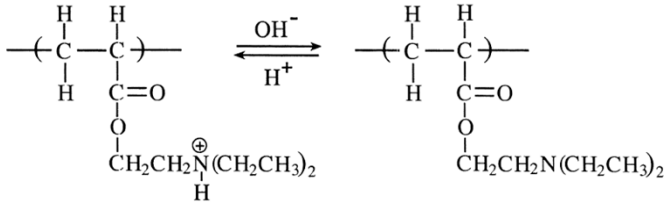

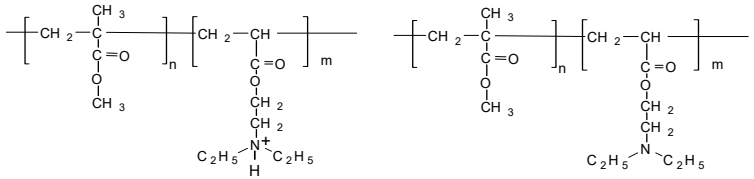

	Monomer	pH-sensitive group
Acidic (Anionic)	(Meth)acrylic acid	-COOH
	Sodium styrene sulfonate	$-SO_3^-$ Na^+
	Sulfoxyethyl methacrylate	$-SO_3H$
Basic (Cationic)	Aminoethyl (meth)acrylate	$-NH_2$
	N,N-dimethylaminoethyl (meth)acrylate	$-N(CH_3)_2$
	N,N-diethylaminoethyl (meth)acrylate	$-N(CH_2CH_3)_2$
	Vinylpyridine	
	Vinylbenzyl triethylammonium chloride	$-N^+(CH_3)_3Cl^-$

Brondsted and Kopecek, ACS Symp. Ser. 480, pp. 285-304 (1992)

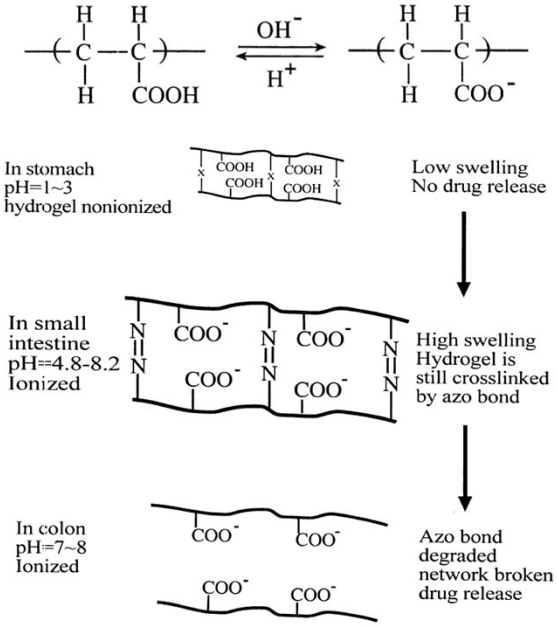

Fig. 5. Schematic illustration of oral colon-specific drug delivery using biodegradable and pH-sensitive hydrogels. The azoaromatic moieties in the cross-links are designated by –N=N–; from Ref. [62].

pH-Sensitive Polymers for Controlled Insulin Release

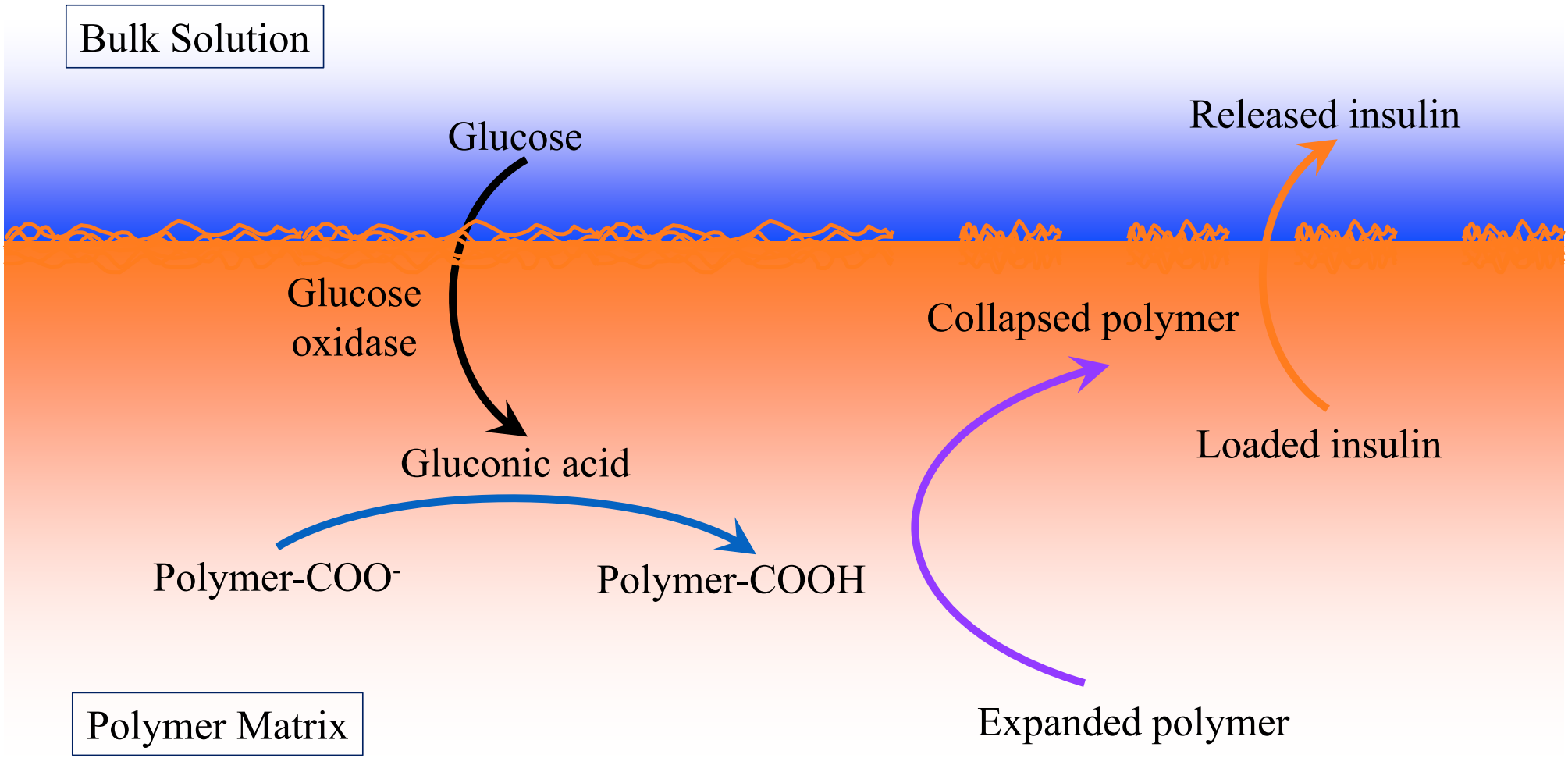

pH-Activatable Polymeric Prodrugs

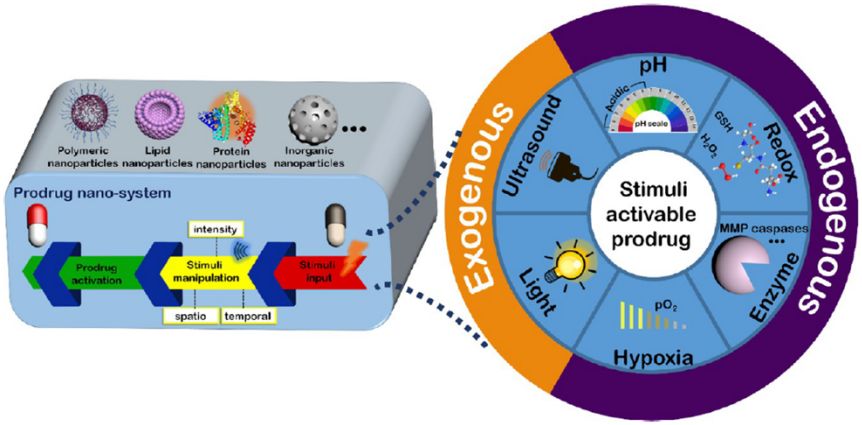

Scheme 1. Schematic illustration of stimuli-responsive activation process of prodrug nanosystems and various kinds of stimuli for prodrug activation

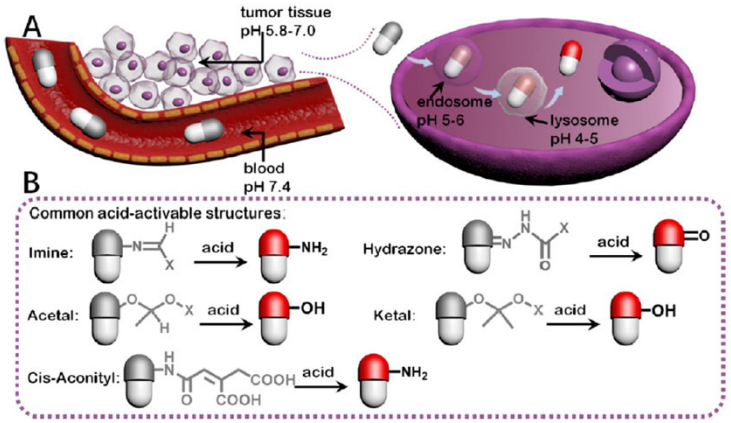

Scheme 2. (A) pH Values in blood, tumor microenvironment, endosome, and lysosome and (B) Representative acid-activable chemical structures

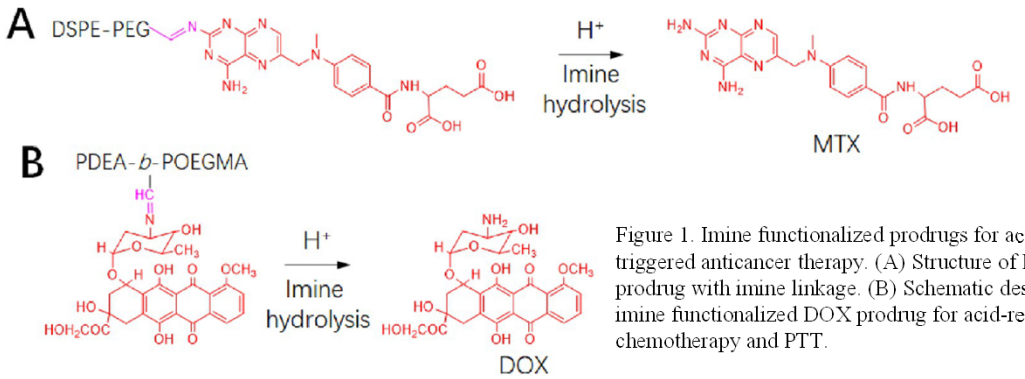

Figure 1. Imine functionalized prodrugs for acid-triggered anticancer therapy. (A) Structure of MTX prodrug with imine linkage. (B) Schematic design of imine functionalized DOX prodrug for acid-responsive chemotherapy and PTT.

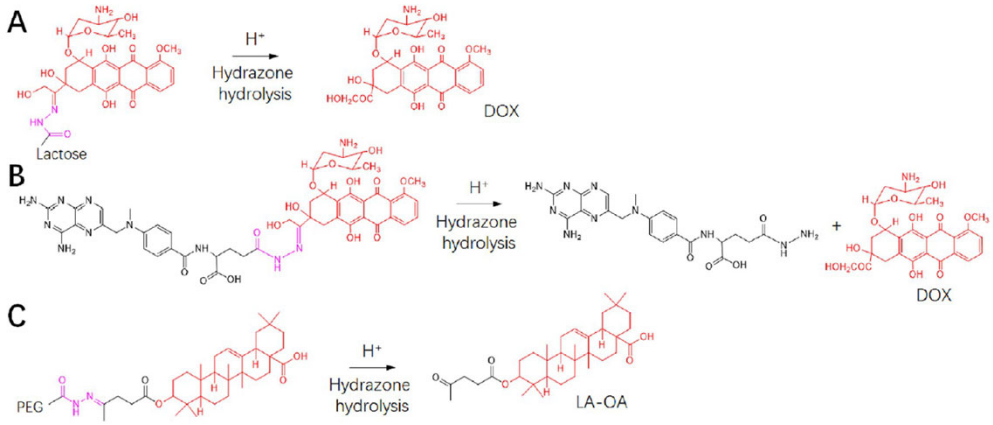

Figure 2. Prodrugs containing hydrazone linkage for acid-responsive activation. (A) Structure of DOX−lactose conjugated amphiphilic prodrug and working mechanism of the acid-triggered activation. (B) Hydrazone-based MTX−DOX prodrug and action mechanism of acid-responsive activation for cancer therapy. (C) Hydrazone functionalized PEG−OA macromolecule and schematic illustration of pH-induced OA activation

Ding 2022, Emerging strategies in stimuli-responsive prodrug nanosystems for cancer therapy

pH-Sensitive Polymers

Molecular structure of polyethylenimine and aldehydes

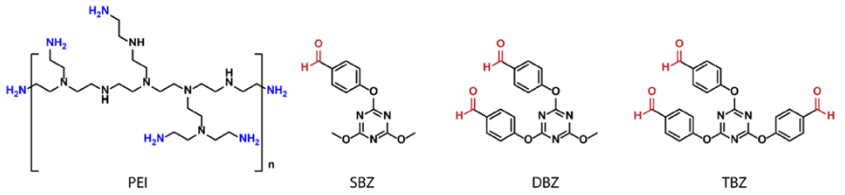

Schiff base reaction between polyethylenimine and aldehydes

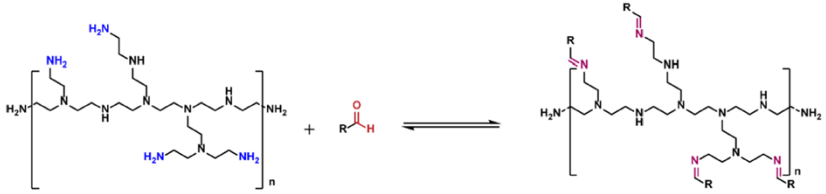

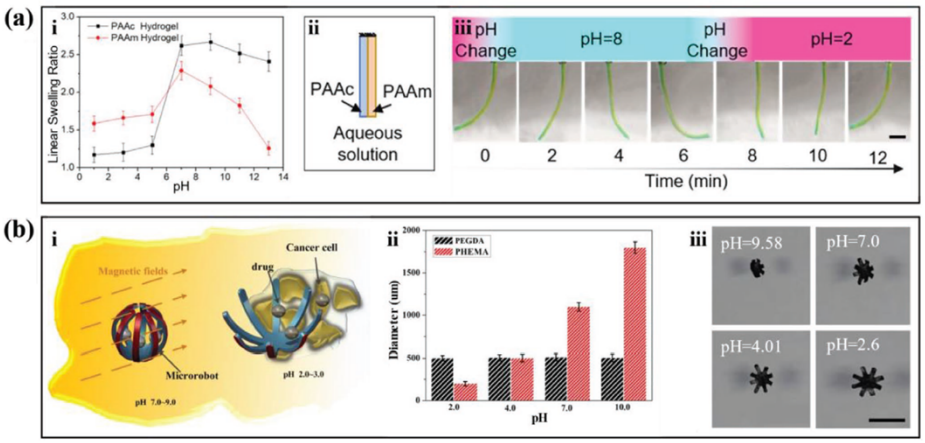

Figure 7. a-i) The swelling ratio of the poly(acrylic acid) (PAAc) hydrogel and the polyacrylamide (PAAm) hydrogel as a function of pH value; a-ii) schematic diagram of the PAAc-PAAm bilayer hydrogel; a-iii) a series of images of the bilayer actuator under different pH value conditions. Scale bar is 2 cm. b-i)Schematic diagram of the working mechanism of the soft actuator, which could move by the magnetic field and perform drug carrying and release by folding/unfolding motions triggered by different pH values; b-ii) a histogram of the expansion ratio of circular polyethylene glycol diacrylate (PEGDA) and poly(2-hydroxyethyl methacrylate) (PHEMA) hydrogels; b-iii) the folding/unfolding motions of the smart film actuators (SFAs) under different pH values. Scale bar is 3 mm.

Zhang 2022, Smart film activators for biomedical applications

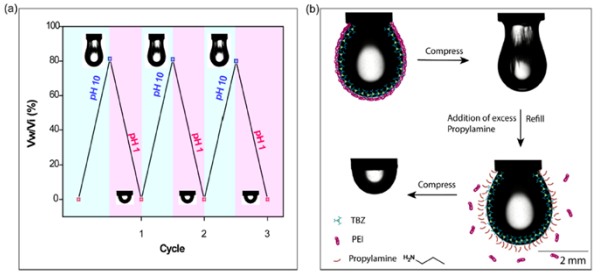

Figure 4. Representation of (a) pH-dependent reversible assembly and disassembly of a droplet by adding an acid/base. Surface coverage was noted after aging the droplet for 200 s. (b) Imine exchange at the PEI/TBZ cross-linked interface with a primary amine, propylamine (concentrations were 1% w/w for PEI, 1.0 mg/mL for TBZ, 5% w/w for propylamine).

After studying the pH-dependent interfacial activity of the TBZ and PEI pair, we explored the reversible and dynamic nature of imine bond formation that would pave the way for numerous stimuli-responsive systems. For this study, the pH of the system was switched from acidic (pH 1) to basic (pH 10), and the resultant interfacial jamming to unjamming transition was noted. Initially, the experiment was conducted at an acidic pH, and once the equilibrium interfacial tension was attained, the volume of the droplet was reduced to examine the wrinkle formation. As previously observed, at an acidic pH, the imine bond formation did not occur, and no wrinkles were observed. Next, the pH of the aqueous solution was adjusted to pH 10 by adding NaOH to the solution. The interfacial jamming was observed, and the surface coverage was 81% as observed earlier. When HCl was added to alter the pH of the system to pH 1, the preformed wrinkles disappeared. Even after compressing the droplet to its minimum volume, there was no evidence of wrinkle formation.

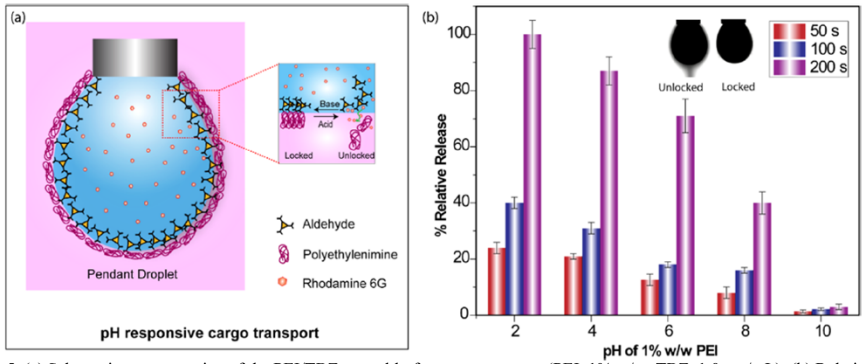

Figure 5. (a) Schematic representation of the PEI/TBZ assembly for cargo transport (PEI, 1% w/w; TBZ, 1.0 mg/mL). (b) Relative release of Rh6G at different pH values of PEI for 50, 100, and 200 s, taken at 530 nm. The inset picture shows the unlocked and locked states of the droplet.

Agashe 2022, Anisotropic compartmentalization of the liquid–liquid interface using dynamic imine chemistry

pH- & Temperature-Sensitive Polymers

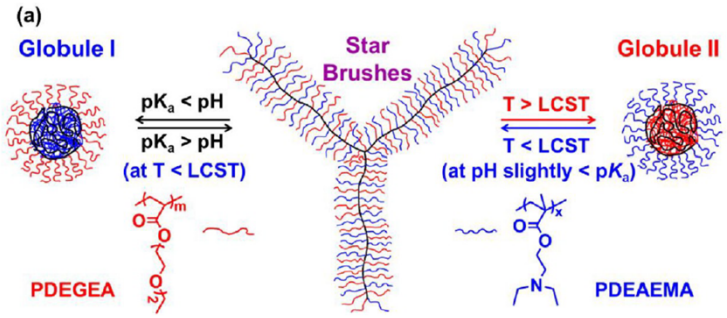

Figure 6. Stimuli-induced star−globule shape transitions of a three-arm star-shaped binary heterografted BBP composed of PDEGEA and PDEAEMA side chains (SBB-TP). (a) Schematic illustration of pH-induced and thermally induced star−globule shape transitions of SBB-TP.

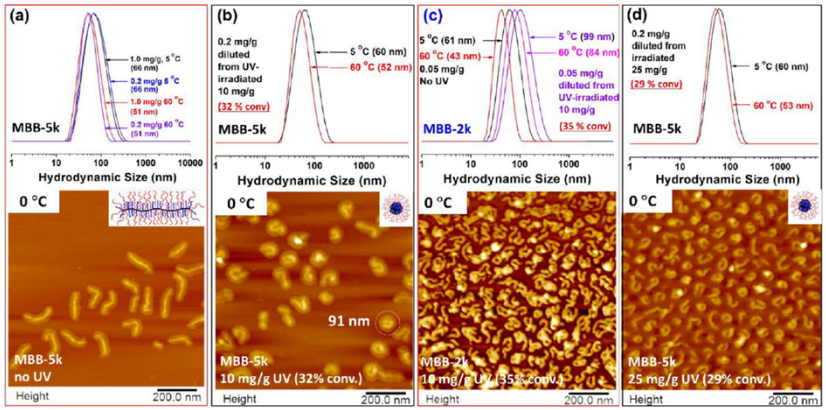

Figure 7. DLS data and AFM images on bare mica for BBP-5k and -2k: (a) nonirradiated BBP-5k; (b−d) diluted from the 10 mg/g BBP-5k solution (b), 10 mg/g MBB-2k solution (c), and 25 mg/g BBP-5k solution (d) after UV irradiation. BBP-5k: Nbb = 707, DPPEO = 114, DP = 43 for the thermoresponsive UV-cross-linkable polymer, σSC = 87.6%. BBP-2k: DPPEO = 45, σSC = 82.7%. The molar ratio of PEO to thermoresponsive UV-crosslinkable polymer in both BBPs was 0.52:0.48.

Zhao 2021, Shape-changing bottlebrush polymers

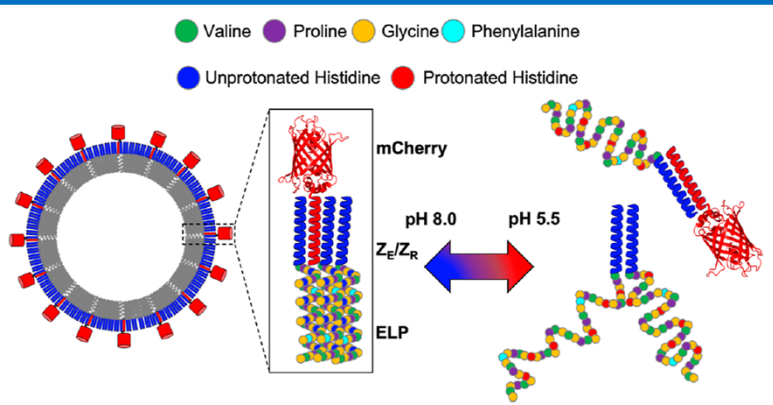

Figure 1. Schematic of the proposed vesicle disassembly caused by the protonation of histidine in acidic environments. The ELP shown representsH15- ZR-ELP, but only shows 10 of the 25 total pentapeptide repeats for simplicity.

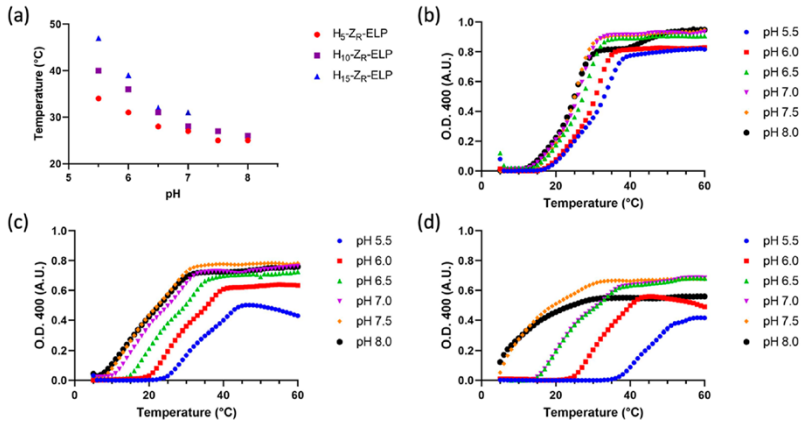

Figure 2. Transition temperature of 30 μMH5-ZR-ELP, H10-ZR-ELP, and H15-ZR-ELP in aqueous solutions containing 1.5 μMmCherry-ZE (0.05 ZE/ ZR ratio), 0.5M NaCl, and either 10 mM sodium phosphate or sodium succinate depending on the pH of the solution. (a) Transition temperature of each ZR-ELP variant as a function of pH. (b) Representative turbidity vs temperature profiles of H5-ZR-ELP, (c) H10-ZR-ELP, and (d) H15-ZR-ELP at pH between 5.5 and 8.0.

Dautel 2022, Protein vesicles with pH-responsive disassembly

Ligand-Sensitive Systems

Glucose Sensitive Systems

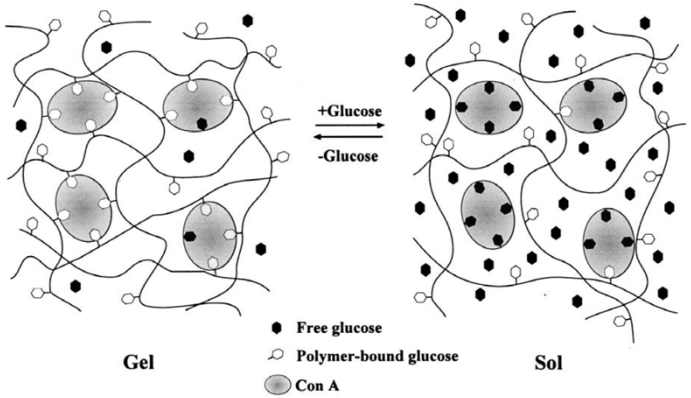

Fig. 6. Sol–gel phase-transition of a glucose-sensitive hydrogel. Large circles represent Con A, a glucose-binding protein. Small open and closed hexagons represent polymer-attached glucose and free glucose, respectively.

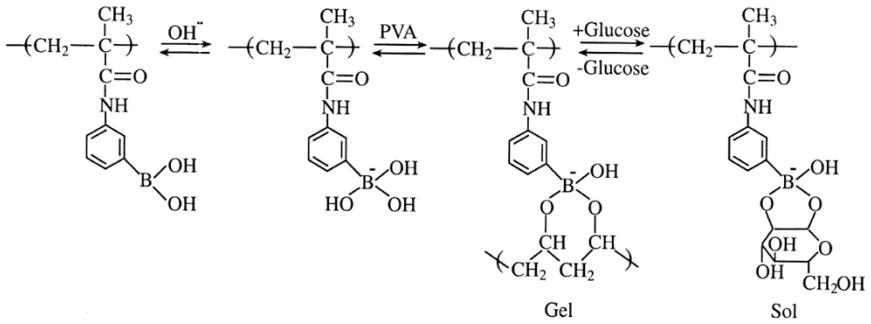

Fig. 7. Sol–gel phase-transition of a phenylborate polymer. At alkaline pH, phenylborate polymer interacts with poly(vinyl alcohol) (PVA) to form a gel. Glucose replaces PVA to induce a transition from the gel to the sol phase.

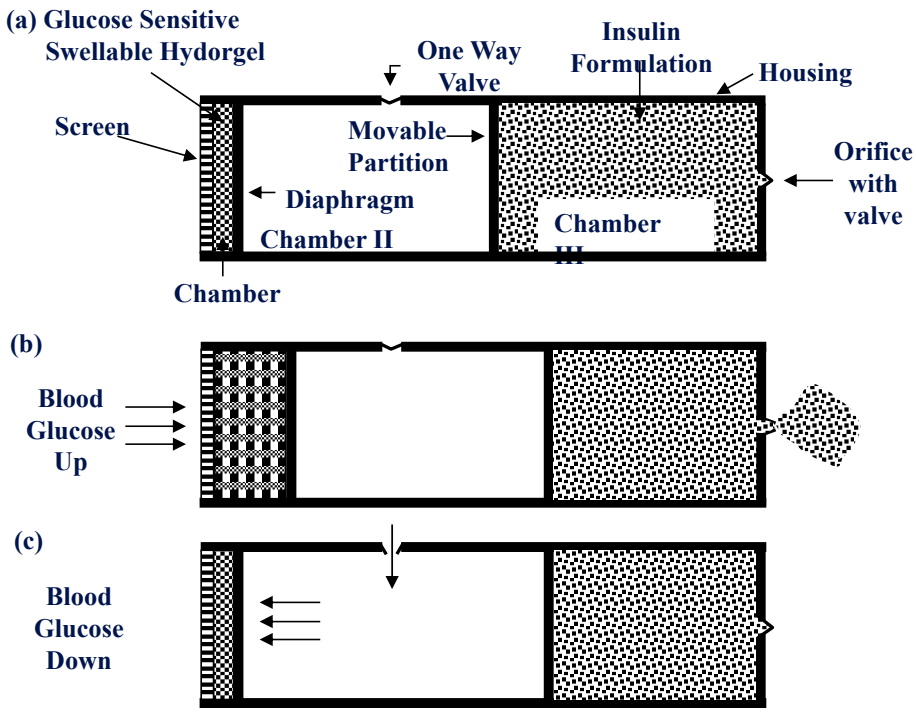

Kinetics
Reproducibility

Qiu 2001, Environment-sensitive hydrogels for drug delivery

Glucose Sensitive Systems

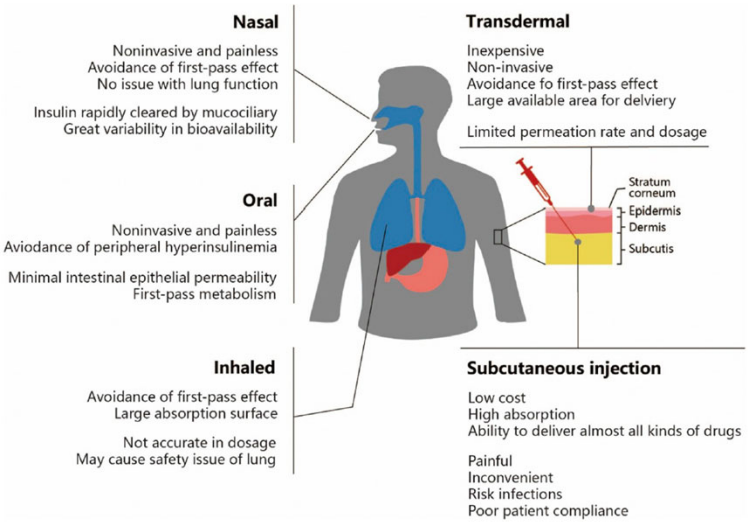

Fig. 3. The advantages and drawbacks of different insulin administrations.

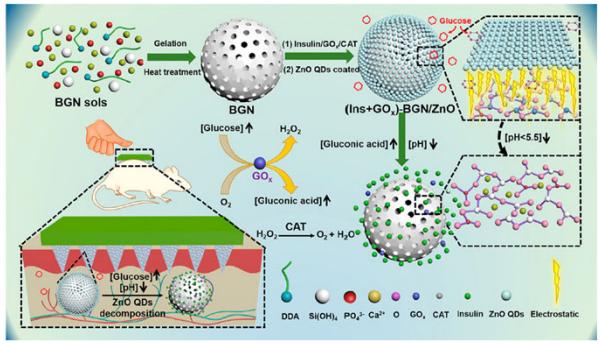

Fig. 31. Preparation of glucose-responsive microneedles integrated with ZnO quantum-dot-capped MBGs for transdermal delivery of insulin.

Shen 2020, Recent progress in design and preparation of glucose-responsive insulin delivery systems

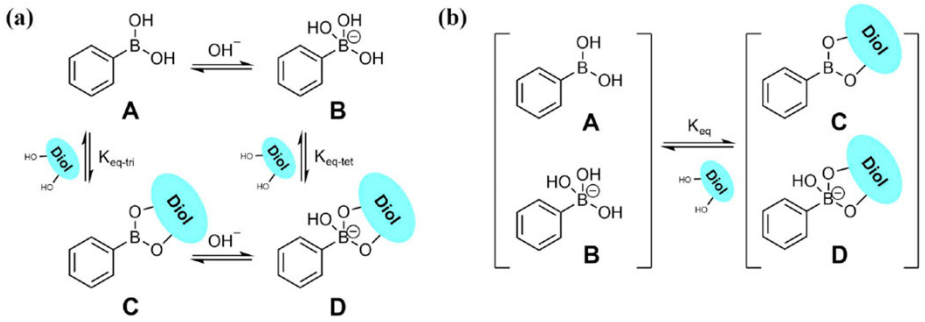

Fig. 4. (a) The equilibrium between charged and uncharged phenylboronic acid and their esters. (b) The equilibrium between phenylboronic acids and their esters. $K_{eq\text{-}tri}$, $K_{eq\text{-}tet}$ and K_{eq} are all equilibrium constants and K_{eq} is named as overall association constant

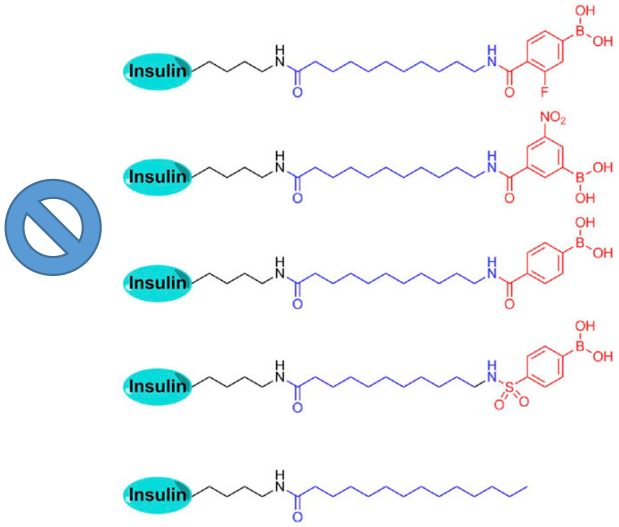

Fig. 17. The structures of aliphatic PBA-modified insulins and the aliphatic insulin [119].

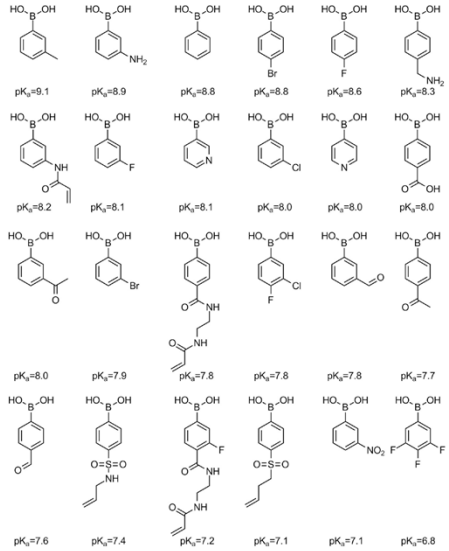

Fig. 7. The pK_a values of PBA and PBA derivatives [64,65,69–71].

Self-Regulated Systems

Changes in Environmental Factors

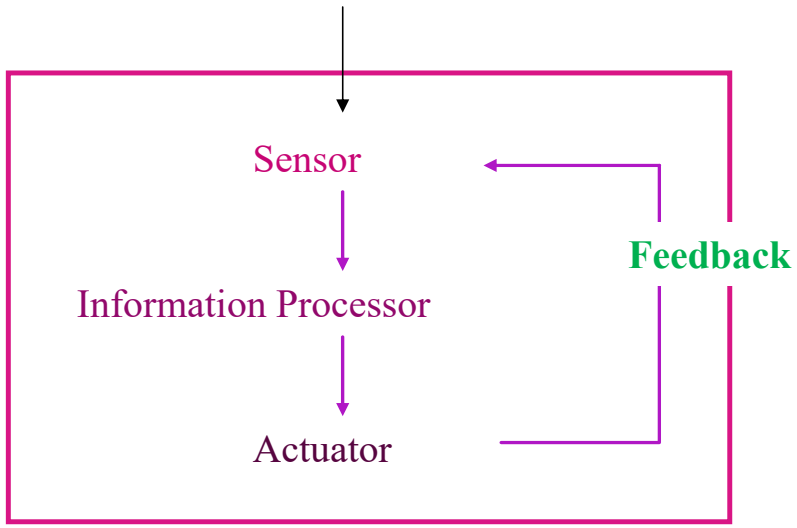

Glucose level changes in blood

Glucose sensor

Determine the amount of insulin to be released

Insulin release

Feedback: Stop insulin release

Specificity, sensitivity
Speed

Accurate dose

Accurate timing

Reversibility
Repeatability
Magnitude

Safety
Biodegradability

Open-loop system

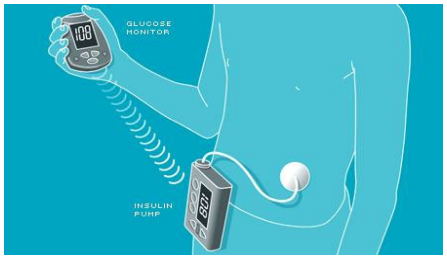

Closed-loop system

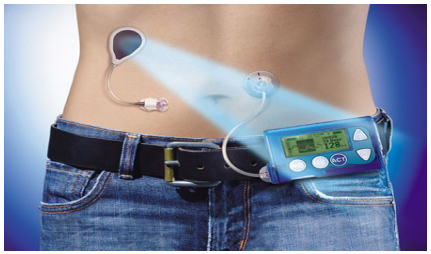

Ligand-Triggered Nanoarchitectures

ABSTRACT: The design of simple and versatile synthetic routes to accomplish triggered-release properties in carriers is of particular interest for drug delivery purposes. In this context, the programmability and adaptability of DNA nanoarchitectures in combination with liposomes have great potential to render biocompatible hybrid carriers for triggered cargo release. We present an approach to form a DNA mesh on large unilamellar liposomes incorporating a stimuli-responsive DNA building block. Upon incubation with a single-stranded DNA trigger sequence, a hairpin closes, and the DNA building block is allowed to self-contract. We demonstrate the actuation of this building block by single-molecule Förster resonance energy transfer (FRET), fluorescence recovery after photobleaching, and fluorescence quenching measurements. By triggering this process, we demonstrate the elevated release of the dye calcein from the DNA–liposome hybrid carriers. Interestingly, the incubation of the doxorubicin-laden active hybrid carrier with HEK293T cells suggests increased cytotoxicity relative to a control carrier without the triggered-release mechanism. In the future, the trigger could be provided by peritumoral nucleic acid sequences and lead to site-selective release of encapsulated chemotherapeutics.

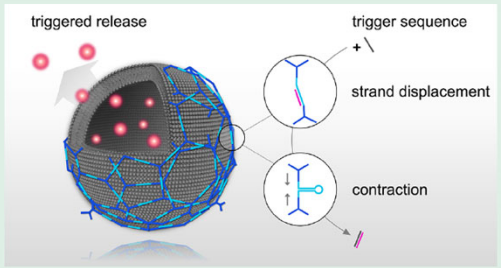

KEYWORDS: *DNA nanotechnology, biomimetics, liposome, triggered release, drug delivery*

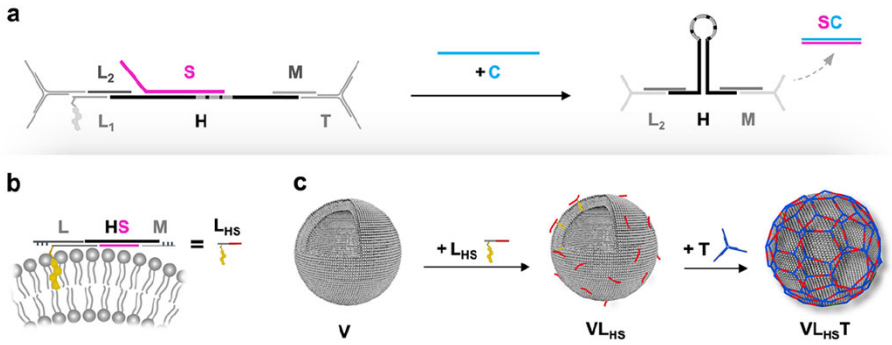

Figure 1. Assembly principle of the active DNA building block and the trigger-responsive DNA–liposomal hybrid nanocarrier. (a) Trigger mechanism of the aDBB. The building block comprises a hairpin H and a preannealed, partially complementary sequence S. Mediated by a toehold at the 5′-terminal of S, a complementary trigger strand C hybridizes with S, allowing H to close. This leads to a contraction of the two opposite ends. (b) The aDBB is first annealed with a cholesterol-TEG-modified linker L (composed of L_2 and the cholesterol-TEG-labeled L_1) and a connecting strand M, to render L_{HS}. (c) L_{HS} is incubated with large unilamellar POPC vesicles (V) and is anchored to the lipid membranes via the cholesterol-TEG modification (rendering VL_{HS}). This allows for polymerization of a triskelion T, which is added in the subsequent step on the surface of the vesicles and hybridizes with M and L_1 (resulting in the final structure $VL_{HS}T$).

Baumann 2022, DNA–liposome hybrid carriers for triggered cargo release

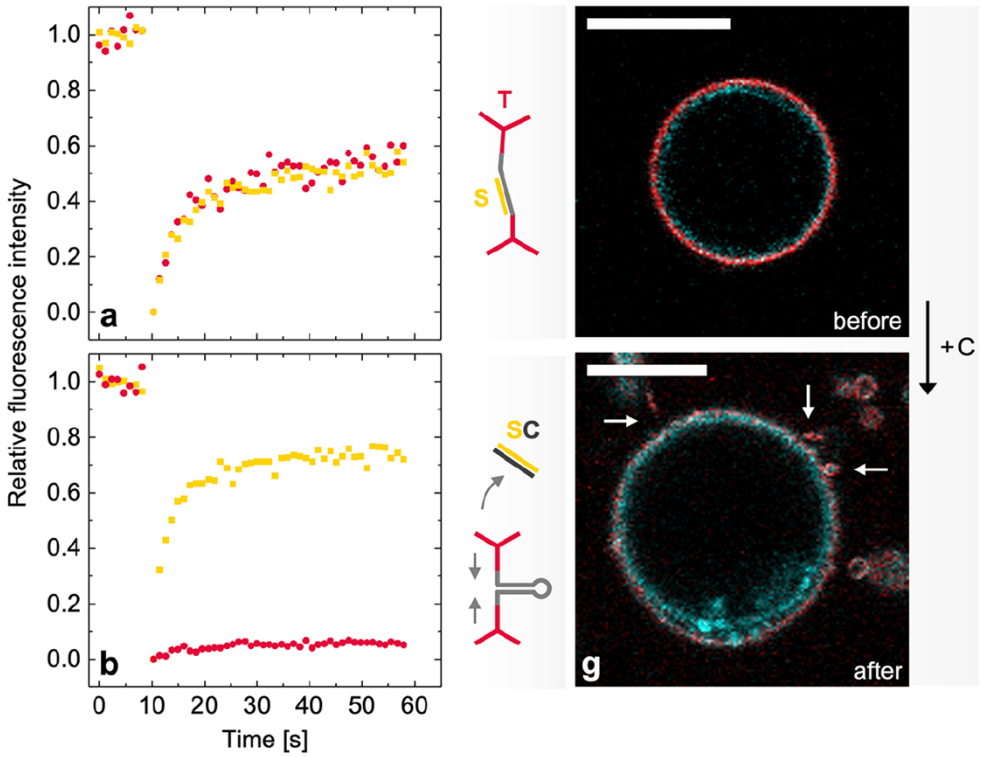

Figure 4. Characterization of DNA-coated GUVs by confocal microscopy and FRAP. (a) Representative FRAP traces recorded on GUVs before the addition of C. S was labeled with ATTO550 (yellow data), and T was labeled with ATTO647N (red data). Both species exhibit similar fluorescence recovery dynamics (described by the recovered fluorescence intensities and recovery halftimes obtained from exponential fitting curves, n = 8). (b) After the addition of C, the fluorescence recovery kinetics of S and T split into two populations: S is characterized by increased mobility, while T remains mostly static. (g) In the presence of a hyperosmotic pressure, visible deformation and tubulation (see arrows) of the coated GUVs could be observed after the displacement of S had been performed (cyan: NBD-labeled PC lipids, red: ATTO647N-labeled T). Scale bars: 10 μm.

Shape Memory Polymers

Important Aspects of Shape Memory Polymer Systems

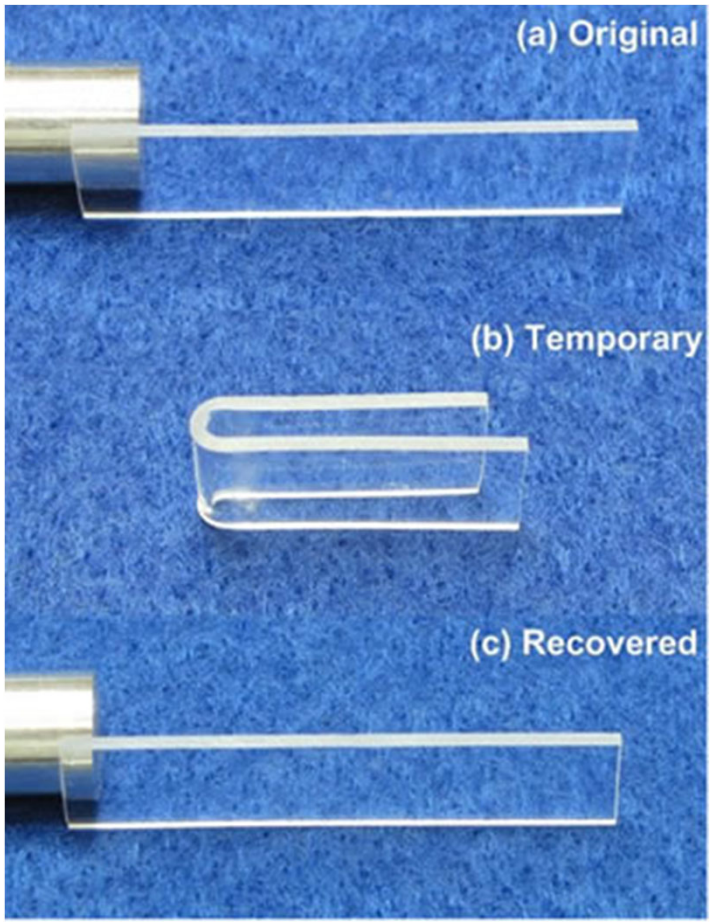

Shape memory polymers have 2 key identifying features

Shape fixity
Shape recovery

Shape fixity allows the material to maintain a temporary shape after molding

Shape recovery allows the material to return to the original shape of the material

Polymer Origami

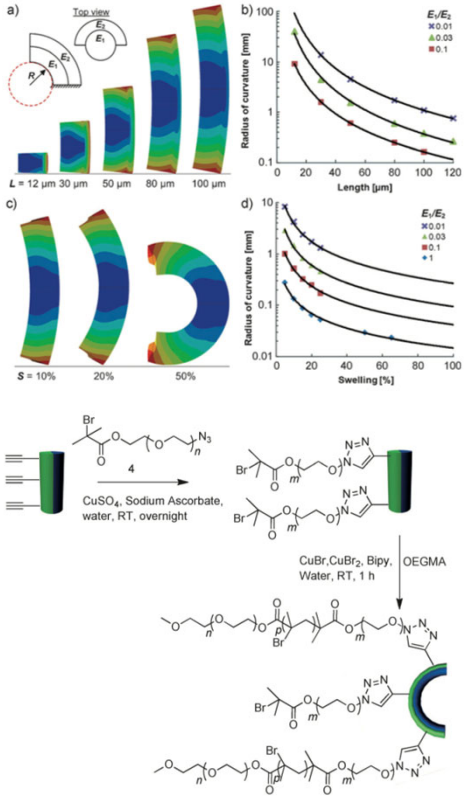

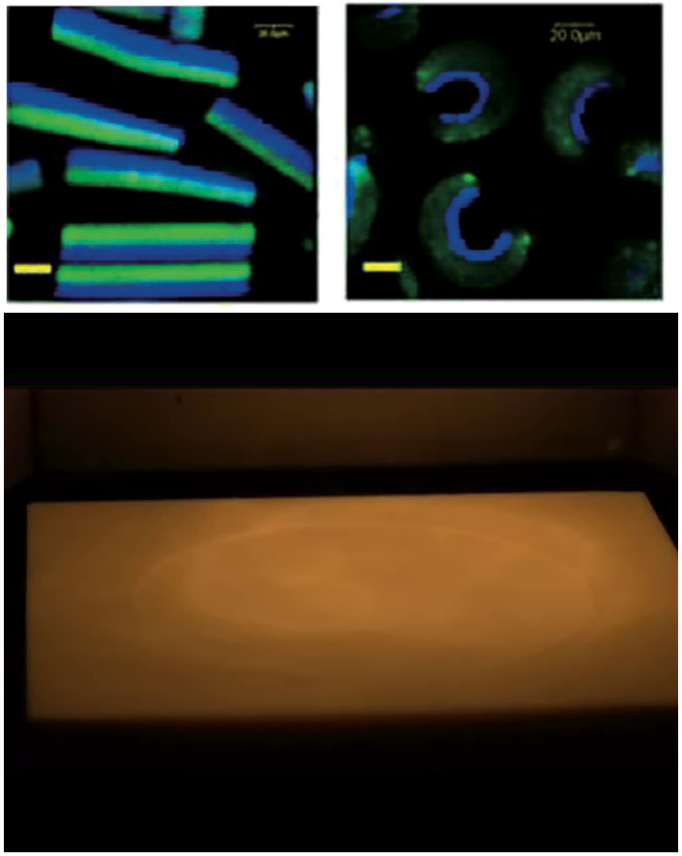

Stimulus allows for folding of a polymer into predefined shape in response to an external stimulus.

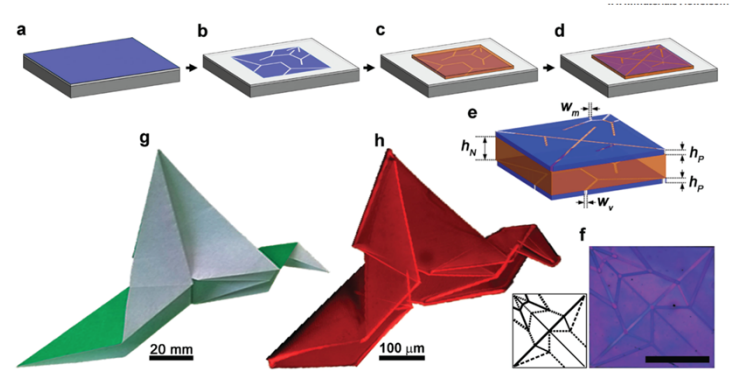

Figure 1. Fabrication of self-folding polymer origami. a) A thin layer of a photo-crosslinkable glassy polymer (PpMS) on a substrate precoated with a sacrificial layer is b) photolithographically patterned with open stripes of width W_v to define the positions and angles of the valley folds. c) Next, a thicker layer of a photo-crosslinkable temperature-responsive polymer (PNIPAM) is coated on top and uniformly crosslinked over the entire area of the bottom PpMS sheet. d) Finally, a third layer of PpMS is coated and patterned with open stripes of width W_m to define the positions and angles of the mountain folds. e) A magnified schematic of the resulting trilayer film (dimensions not to scale), with h_N and h_P as the respective thicknesses of PNIPAM and PpMS layers. f) An optical image of a trilayer film patterned to fold into Randlett's flapping bird (scale bar: 400 μm), along with a schematic indicating the locations and widths of mountain (solid lines) and valley (dotted lines) folds. g) A photograph of Randlett's flapping bird folded using paper, h) alongside a fluorescence image of the self-folded trilayer film.

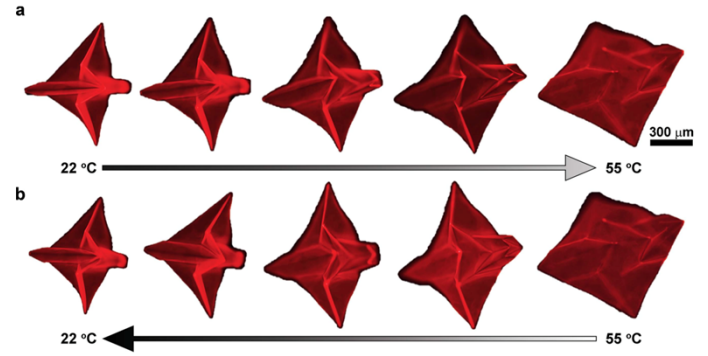

Figure 4. Thermal actuation of self-folding origami. a) When the temperature is increased, the hydrogel polymer layer deswells, causing the Randlett's bird to revert to an unfolded, nearly flat, shape by 55 °C. b) Upon cooling to 22 °C, reswelling back to the folded state occurs through a similar pathway. Dry thicknesses of h_P = 70 nm and h_N = 1.5 μm are used, while the size of the square sheet is 800 μm on a side.

Angew. Chem. Int. Ed. 2012, 51, 660 –665

Science Advances 08 Jan 2016: Vol. 2, no. 1, e1501297 DOI: 10.1126/sciadv.1501297

Adv. Mater. 2015, 27, 79–85

Shape Memory Polymers in Aerospace Applications

http://acadia.org/papers/2QPH7Y

Figure 6: The sequential recovery of a multimaterial flower.

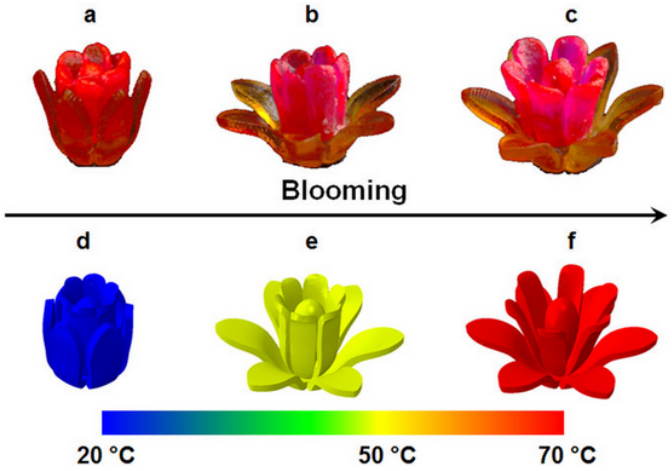

The multimaterial flower in the original shape (**c**) was first programmed into the temporary bud state at 20 °C (**a**). The outer petals opened first after heating to 50 °C (**b**) and then, the flower fully bloomed at 70 °C (**c**). (**d**)–(**f**) represent the FE simulations of the corresponding flower blooming process.

http://www.nature.com/articles/srep31110

Figure 5: 3D printed multimaterial grippers.

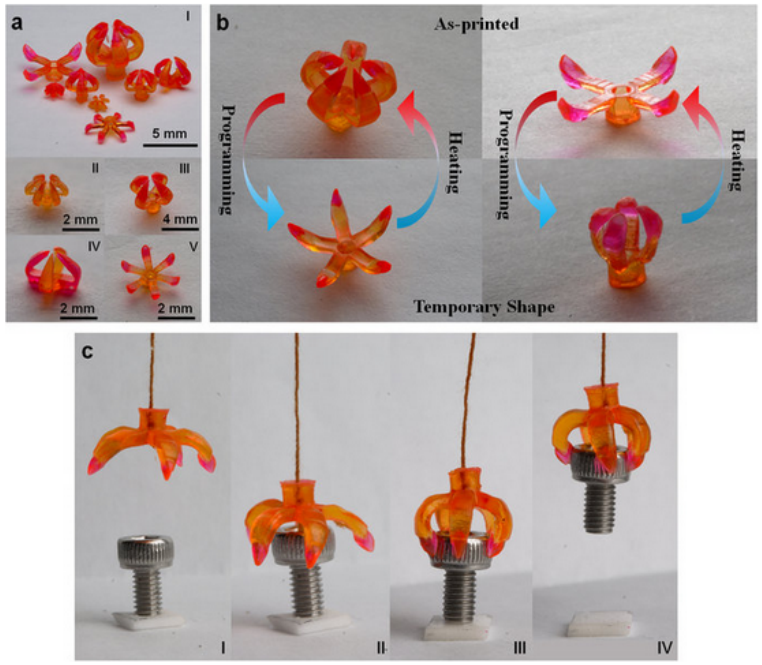

(**a**) Multimaterial grippers were fabricated with different designs. (**b**) The demonstration of the transition between as printed shape and temporary shape of multimaterial grippers. (**c**) The snapshots of the process of grabbing an object.

Shape Adaptive Multilayered Polymer Composite

Variable stiffness shape memory polymer triggered by both Joule heating and dielectric loss NASA's Langley Research Center has developed a novel shape memory polymer (SMP) made from composite materials for use in morphing structures. In response to an external stimulus such as a temperature change or an electric field, the thermosetting material changes shape, but then returns to its original form once conditions return to normal. Through a precise combination of monomers, conductive fillers, and elastic layers, the NASA polymer matrix can be triggered by two effects--Joule heating and dielectric loss--to increase the response. The new material remedies the limitations of other SMPs currently on the market--namely the slow stimulant response times, the strength inconsistencies, and the use of toxic epoxies that may complicate manufacturing. NASA has developed prototypes and now seeks a partner to license the technology for commercial applications.

Electroactive polymers (EAPs) are a type of flexible, elastic polymer (elastomer) that change size or shape (i.e., bend, contract or expand) when stimulated by an electric field. EAPs are generally categorized by their mode of activation: electronic or ionic. Electronic EAPs include electrostrictive elastomers and dielectric electroactive polymers (DEAPs), while an example of an ionic EAP is the ionic polymer metal composite (IPMC). In electronic EAPs, the electric field applies coulomb attractive forces to the electrodes. This causes the change in size and shape due to compressive forces. With ionic EAPs, the mobility and diffusion of ions changes the shape.

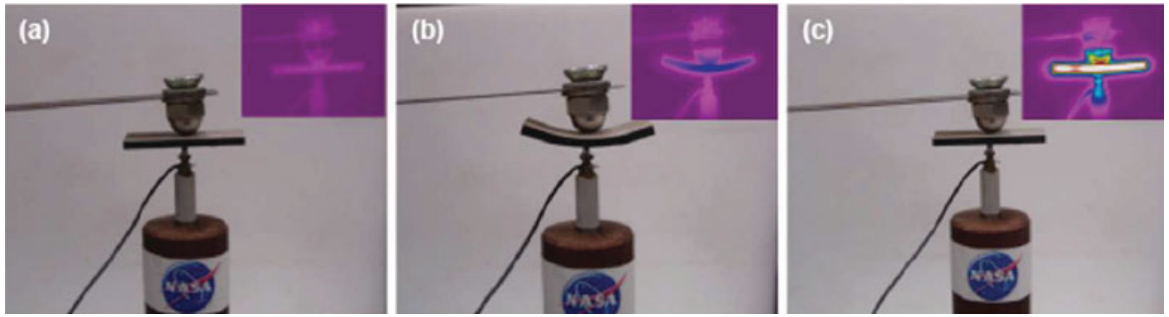

Electric field activated shape memory behavior of variable stiffness polymer composite (VSPc). (a) permanent shape, (b) programmed temporary shape, and (c) recovered permanent shape (inset: infrared images).

https://technology.nasa.gov/patent/LAR-TOPS-39
http://www.azom.com/article.aspx?ArticleID=13516

Stimuli-responsive Shape Memory Polymer Composites

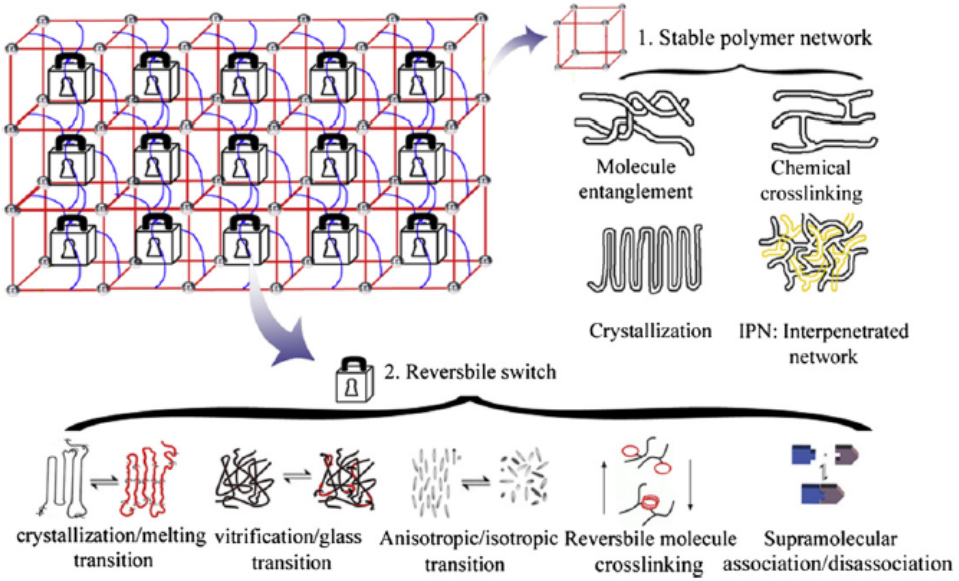

Fig. 1. Various molecular structures of SMPs. A stable network and a reversible switching transition are the prerequisites for the SMPs to show SME. The stable network can be molecule entanglement, chemical cross-linking, crystallization, and IPN; the reversible switching transition can be crystallization melting transition, vitrification-glass transition, anisotropic-isotropic transition, reversible chemical cross-linking, and associatione-disassociation of supramolecular structures

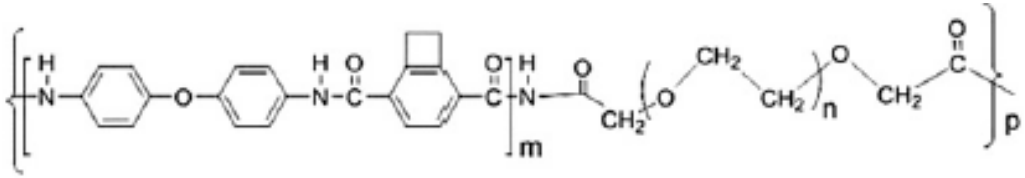

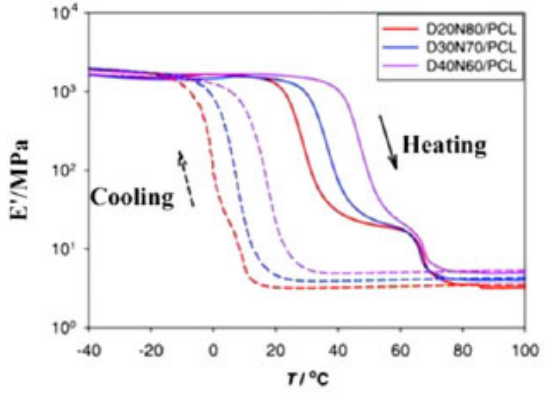

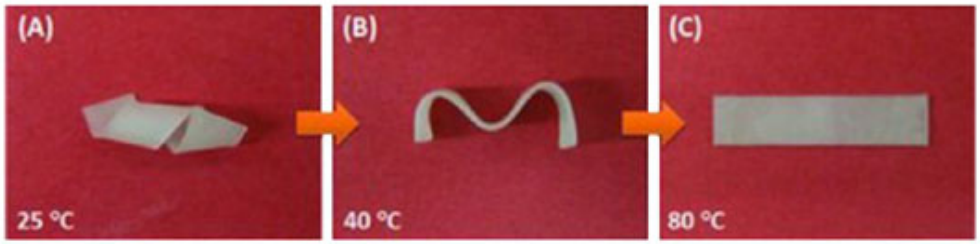

The sequential recovery of the epoxy/polycaprolactone composite (A) from a temporary shape, (B) to temporary shape b, and (C) to permanent shape c.

Harper Meng, Guoqiang Li. A review of stimuli-responsive shape memory polymer composites. Polymer 54: 2199-2221, 2013.

Hydrogel with Fast Shape Memory and On-demand Drug Release

Fig. 2 | Mechanical and shape-memory properties of PTK hydrogel. a Tensile stress-strain curves of PMI, PKG, PTA, and PTK hydrogels. **b** Successive loading-unloading test of PMI and PTK hydrogels. **c** The retention ratio of the initial stress at the 0, 20, 200, 1000, 3000, 6000, 10000, and 20000 cycles during the successive loading-unloading test of PMI and PTK hydrogel. **d** The lap-shear adhesive strength of PTA and PTK hydrogels with cartilage. Photographs of the shape-memory performances of PTK hydrogel with the temporary helix shape (**e**) and coil shape (**f**). Scale bar: 5 mm. Data in **d** are presented as mean values ± SD. ($n = 3$ independent samples).

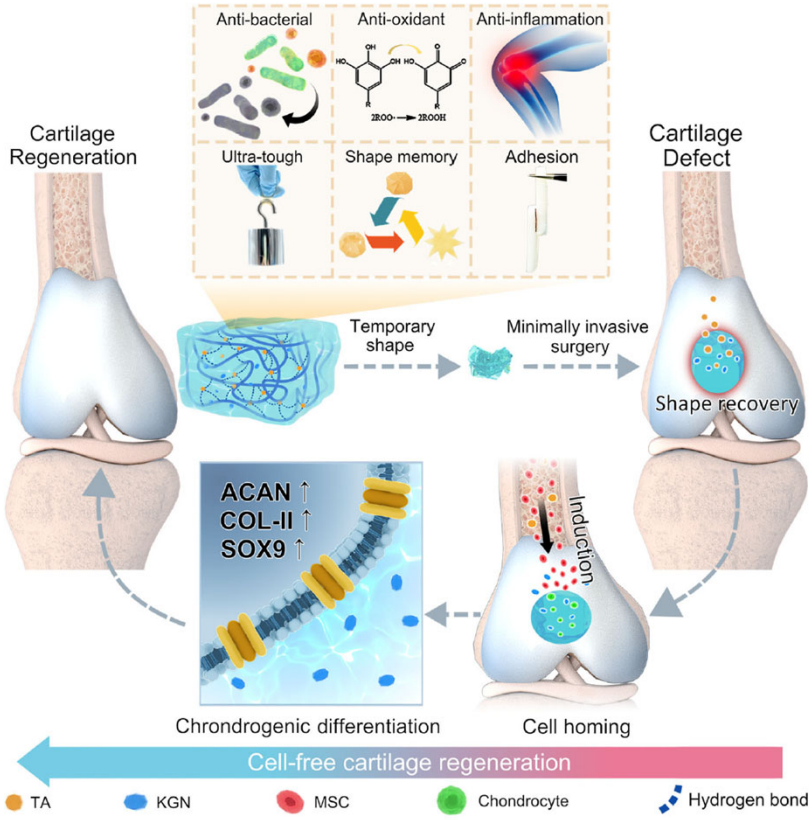

Yang 2023, Ultra-durable cell-free bioactive hydrogel with fast shape memory and on-demand drug release for cartilage regeneration

Is This A Shape Memory Polymer?

Pressure-Sensitive Polymers

Pressure-Sensitive Polymers

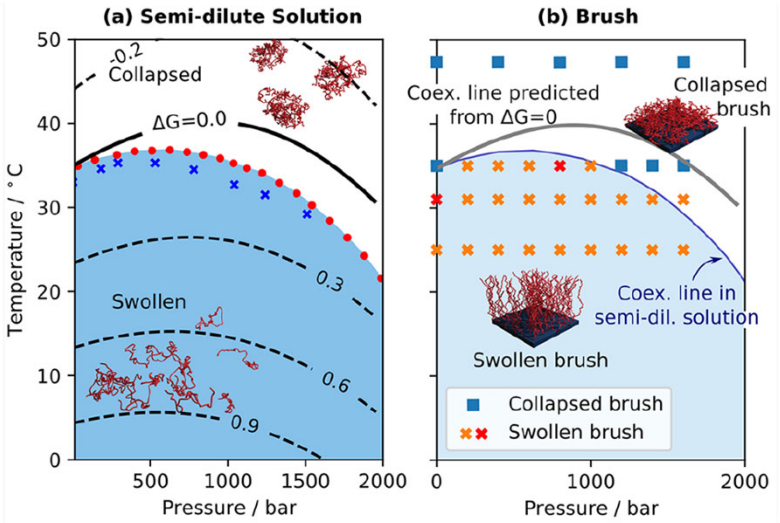

Figure 3. Phase diagrams of PNIPAM in semidilute solution and grafted on planar substrates. (a) Pressure−temperature phase behavior of a 3 wt % PNIPAM semidilute solution in D_2O. Red points and blue crosses indicate experimentally determined phase boundaries as reported in refs 32 and 38, respectively. The contour lines are isoenergetic lines of fixed ΔG (values given in kJ mol^{-1}), calculated with eq 1 using the parameters determined by calorimetry and volumetry. (b) Pressure−temperature phase behavior of PNIPAM brushes in water. Squares and crosses indicate $P-T$ coordinates for collapsed and swollen brushes, respectively (see text for definitions). For the sake of comparison, the experimentally determined coexistence line in the semidilute solution is drawn. The two red crosses indicate the $P-T$ coordinates for PNIPAM brushes under the following conditions: (31 °C, 1 bar) and (35 °C, 800 bar), which are equidistant from the coexistence line and whose volume fractions are compared later in the text.

Micciulla 2023, Pressure-induced phase transitions of nonionic polymer brushes

PNIPAM brushes in aqueous media.

Pressure-induced hydration of nonionic polymers at low pressure is universal as it is dictated by water and is polymer-independent. In contrast, the pressure-induced dehydration at high pressure is strongly polymer-specific. The outcomes apply to a wide class of nonionic polymers and can aid the design of responsive coatings with the desired pressure-responsive behavior.

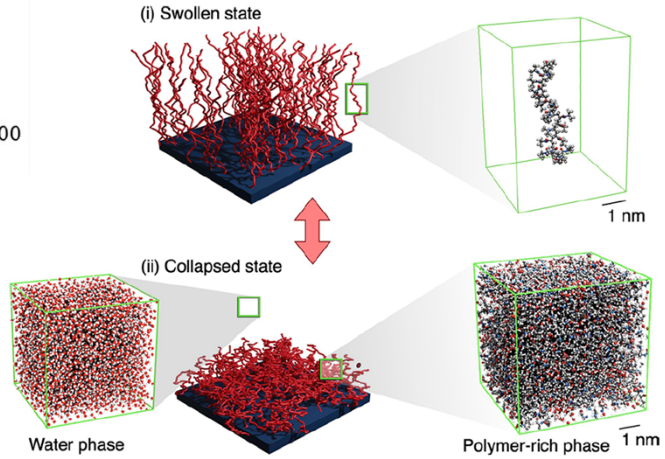

Figure 5. Brush states and simulation setup. (i) The swollen state (schematic, left), where adjacent polymer chains are far apart, is simulated as a stretched and restrained PNIPAM chain in water (MD snapshot, right; water molecules not shown for visibility). (ii) The collapsed state (schematic, middle) is modeled separately as a dense aggregate of PNIPAM chains with water (MD snapshot, right) and a bulk water phase (MD snapshot, left).

They clearly indicate that increasing the temperature causes the collapse of the polymer brush, resulting in a lower degree of hydration and smaller brush thickness. In contrast, increasing the hydrostatic pressure in the system causes the brush to swell, as indicated by increase of the degree of hydration and brush thickness. The phenomenon is particularly evident at 31 and 35 °C for PNIPAM brushes and at all investigated temperatures for PDMAEMA brushes. Interestingly, the maximal thickness and degree of hydration of PNIPAM brushes occur between 600 and 800 bar for curves recorded at 31 and 35 °C. The pressure-induced swelling observed here is in agreement with studies on aqueous solutions of PNIPAM, whereby it was shown that up to moderate pressures of 1000 bar the solubility of PNIPAM increases with increasing pressure.[32,33]

Materials. The silicon substrates (50 × 50 × 10 mm^3) for the preparation of polymer brushes were purchased by Sil'Tronix (Archamps, France). *N*-Isopropylacrylamide (NIPAM, 97%), 2-(dimethylamino)ethyl methacrylate (DMAEMA, 98%, stabilized by monomethyl ether hydroquinone), 2,2′-bipyridyl (bipy, ReagentPlus, ≥99%), *N*,*N*,*N*′,*N*″,*N*″-pentamethyldiethylenetriamine (PMDETA, 99%), copper(I) and copper(II) chloride (CuCl and $CuCl_2$, >99%), and methanol were all purchased from Sigma-Aldrich (France). All reagents were used as received without any further purification. All samples were prepared using D_2O from Eurisotop.

Polymers Responsive to Electric and Magnetic Fields

Electrifying Plastics

Flexible circuits by lamination

PLASTIC ELECTRONICS

Researchers at Bell Laboratories and the University of Texas at Austin, led by John A. Rogers, have developed a new method to fabricate plastic circuits with organic semiconductors using 'soft', conformable electrical contacts and a lamination process [*PNAS* (2002) 99, 10252-10256]. The printed circuits have excellent flexibility and are able to withstand stirred, soapy water for long periods. Low cost, flexible, durable, and lightweight plastic circuits have great potential for many devices, including electronic paper, wearable sensors, and smart cards.

The key aspect of the approach is the fabrication of different parts of the circuit on different substrates. The two substrates are then bonded together. "A thin elastomeric substrate supports the electrodes and interconnections. Laminating this substrate against another plastic substrate that supports the gate, dielectric, and semiconductor levels establishes effective electrical contacts and completes the circuits," explain the authors. The electrical properties of these laminated transistors are similar to other organic semiconductor devices produced using more standard techniques.

The laminated circuits have two advantages over other fabrication technologies. The embedded circuits have much better mechanical flexibility than circuits deposited in the usual way on the surfaces of substrates. The flexibility arises because the circuit lies near the neutral mechanical plane (0% strain) at the center of the device. The embedded circuits are also naturally encapsulated, providing protection from the environment. Negligible changes in the transistor properties after 15 minutes in stirred, soapy water were observed.

The researchers hope that their work will provide a general method for providing non-invasive electrical contacts to fragile or ultra-thin organic materials, and will be useful for measuring charge transport in these systems.

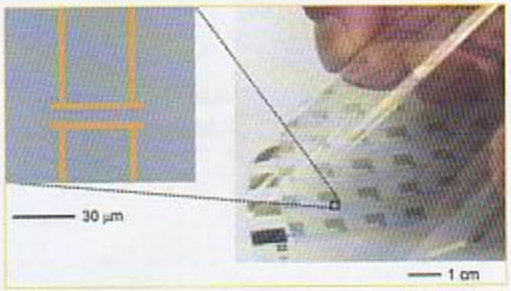

A laminated circuit. Inset shows source/drain electrodes (gold) laminated against a pentacene layer (blue). (Courtesy of PNAS.)

ELECTRIFYING PLASTICS

Nobel Prize in Chemistry honors three who pioneered a new materials field

Alan G. MacDiarmid missed the fateful phone call from Stockholm that many scientists can't help dreaming about. But he learned the momentous news soon enough from a colleague who had seen it on the Internet: MacDiarmid, 73, a chemistry professor at the University of Pennsylvania, had won the 2000 Nobel Prize in Chemistry along with Alan J. Heeger, 64, a professor of physics and materials science at the University of California, Santa Barbara, and Hideki Shirakawa, 64, a chemistry professor who retired earlier this year from the University of Tsukuba, in Japan.

The three were honored last week by the Royal Swedish Academy of Sciences, which administers the Nobel Prizes, for opening and developing the important new field of electrically conductive polymers. They will share the monetary award of more than $900,000.

Before Shirakawa, MacDiarmid, and Heeger made their seminal discovery in 1977, the idea that a plastic could conduct electricity as well as a metal would have seemed ludicrous. Organic polymers were—and for the most part, still are—known as insulators. But the three researchers found that by doping a known conjugated polymer (polyacetylene), they could make it conduct a charge with unprecedented ease.

Since then, scientists have synthesized a number of other conducting polymers as well as a host of related polymers that have semiconducting and light-emitting properties. All applications that involve the movement of charge through a polymer "owe some debt" to the 1977 discovery, says organic chemist Howard E. Katz of Lucent Technologies' Bell Laboratories in Murray Hill, N.J.

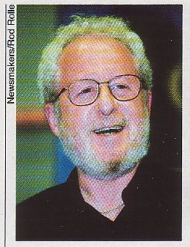
Newsmakers/Reuters/Rick Rickle

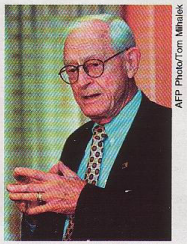
AFP Photo/Tom Mihalek

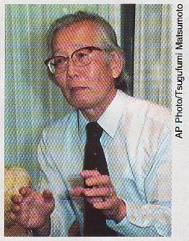
AP Photo/Tsugufumi Matsumoto

Clockwise from above: Heeger, MacDiarmid, and Shirakawa

That discovery, he adds, led to new types of organic materials that combine the processing advantages and mechanical properties of plastics with the electronic and optical properties of metals and inorganic semiconductors. And these materials, in turn, led to the development of organic and polymeric light-emitting diodes, field-effect transistors, and photovoltaic devices.

Conducting polymers have yet to take the marketplace by storm, but they are beginning to have a commercial impact, says Arthur J. Epstein, a professor of physics and chemistry at Ohio State University.

For example, conducting polymers are being used as antistatic coatings and corrosion inhibitors, and one even plays "a major role as a radar-absorbing screen coating in stealth bombers," according to chemistry professor Andrew B. Holmes, who directs the Melville Laboratory for Polymer Synthesis at the University of Cambridge. He tells C&EN that one conductive polymer is making its way into mobile phone displays based on a light-emitting polymer.

Other applications of conducting polymers that could emerge in coming years include lightweight batteries for cars, electromagnetic shielding, ultrathin computer monitors and TV sets, artificial nerves, and sensors, according to Daryle H. Busch, president of the American Chemical Society.

As often happens in science, the 1977 discovery began with an accident. In the early 1970s, a graduate student in Shirakawa's lab at Tokyo Institute of Technology prepared a new form of polyacetylene after he mistakenly added 1,000 times more catalyst to the reaction mixture than the recipe called for. The film of all-*trans*-polyacetylene produced in the reaction looked like aluminum foil, not the dark material the chemists had been expecting.

MacDiarmid later met Shirakawa in Tokyo and heard about his discovery. MacDiarmid invited the Japanese chemist to Penn to collaborate with him and Heeger, who then was also on the Penn faculty, on further studies of this metallic-looking polymer.

During that visit at Penn in 1977, the three researchers tried doping the polyacetylene with iodine. Not only did the silvery polymer film become golden, but its conductivity increased more than a billionfold—to 10^5 siemens per meter. By comparison, DuPont's Teflon has a conductivity of 10^{-16} S m^{-1} and silver and copper have conductivities of 10^8 S m^{-1}.

On exposure to iodine, polyacetylene is oxidatively doped: The polymer chain loses an electron, leaving a hole or positive charge, while the pilfered electron resides on the counterion I_3^-. When such a hole is filled by an electron jumping in from a neighboring position, a new hole

Some conjugated polymers can be made conductive

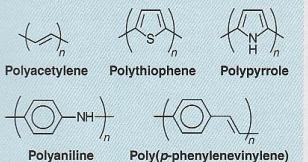

Organic Light-Emitting Diode

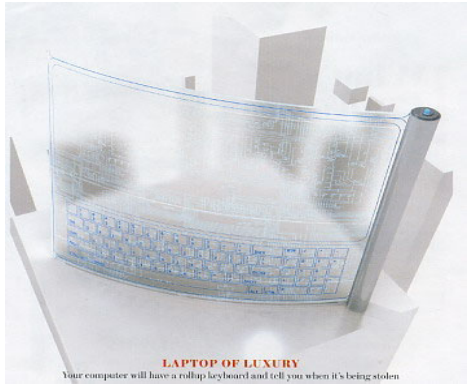

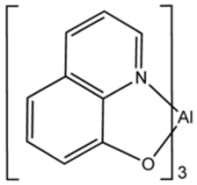

Tris(8-hydroxyquinolinato) aluminium

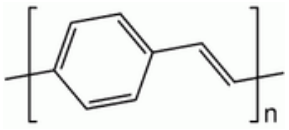

Poly(*p*-phenylene vinylene)

Science&Technology Electronics

PIXEL POWER Flexible electronic "pages" look like the future of paper. Ultrathin displays (left) may fan sales of e-books like those developed by Sony and Philips

Just Two Words: Plastic Chips

They can endow just about anything with computer smarts—and they'll be cheap

IT'S CALLED THE SEDUCTION room. Eastman Kodak Co. uses it to woo visitors with the vivid colors that light up new-breed video screens. They're made from organic light-emitting diodes, or OLEDs. And in the room's side-by-side comparisons with ordinary liquid-crystal displays (LCDs), the difference is impressive: Colors are more vibrant, resolution is crisper, and the OLED screens can be viewed from farther off to the sides without visual loss.

Kodak fell for OLEDs long ago. In 1979, researcher Ching Tang was looking for an inexpensive plastic solar cell to convert light into electricity. Ironically, says Willy C. Shih, president of Kodak's Display & Components Group, Tang stumbled on a polymer recipe that "did just the opposite." His plastic converted electricity into light—with unprecedented efficiency for an organic compound. Kodak has been smitten ever since.

Today, the whole display industry loves plastics. Every maker of TV sets and computer monitors is working on OLED screens. In Japan, a dozen companies and four universities are collaborating to build a 60-inch OLED display by 2007, says Kimberly Allen, director for technology research at market watcher iSuppli Corp. Don't look for anything larger than a laptop screen much before then. One reason: The little organic light bulbs that make up the picture elements, or pixels, burn out after about 8,000 hours of use. That's fine for cell phones, which only get used intermittently. But desktop monitors in offices would last only a year or so. Shih says Kodak's latest chemicals promise a tenfold boost in performance.

Displays, though, barely scratch the surface of what's coming in plastic electronics. A typical home probably has only a handful of displays, but it has hundreds of food containers, toys, medicine bottles, and other items, each of which could be endowed with a modicum of computer smarts if brittle and costly silicon and glass can be replaced with plastic. With the advent of cheap plastic circuits, food packages could sport a "sell by" imprint that keeps track of time and turns bright red when the limit is reached. Kids could converse with even low-priced toys, not just the premium ones. "And a sensor in my daughter's asthma inhaler could warn when it's close to empty," says Elsa Reichmanis, director of polymer materials research at Lucent Technologies Inc.'s Bell Laboratories. "The possible consumer applications are endless."

Moreover, in a world of polymer electronics, virtually any company could become a chipmaker. Thanks to inks made from conductive and semiconductive polymers, it will soon be possible to print proletarian circuits on almost any surface using an inkjet printer or offset press. A billion-dollar semiconductor factory isn't needed, notes Jim Tully, chief of Gartner Inc.'s research arm in Europe, "so this will open the door for a large number of manufacturers" to make poly chips for a host of everyday products.

THINGS THAT THINK

POLYMER ELECTRONICS can't challenge silicon in heavy-duty number-crunching jobs now, although that may be just a matter of time. Plastic transistors today are positively poky compared with silicon versions, concedes Alan J. Heeger, the University of California at Santa Barbara physicist who shared a Nobel prize in 2000 for helping to create the first conductive polymer in 1977. But the speed of poly transistors has been rising steadily. "Every improvement," says Heeger, "expands the potential market."

How much might the poly-chip market be worth? Motorola Inc. sees an op-

Printers could spew out plastic chips like so much newspaper

Graphene

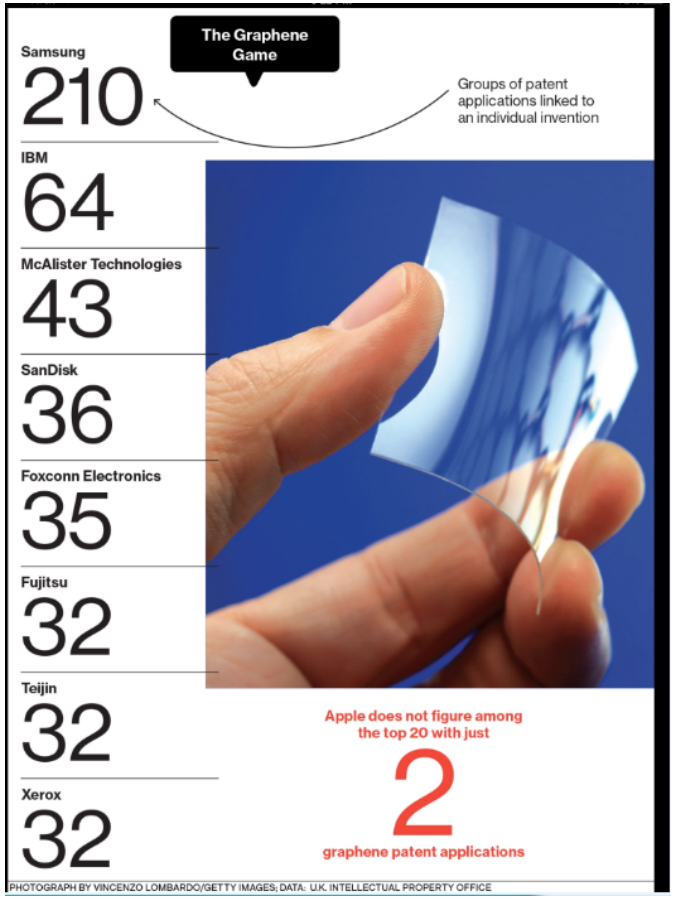

Electrochromic Polymers

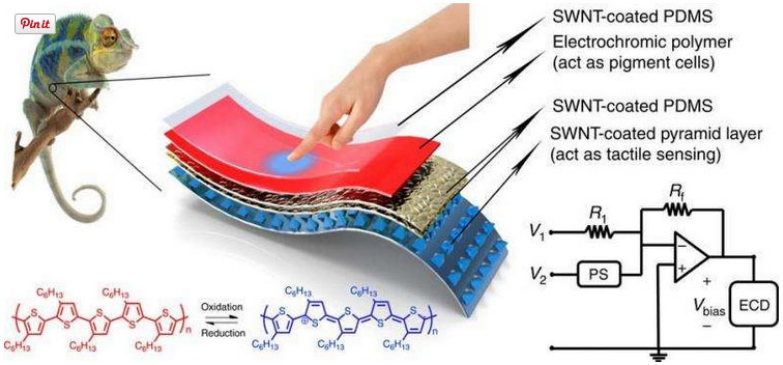

http://phys.org/news/2015-09-chameleon-inspired-stretchable-e-skin.html

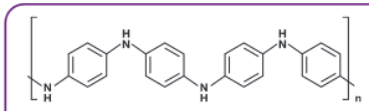	Leucoemeraldine	Colourless Fully reducing Insulating
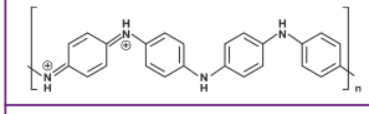	Emeraldine salt	Green Partially oxidised Conducting
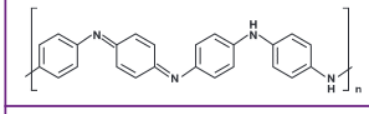	Emeraldine base	Blue Partially oxidised Insulating
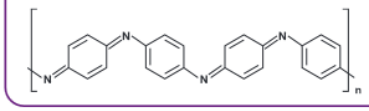	Pernigraniline	Purple Fully oxidised Insulating

http://www.rsc.org/images/RSCelectro_tcm18-159224.pdf

'Green' Paper- Thin, Flexible Electronics

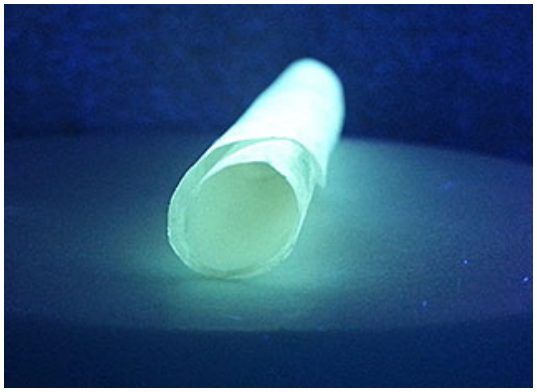

The researchers developed a thin, clear nanocellulose paper made out of wood flour and infusaed it with biocompatible quantum dots—tiny, semiconducting crystals—made out of zinc and selenaium. The paper glowed at room temperature and could be rolled and unrolled without cracking.

http://www.rdmag.com/news/2015/05/toward-green-paper-thin-flexible-electronics?et_cid=4581167&et_rid=54728378&location=top

New printing process makes three-dimensional objects glow

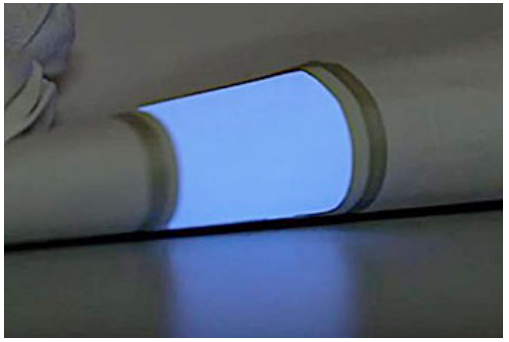

Conventional electroluminescent (EL) foils can be bent up to a certain degree only and can be applied easily onto flat surfaces. The new process developed by Karlsruhe Institute of Technology (KIT) in cooperation with the company of Franz Binder GmbH & Co. now allows for the direct printing of electroluminescent layers onto three-dimensional components. Such EL components might be used to enhance safety in buildings in case of power failures. Other potential applications are displays and watches or the creative design of rooms. The development project was funded with EUR 125,000 by the Deutsche Bundesstiftung Umwelt (German Foundation for the Environment).

http://www.rdmag.com/news/2015/05/new-printing-process-makes-three-dimensional-objects-glow?et_cid=4581167&et_rid=54728378&type=cta

Metal Rubber: Layer by Layer (LBL) Coating

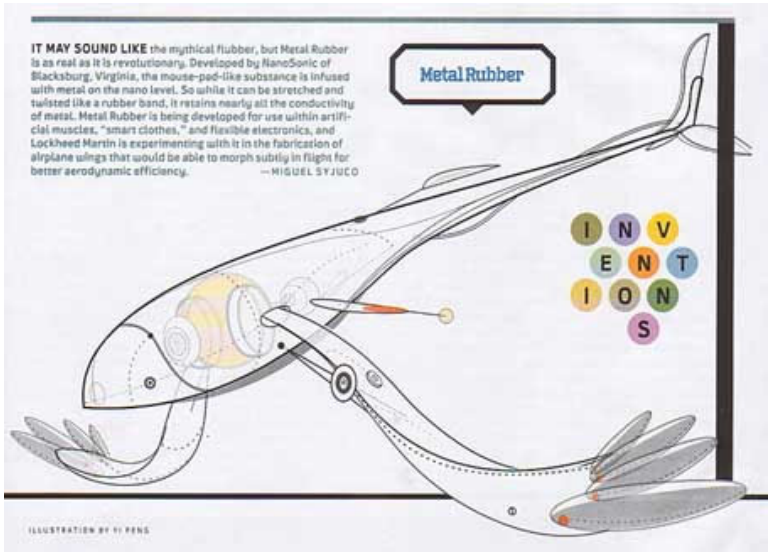

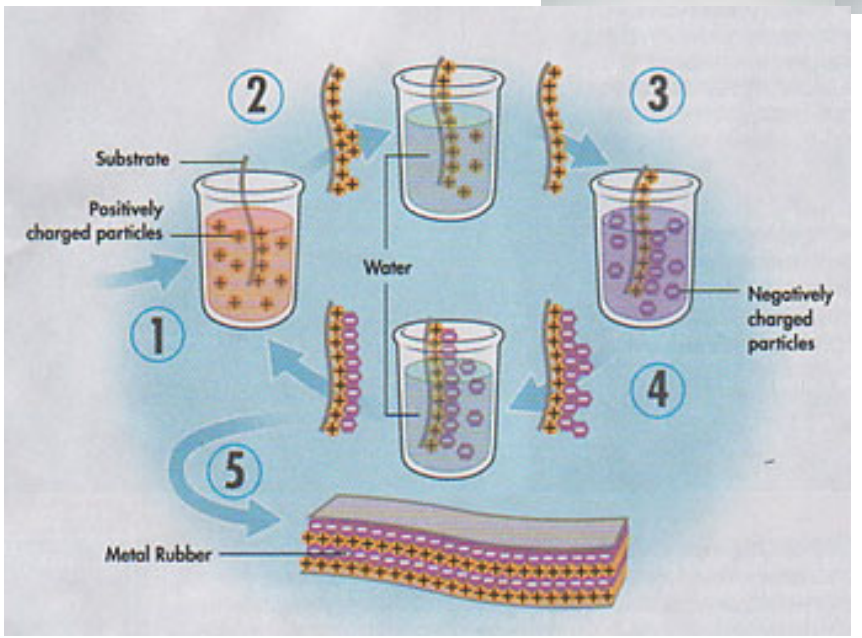

MAKING METAL RUBBER FROM SCRATCH
Dip charged substrate into container of positively charged water-based solution (1). Rinse substrate in water to remove unbound particles (2). Dip substrate into negatively charged solution (3). Rinse and repeat (4, 5).

NanoSonic's Metal Rubber™ is a highly electrically conductive and highly flexible elastomer. It can be mechanically strained to greater than 1000 percent of its original dimensions while remaining electrically conductive. As Metal Rubber can carry data and electrical power and is environmentally rugged, it opens up a new world of applications requiring robust, flexible and stretchable electrical conductors in the aerospace/defense, electronics and bioengineering markets.

http://www.nanosonic.com/80/4/metalrubber.html
http://videos.howstuffworks.com/sciencentral/2938-metal-rubber-video.htm

Popular Science. August 2004. p. 36.

Conductive Polymers

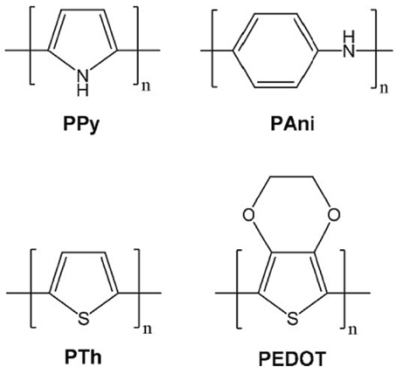

Fig. 2. Structures of most widely investigated CPs in biomedical applications.

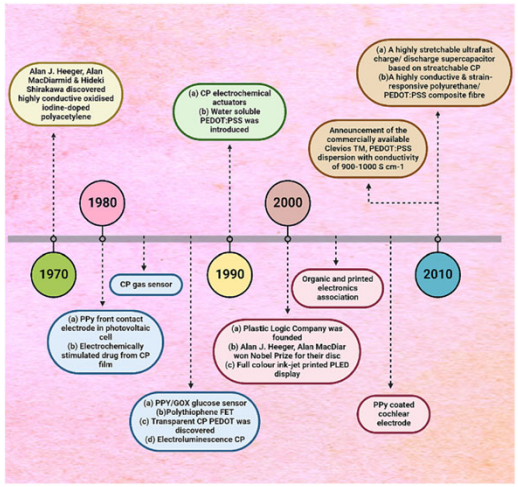

Fig. 3. A timeline detailing the evolution of CPs and their applications over past decades.

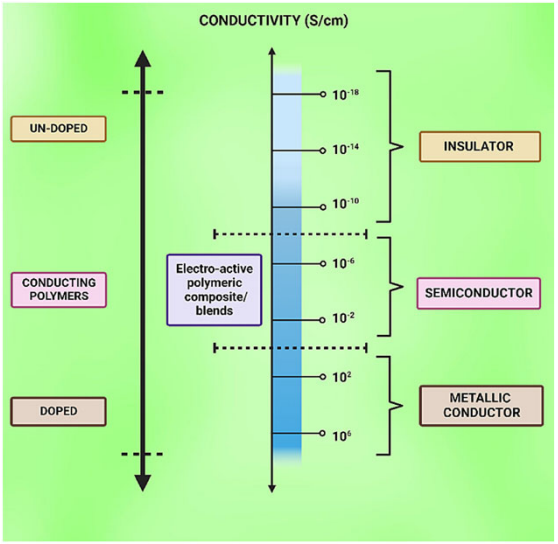

Fig. 1. Range of conductivity for CPs, CPs composites, and blends.

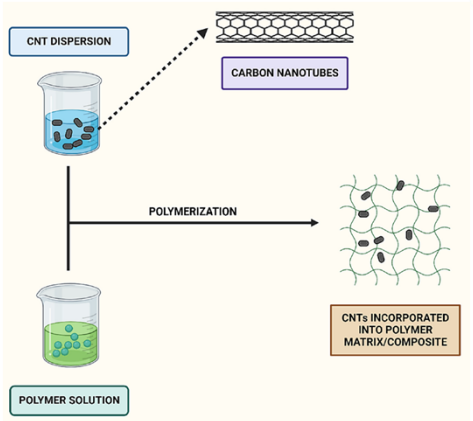

Fig. 7. Overview of in-situ polymerization method for the synthesis of CPs composites.

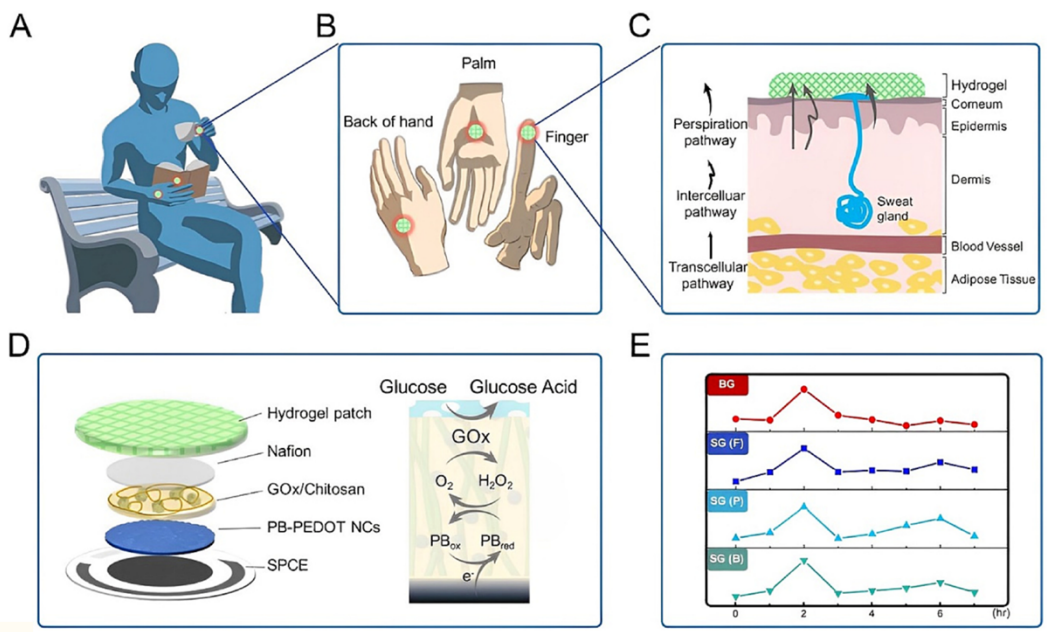

Fig. 11. Schematic representation of the design, mechanism involved, and the usage of natural sweat as a sample for glucose sensor. (A) The hydrogel patch can be placed at different positions on the body for the sampling of sweat during resting time. (B) The positions to place the patch on the hand for sweat collection are the palm, back of the hand, and fingers. (C) The favourable glucose sweat sampling pathways for natural sweat hydrogel patches. (D) Schematic representation of the multiple layers in PB-PEDOT NC enzymatic electrode of the sweat glucose monitoring device and the working mechanism GOx with the PB probe. (E) The sweat glucose monitoring device can identify sweat glucose levels without externally applied stimulation or high-intensity physical activity at various locations such as the palm, back of the hand, and finger.

Raj 2023, Conductive polymers and composites-based systems

Conductive Hydrogels

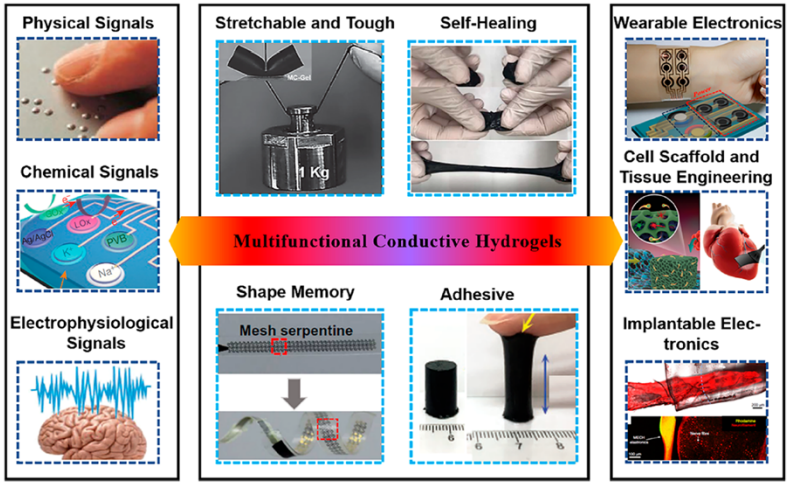

Figure 1. Functional conductive hydrogels for bioelectronics in biomedical applications. The left column presents the conductive hydrogels used for physical, chemical, and electrophysiological signals detection, respectively. The middle column summarizes important functions of conductive hydrogels. The right column shows the application of conductive hydrogels in the areas of wearable electronics, cell scaffold and tissue engineering, and implantable electronics, respectively.

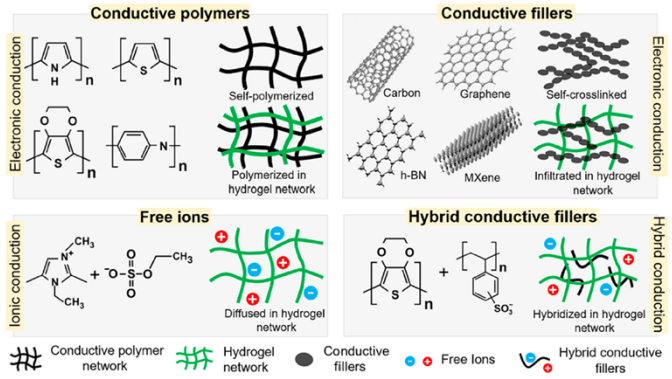

Figure 2. Structures of several types of conductive hydrogels. Conductive hydrogel can be synthesized by using conductive polymers, conductive fillers, free ions, and their mixtures. The formed hydrogels can be classified as electronic, ionic, and the hybrid electronic–ionic conducting hydrogels.

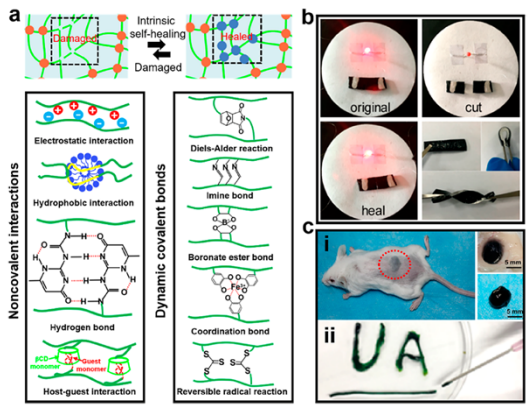

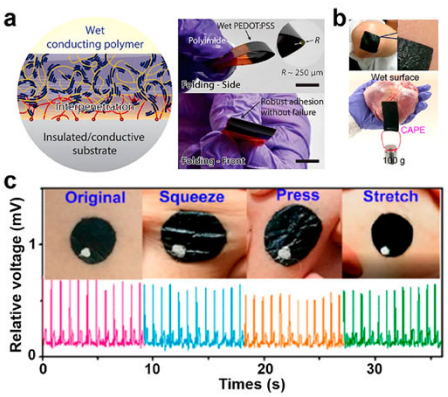

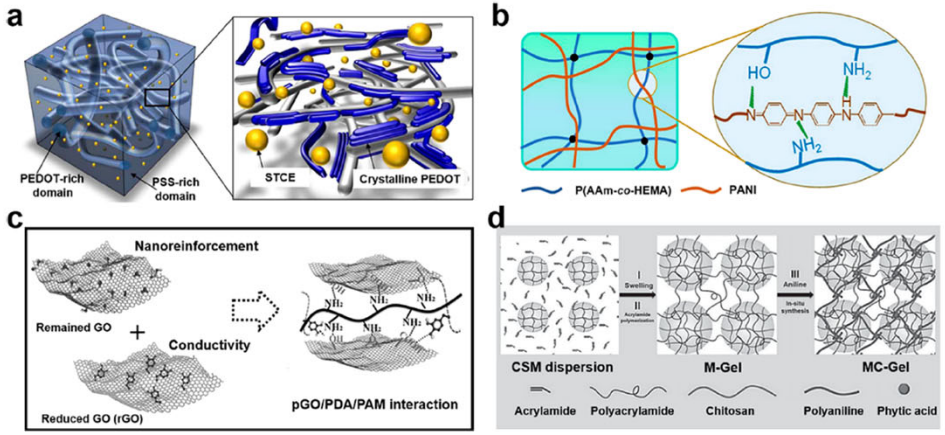

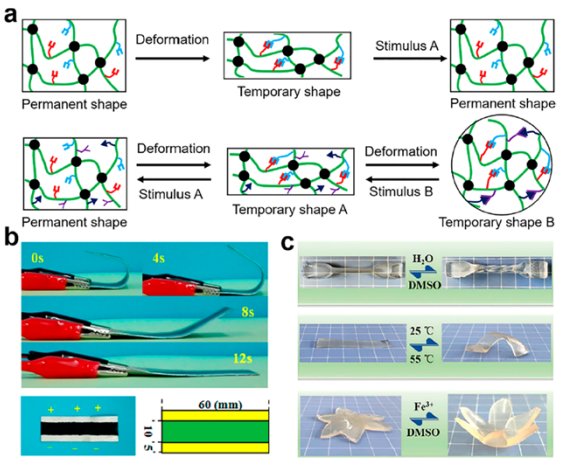

Fu 2020, Functional conductive hydrogels for bioelectronics

Magnetic Gels

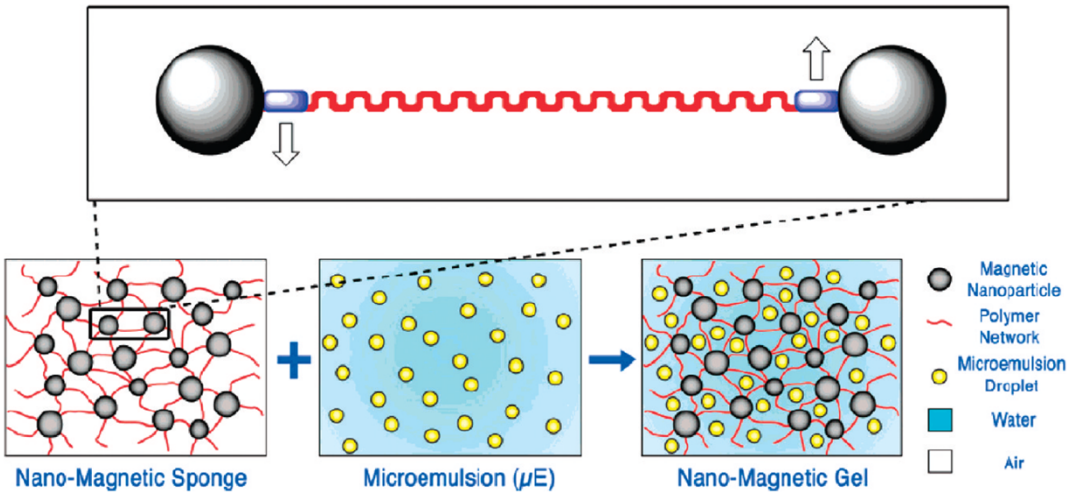

FIGURE 4. Schematic representation of the gel with a microemulsion and ferrite magnetic nanoparticles. The inset shows cross-linked nanoparticles (black spheres) bonded to methacrylate residues (blue rectangles) and a PEG chain (red line); arrows represent the binding group to the polymer network of acrylamide and bisacrylamide.

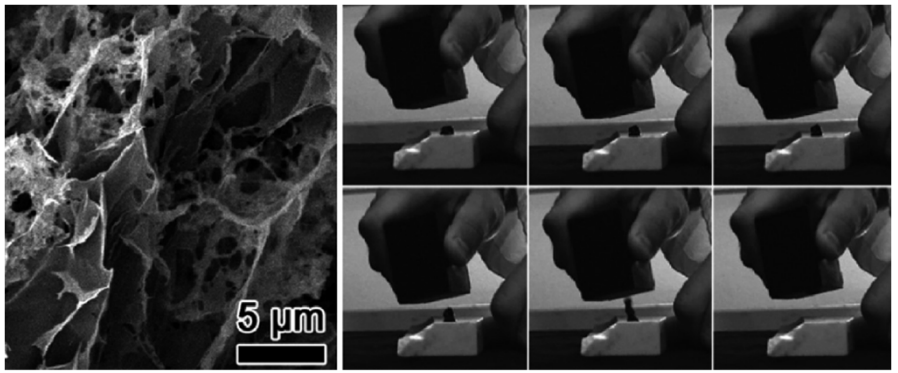

FIGURE 5. (left) SEM micrograph showing the microscaled pores, together with the acrylamide gel layers where the magnetic nanoparticles are copolymerized (brighter regions). (right) Sequence from top left to lower right illustrating the removal of a microemulsion-loaded gel from the surface of marble by an external magnet.

Magnetic chemical gels for art conservation have been described recently. They were prepared by embedding ferrite magnetic nanoparticles (coated with a dicarboxylic derivative obtained through the esterification of poly(ethylene glycol) (PEG) with maleic anhydride) in a polyacrylamide matrix (Figure 4). The nanoparticles are attached by chemical means to the PEG through the carboxylate functional groups, while the two double bonds per molecule resulting from the esterification anchor the nanoparticles chemically within the gel matrix. Radical copolymerization of these functionalized nanoparticles with acrylamide and N,N'-methylene bisacrylamide produces a nanomagnetic gel where both the physicochemical properties of acrylamide-based gels and the magnetic response of ferrite nanoparticles are retained.

These gels behave as "containers" for aqueous droplets; they can be freeze-dried to obtain magnetic xerogels and then rehydrated like "sponges" to ca. 10× their dried weight. Even in their hydrated state, the gels can be cut with a knife to a desired shape and moved with an external magnet. The emulsions that have been used previously in the removal of Paraloid coatings from the surfaces of artwork.

Carretti 2009, New frontiers in materials science for art conservation: Responsive gels and beyond.

Magnetic Hydrogel for Controlled Release

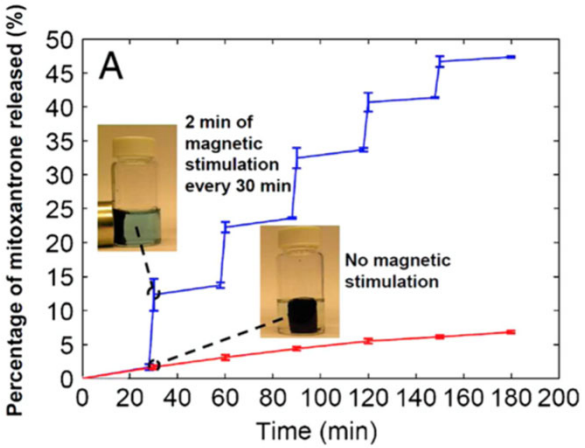

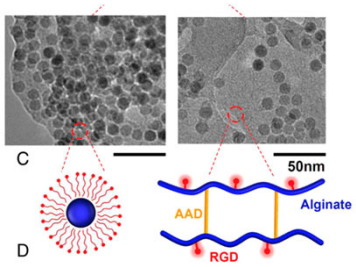

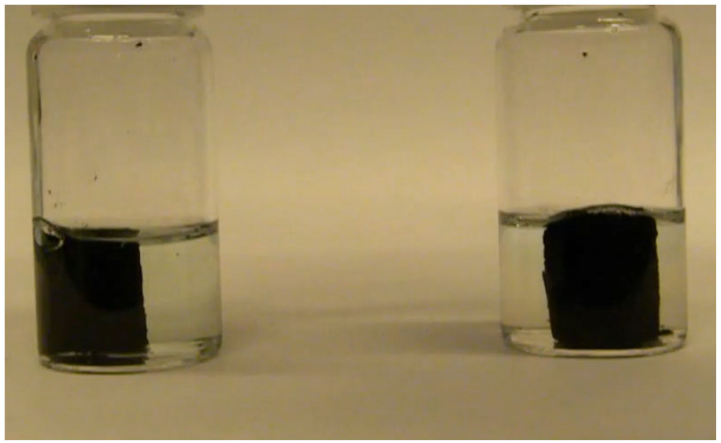

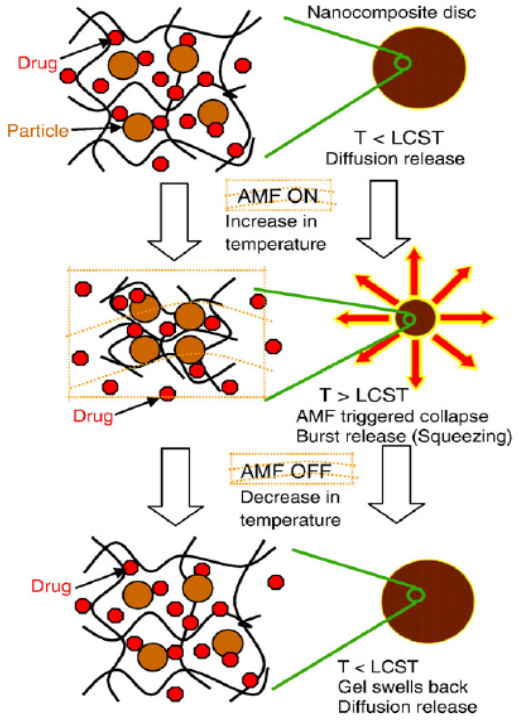

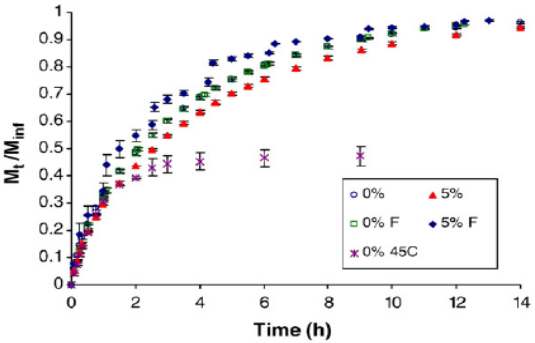

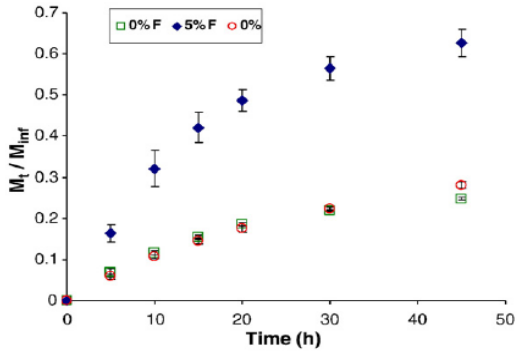

www.pnas.org/cgi/doi/10.1073/pnas.1007862108

Satarkar NS and Hilt JZ. *J Control Release 130: 246,* 2008

Magnetic Field-Responsive Hydrogels

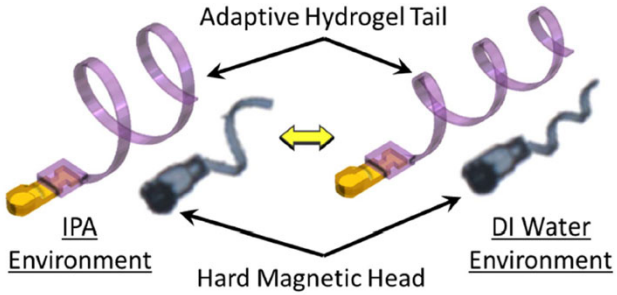

Fig. 1. Schematic of the Helical Adaptive Multi-material MicroRobot (HAMMR). It consists of a hard magnetic head and an adaptive helical hydrogel structures that deforms between a loose and compact configuration depending on the solvent environment. The HAMMR locomotion is controlled with a rotating magnetic field.

***Abstract*—Adaptive locomotion is an advanced function of microrobots that can be achieved using smart materials. In this letter, a responsive hydrogel is utilized as a smart material and used to fabricate Helical Adaptive Multi-material MicroRobots (HAMMRs) with deformable tails to achieve adaptive locomotion capabilities. Moreover, a novel fabrication method is proposed to realize these types of helical microrobots with enhanced swimming performances by taking advantage of a strong magnetic head and deformable tail. The deformations of different tail designs and the fabricated microrobots are tested in different solvents. The swimming performances of the swimming microrobots are investigated experimentally under a rotating magnetic field and verified with theoretical calculations. The HAMMRs show significant deformations upon stimulation and changes in swimming performance which are in agreement with the scaled calculation result. Finally, the HAMMRs present an enhanced mobility with a highest published translational velocity for an adaptive swimming microrobot of 8.1 body length per second.**

***Index Terms*—Micro/nano robots, soft robot materials and design, soft robot applications.**

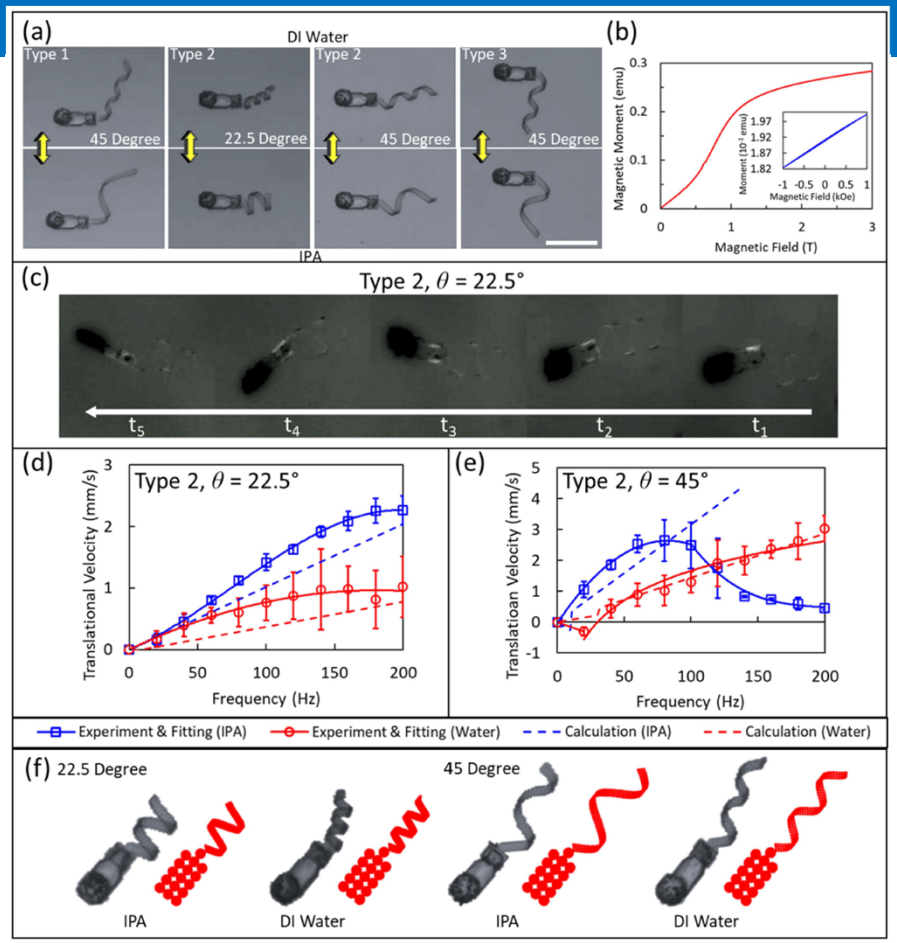

Fig. 5. Responsive deformation and frequency responses of HAMMRs. (a) Deformation of different types and parameters of HAMMRs in DI water and IPA. Scale bar: 200 μm. (b) Magnetization and measurement of SU-8/MMPs film. (c) Swimming motion at 1 Hz of a Type 2 microrobot with a modulating angle of 22.5°. (d) Frequency response of a Type 2 HAMMR with a tail modulating angle of 22.5°. (e) Frequency response of a Type 2 HAMMR with a tail modulating angle of 45°. Curves and symbols in blue are data for HAMMRs in IPA while data in water are represented in red. Solid curves are fitted curves and dash lines are velocities predicted by the dynamics calculations. At least three microrobots are tested for each data point. (f) Discretizations of the microrobot geometries in (d) and (e) for the calculations using the multipole expansion method.

Tan 2023, Design, fabrication, and characterization of a helical adaptive multi-material microrobot (HAMMR)

Ultrasound-Responsive Hydrogels

ABSTRACT: The development of tunable, ultrasound-responsive hydrogels that can deliver protein payload on-demand when exposed to focused ultrasound is described in this study. Reversible Diels−Alder linkers, which undergo a retro reaction when stimulated with ultrasound, were used to cross-link chitosan hydrogels with entrapped FITC-BSA as a model protein therapeutic payload. Two Diels−Alder linkage compositions with large differences in the reverse reaction energy barriers were compared to explore the influence of linker composition on ultrasound response. Selected physicochemical properties of the hydrogel construct, its basic degradation kinetics, and its cytocompatibility were measured with respect to Diels−Alder linkage composition. Focused ultrasound initiated the retro Diels−Alder reaction, controlling the release of the entrapped payload while also allowing for real-time visualization of the ongoing process. Additionally, increasing the focused ultrasound amplitude and time correlated with an increased rate of protein release, indicating stimuli responsive control.

KEYWORDS: *chitosan, hydrogels, ultrasound, controlled release, click chemistry, Diels−Alder*

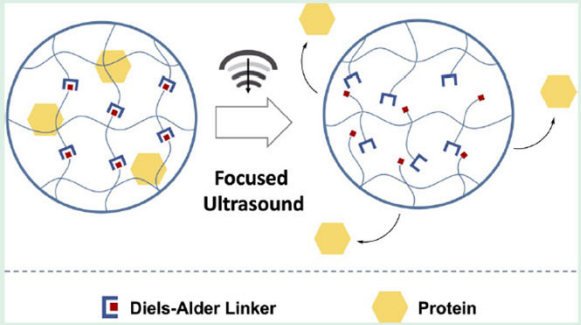

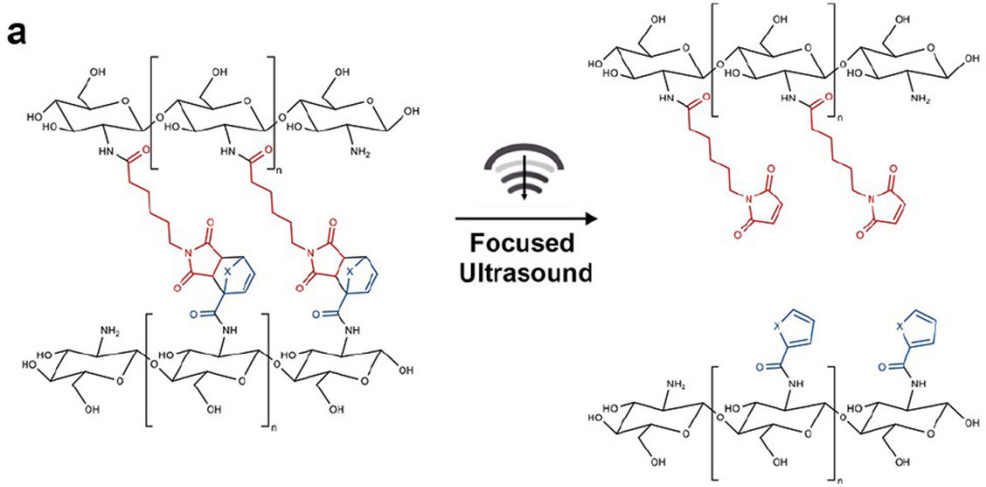

Figure 5. Ultrasound-mediated protein release from hydrogels. (a) Retro Diels−Alder reaction prompted by focused ultrasound for chitosan hydrogels cross-linked with either FDA or TDA. (b) Focused ultrasound dependent release of FITC-BSA from Ch-GLU, Ch-FDA, and Ch-TDA hydrogels (n = 3). *Significant difference ($p < 0.05$). (c) Real-time B-mode ultrasound imaging during focused ultrasound (5 min with a positive peak pressure of 37 MPa and peak negative pressure of 16 MPa) treatment of Ch-GLU, Ch-FDA, and Ch-TDA. A diagram and pictures of the setup used for focused ultrasound are available in the Supporting Information (Figures S1 and S2).

Arrizabalaga 2022, Ultrasound-responsive hydrogels for on-demand protein release

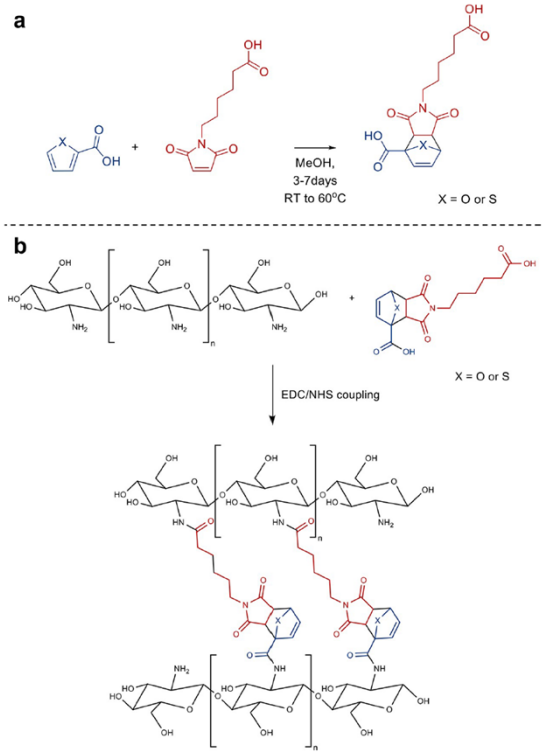

Figure 1. (a) Diels−Alder reaction between 6-maleimidohexanoic acid and a thiophene or furan-based diene. (b) Cross-linking of chitosan with a Diels−Alder linker (FDA or TDA) via EDC/NHS coupling reaction.

Light-Responsive Systems

Light-Sensitive Polymer and Hydrogels

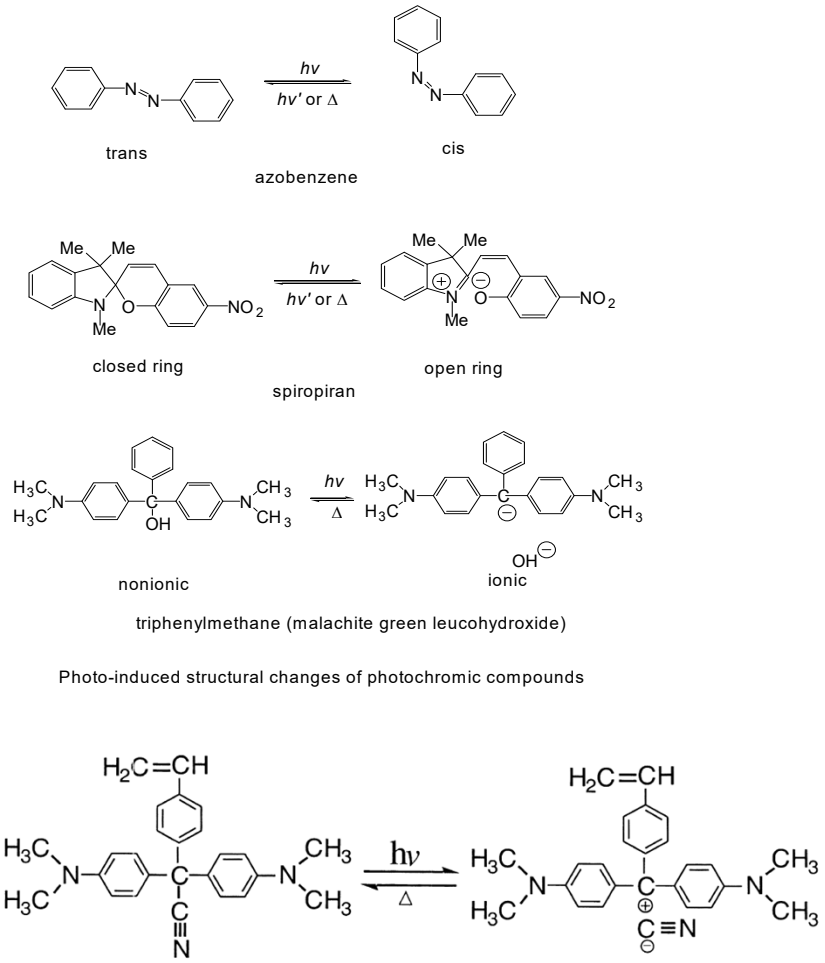

Fig. 8. Structure of leuco derivative molecule bis(4-(dimethylamino)phenyl)(4-vinylphenyl)methylleucocyanide

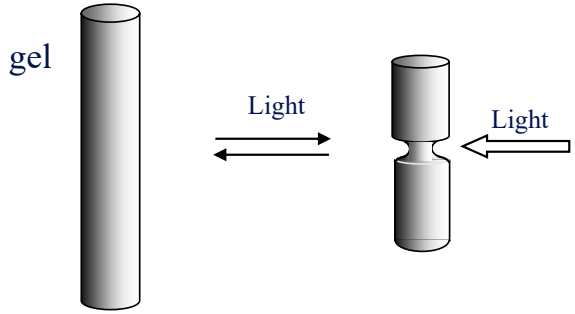

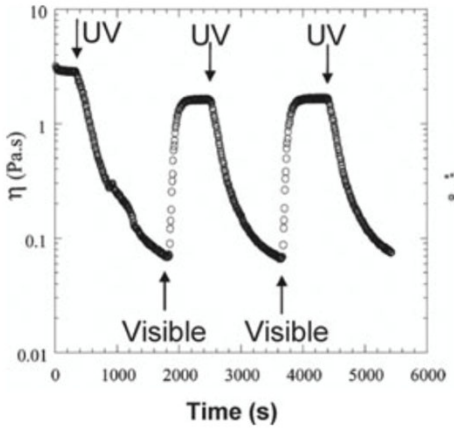

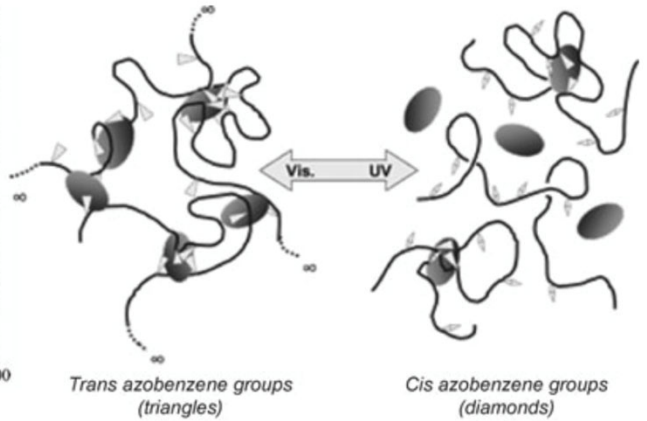

Photochemistry and Photobiology, 2009, 85: 848–860

Irreversible Light-Sensitive systems

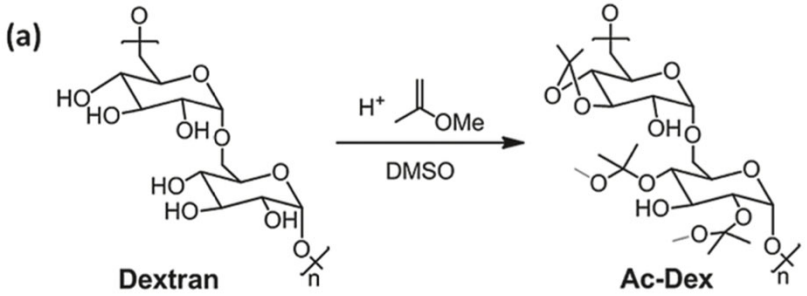

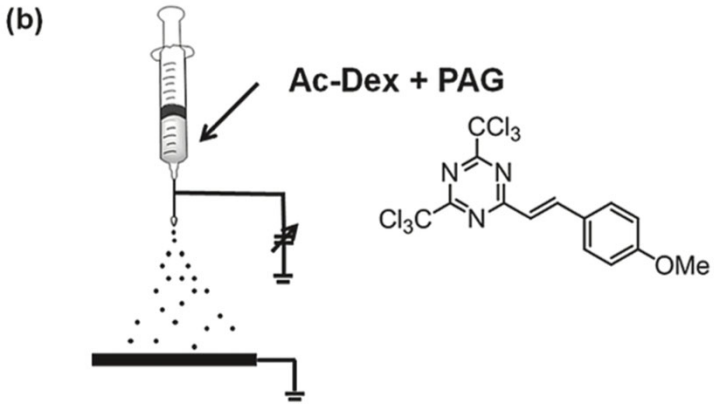

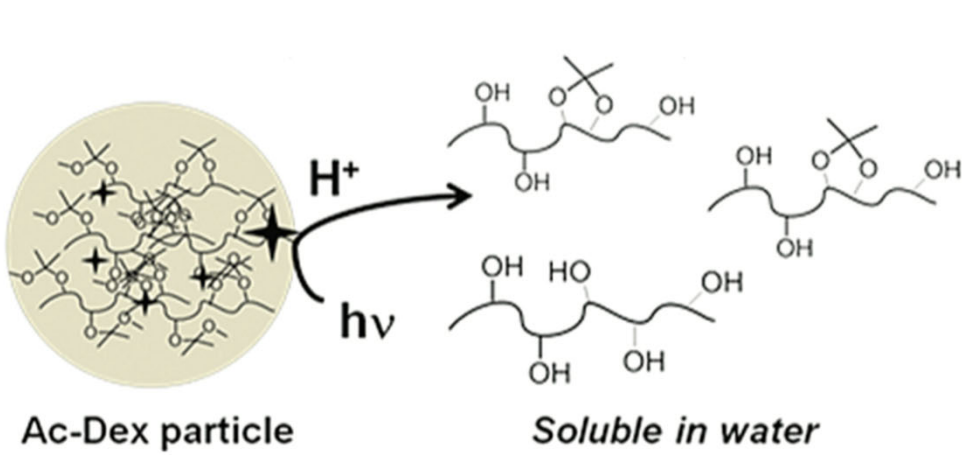

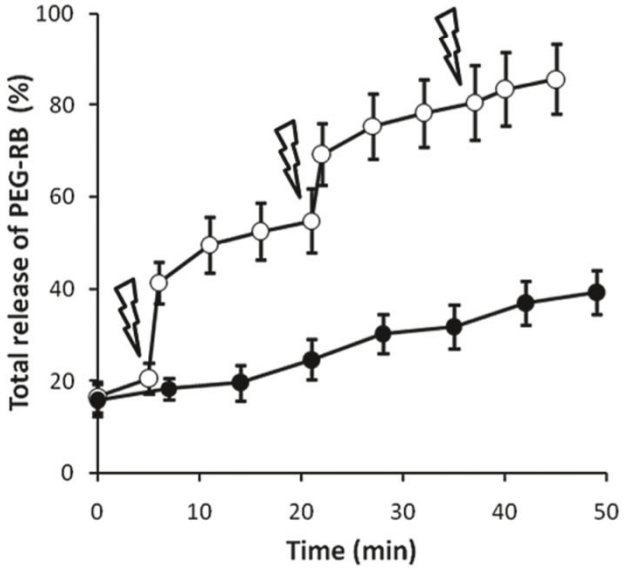

Acetylated Dextran is not soluble, the acetylation is sensitive to acidic conditions

Light induces a change in pH solubalizing the dextran

Small 2013, 9, No. 18, 3051–3057

Light- or Electric-Sensitive Hydrogels

ABSTRACT: In our continuing pursuit to generate, understand, and control the morphology of organic nanofilaments formed by molecules with a bent molecular shape, we here report on two bent-core molecules specifically designed to permit a phase or morphology change upon exposure to an applied electric field or irradiation with UV light. To trigger a response to an applied electric field, conformationally rigid chiral (*S,S*)-2,3-difluorooctyloxy side chains were introduced, and to cause a response to UV light, an azobenzene core was incorporated into one of the arms of the rigid bent core. The phase behavior as well as structure and morphology of the formed phases and nanofilaments were analyzed using differential scanning calorimetry, cross-polarized optical microscopy, circular dichroism spectropolarimetry, scanning and transmission electron microscopy, UV−vis spectrophotometry, as well as X-ray diffraction experiments. Both bent-core molecules were characterized by the coexistence of two nanoscale morphologies, specifically helical nanofilaments (HNFs) and layered nanocylinders, prior to exposure to an external stimulus and independent of the cooling rate from the isotropic liquid. The application of an electric field triggers the disappearance of crystalline nanofilaments and instead leads to the formation of a tilted smectic liquid crystal phase for the material featuring chiral difluorinated side chains, whereas irradiation with UV light results in the disappearance of the nanocylinders and the sole formation of HNFs for the azobenzene-containing material. Combined results of this experimental study reveal that in addition to controlling the rate of cooling, applied electric fields and UV irradiation can be used to expand the toolkit for structural and morphological control of suitably designed bent-core molecule-based structures at the nanoscale.

KEYWORDS: *bent-core liquid crystal, B4 phase, morphology, chirality, electric field, UV irradiation*

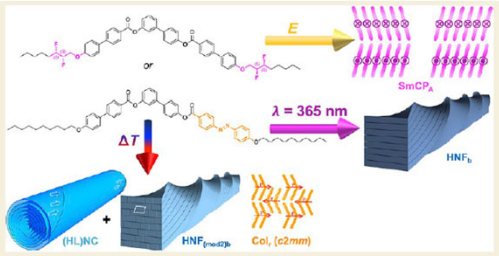

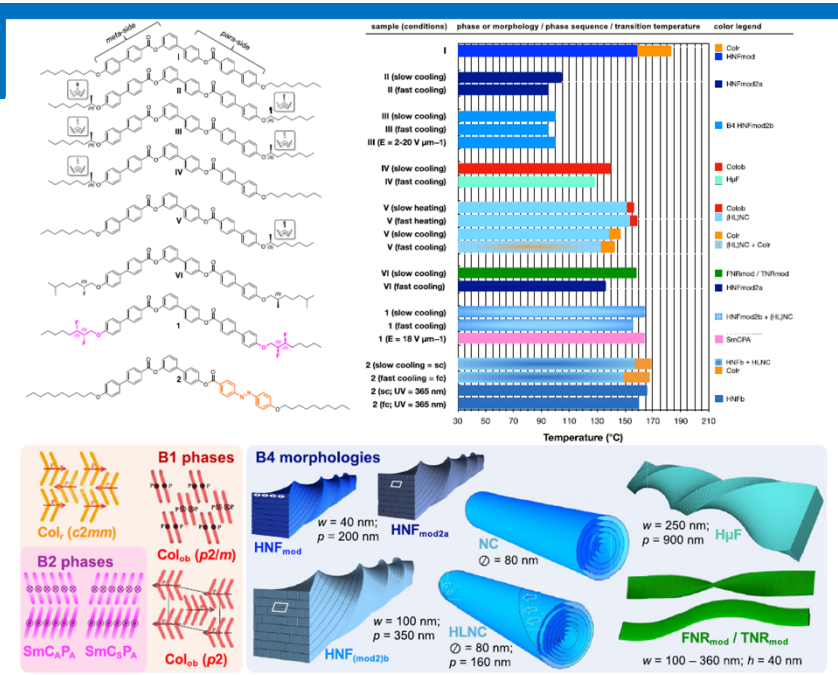

Figure 1. Comparison of the phase sequence, phase structure, B4 morphology, and phase transition temperatures depending on the chemical structure—position, branching points, as well as the number and configuration of chiral center(s) in the aliphatic side chains—of the parent compounds **I**–**VI**[20,22,23,25,26] (chiral center configurations only affect the handedness of the final filaments) with the here-investigated new compounds **1** and **2** (Arabic numerals). Models for the different B1 and B2 phase structures as well as the B4 morphologies are shown at the bottom. The color coding in the bar diagram and models is used throughout in the data plots for various B4 morphologies and B1 or B2 phases.

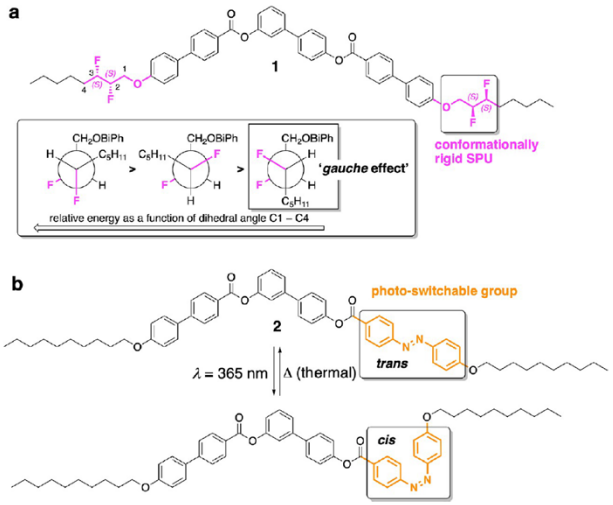

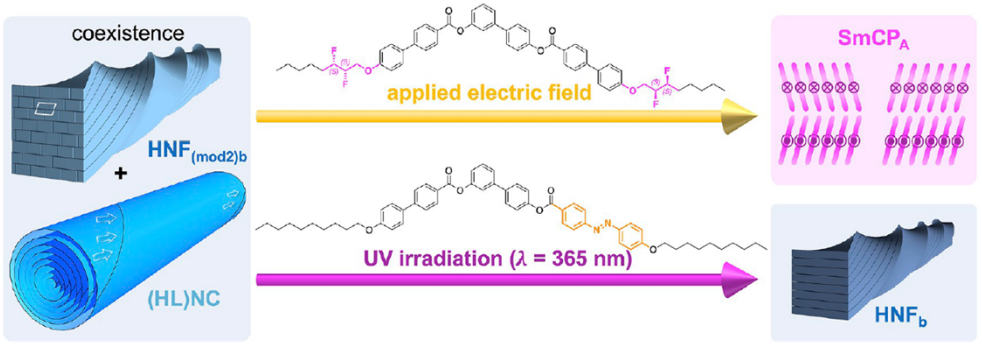

Figure 12. Graphical summary of the response of compounds **1** and **2** to applied external stimuli in addition to thermal control by adjusting the cooling rate from the isotropic liquid phase.

Sezgin 2023, Controlling the structure and morphology of organic nanofilaments using external stimuli

Light-Sensitive Hydrogels

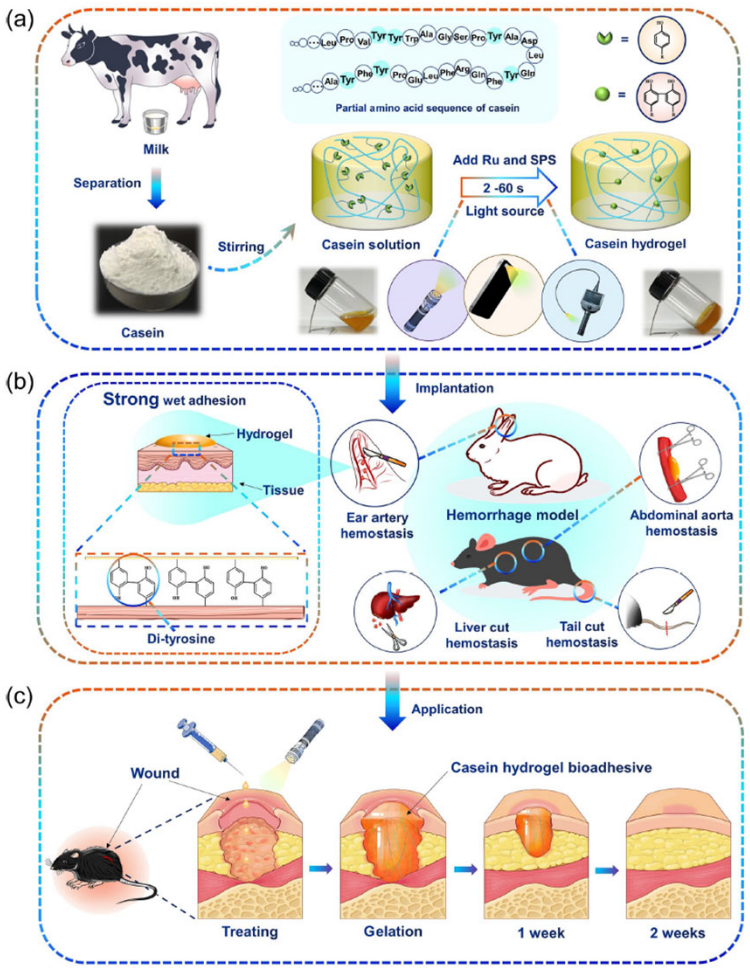

Fig. 1 Schematic illustration of the preparation and the reaction process of casein hydrogels which accelerates hemostasis and wound healing. (**a**) Casein from milk can be crosslinked through white-light activated di-tyrosine bonds formation initiated by Ru/SPS to form hydrogel; (**b**) Adhesion mechanism and hemostatic property of the casein hydrogel bioadhesive for massive arterial and visceral hemorrhage; (**c**) The process of wound healing with casein hydrogel bioadhesive treatment

Abstract Background Post-traumatic massive hemorrhage demands immediately available first-aid supplies with reduced operation time and good surgical compliance. In-situ crosslinking gels that are flexibly adapting to the wound shape have a promising potential, but it is still hard to achieve fast gelation, on-demand adhesion, and wide feasibility at the same time. Methods A white-light crosslinkable natural milk-derived casein hydrogel bioadhesive is presented for the first time. Benefiting from abundant tyrosine residues, casein hydrogel bioadhesive was synthesized by forming di-tyrosine bonds under white light with a ruthenium-based catalyst. We firstly optimized the concentration of proteins and initiators to achieve faster gelation and higher mechanical strength. Then, we examined the degradation, cytotoxicity, tissue adhesion, hemostasis, and wound healing ability of the casein hydrogels to study their potential to be used as bioadhesives. Result Rapid gelation of casein hydrogel is initiated with an outdoor flashlight, a cellphone flashlight, or an endoscopy lamp, which facilitates its usage during first-aid and minimally invasive operations. The rapid gelation enables 3D printing of the casein hydrogel and excellent hemostasis even during liver hemorrhage due to section injury. The covalent binding between casein and tissue enables robust adhesion which can withstand more than 180 mmHg blood pressure. Moreover, the casein-based hydrogel can facilitate post-traumatic wound healing caused by trauma due to its biocompatibility. Conclusion Casein-based bioadhesives developed in this study pave a way for broad and practical application in emergency wound management.
Keywords Casein, photocrosslink, Bioadhesive, Hemostasis, Wound healing

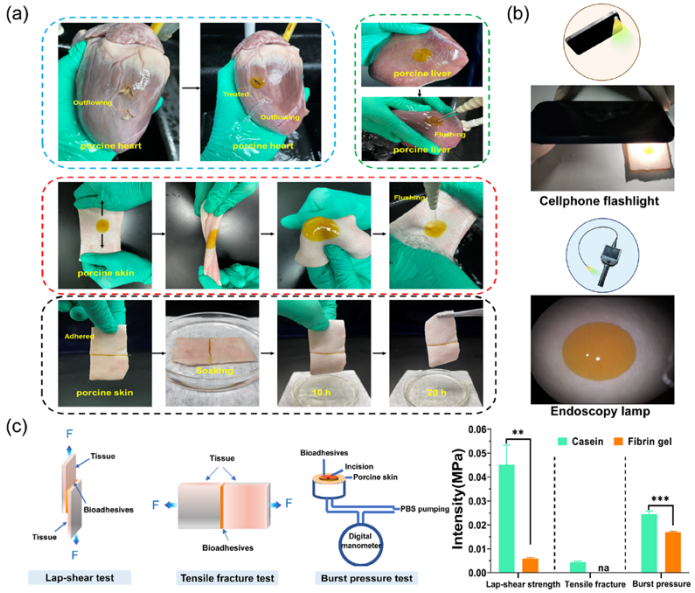

Fig. 3 (a) Quick adhesion of casein hydrogel bioadhesives gelling in-situ in porcine heart, liver and skin, (b) Casein hydrogel photographs under cellphone flight and endoscopy lamp, (c) The lap-shear testing, tensile fracture testing and testing of adhesion performance with casein hydrogel bioadhesive and fibrin gel gelling in-situ on porcine skin (n = 3).

Zhu 2023, White-light crosslinkable milk protein bioadhesive with ultrafast

UV-Sensitive Systems

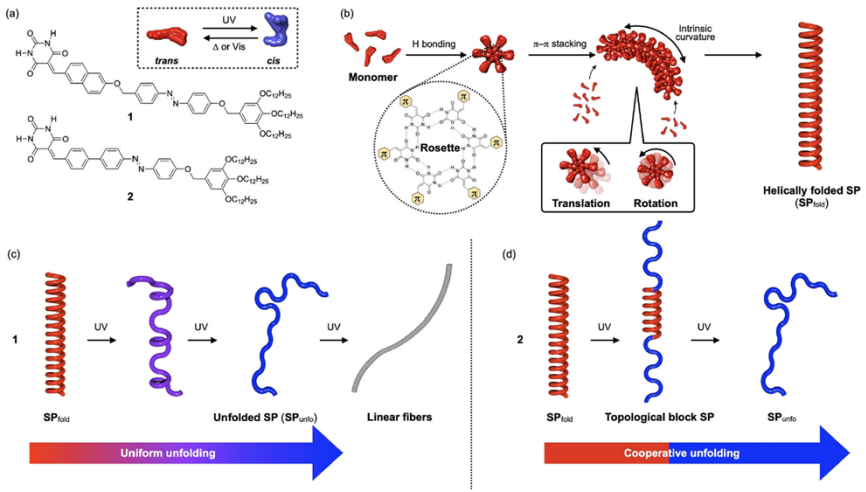

Figure 1. a) Molecular structures **1** and **2**. b) Formation mechanism of the SP_{fold}. c,d) Photo-induced unfolding processes of SP_{fold} composed of **1** (c) and **2** (d).

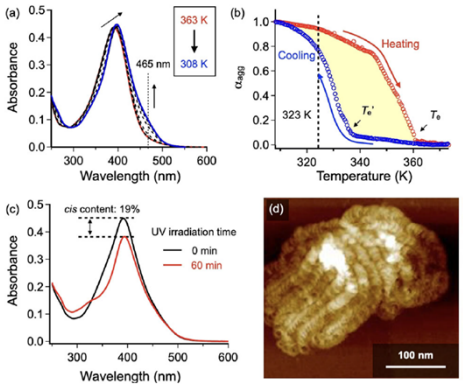

Figure 2. a) Temperature-dependent UV–Vis spectra of **2** ($c = 10$ μM) in MCH upon cooling from 373 to 308 K at a rate of 1.0 K min^{-1}. The cooling was ceased at 308 K to avoid precipitation upon further cooling to room temperature. b) Cooling (blue) and heating (red) curves of **2** ($c = 10$ μM) at a rate of 1.0 K min^{-1} obtained by plotting degree of aggregation α_{agg} (calculated from absorption change at 465 nm) as a function of temperature in MCH. c) UV–Vis absorption spectra of SP_{fold} of **2** in MCH before and after UV-light irradiation at 308 K for 60 min. d) AFM image of the SP_{fold} of **2** spin-coated onto highly oriented pyrolytic graphite (HOPG) after UV-light irradiation in MCH at 308 K for 60 min.

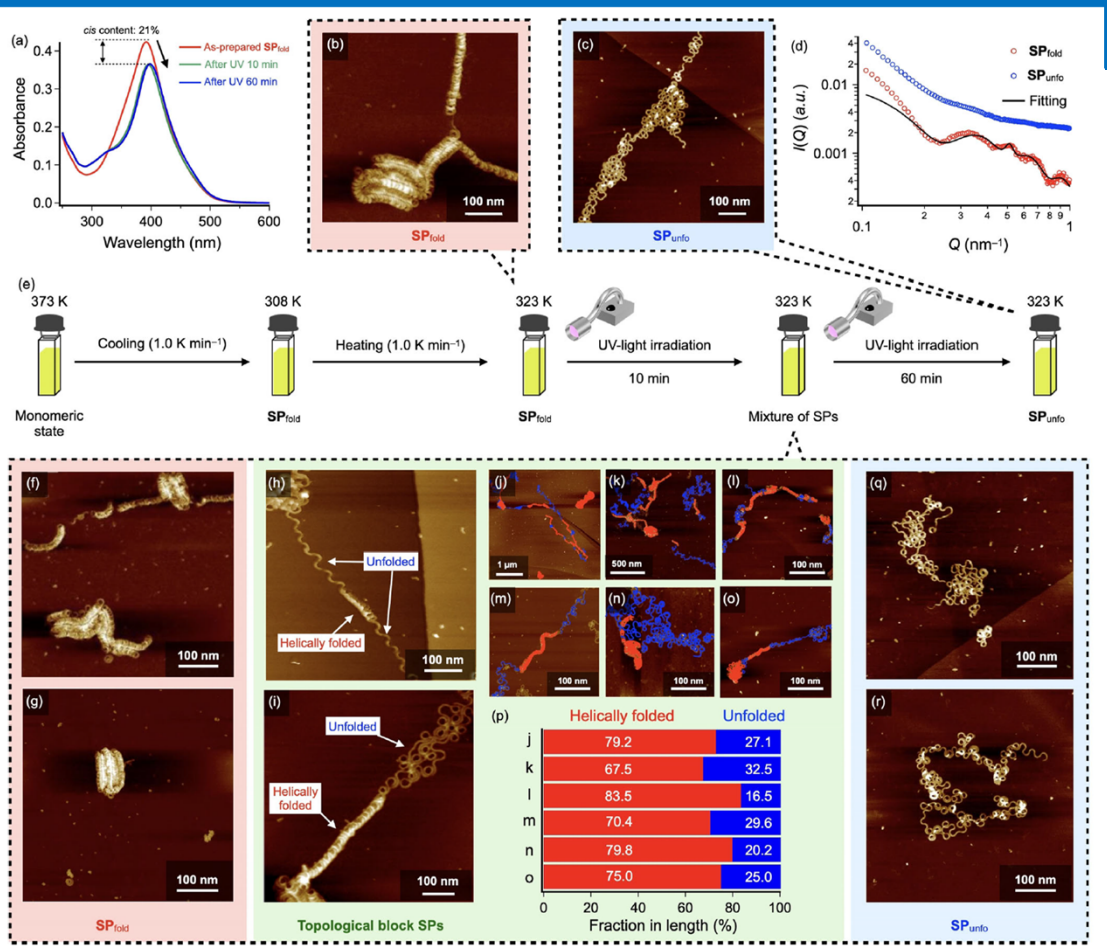

Figure 3. a) UV–Vis spectra of a MCH solution of **2** ($c = 10$ μM) during UV-light irradiation at 323 K. b,c) AFM images of SP_{fold} of **2** before UV-light irradiation (b) and SP_{unfo} of **2** after UV-light irradiation for 60 min at 323 K (c). d) Change of SAXS profiles of a SP_{fold} solution of **2** ($c = 50$ μM) upon UV-light irradiation at 323 K (from red to blue). The black line is a fit to the data using a core-multishell cylinder model. e) Schematic representation of procedure on photo-induced unfolding of SP_{fold} of **2** (f-o,q,r) AFM images of SP_{fold} (f,g), topological block SPs (h-o), and SP_{unfo} (q,r) found in a solution of **2** upon UV-light irradiation for 10 min at 323 K. In (j-o), helically folded and unfolded domains were colored with with red and blue, respectively. p) Fractions in length of helically folded and unfolded domains in the topological block SPs.

Tashiro 2021, Non-uniform photoinduced unfolding of supramolecular polymers leading to topological block nanofibers

Light-Sensitive Drug Release

On-Demand Opioid Effect Reversal with an Injectable Light-Triggered Polymer-Naloxone Conjugate

Wei Zhang, Dali Wang, Claire A. Ostertag-Hill, Yiyuan Han, Xiyu Li, Yueqin Zheng, Berwyn Lu, and Daniel S. Kohane*

Cite This: *Nano Lett.* 2023, 23, 10545−10553 | Read Online

ACCESS | Metrics & More | Article Recommendations | Supporting Information

ABSTRACT: Misuse of opioids can lead to a potential lethal overdose. Timely administration of naloxone is critical for survival. Here, we designed a polymer−naloxone conjugate that can provide on-demand phototriggered opioid reversal. Naloxone was attached to the polymer poly(lactic-*co*-glycolic acid) via a photocleavable coumarin linkage and formulated as injectable nanoparticles. In the absence of irradiation, the formulation did not release naloxone. Upon irradiation with blue (400 nm) light, the nanoparticles released free naloxone, reversing the effect of morphine in mice. Such triggered events could be performed days and weeks after the initial administration of the nanoparticles and could be performed repeatedly.

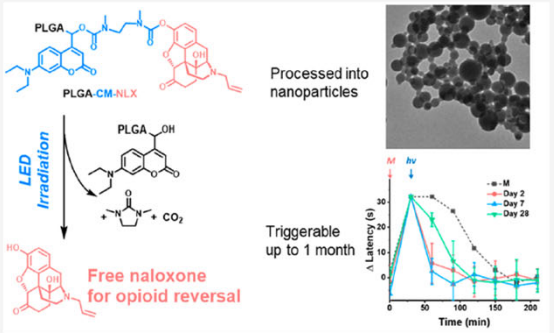

KEYWORDS: *Stimulus-responsive, photocleave, drug delivery, prodrug, naloxone, opioid*

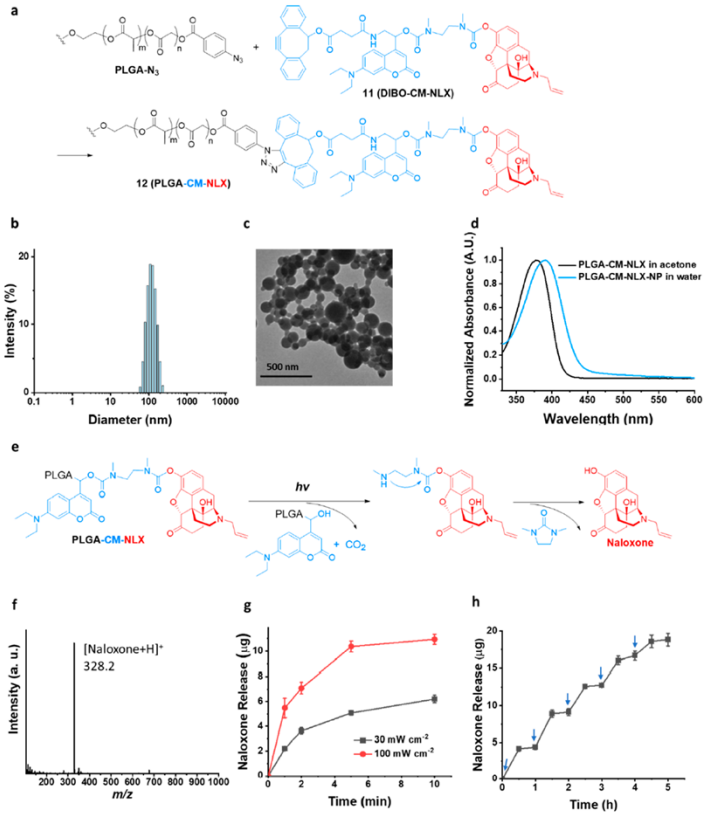

Figure 1. Synthesis, characterization, and in vitro photocleavage. (a) Synthesis of PLGA-CM-NLX. (b) DLS of the PLGA-CM-NLX nanoparticles. (c) TEM image of the PLGA-CM-NLX nanoparticles. (d) UV−vis spectra of the PLGA-CM-CM-NLX in acetone and nanoparticles in water. (e) Scheme of photocleavage releasing naloxone from PLGA-CM-NLX. (f) Mass spectrum of the cleaved naloxone. (g) Release of naloxone by photocleavage of NLX-NP (10 mg mL−1) over time with a 400 nm LED at different irradiances (n = 4, data are means ± SD). (h) Repeated phototriggered naloxone release from NLX-NP (arrows represent 2 min of irradiation with a 400 nm LED at 30 mW cm−2, n = 4, data are means ± SD).

Zhang 2023, On-demand opioid effect reversal with an injectable light-triggered polymer-naloxone conjugate

Enzyme-Responsive Systems

Enzyme-Degradable Polypeptide–PolyHIPE

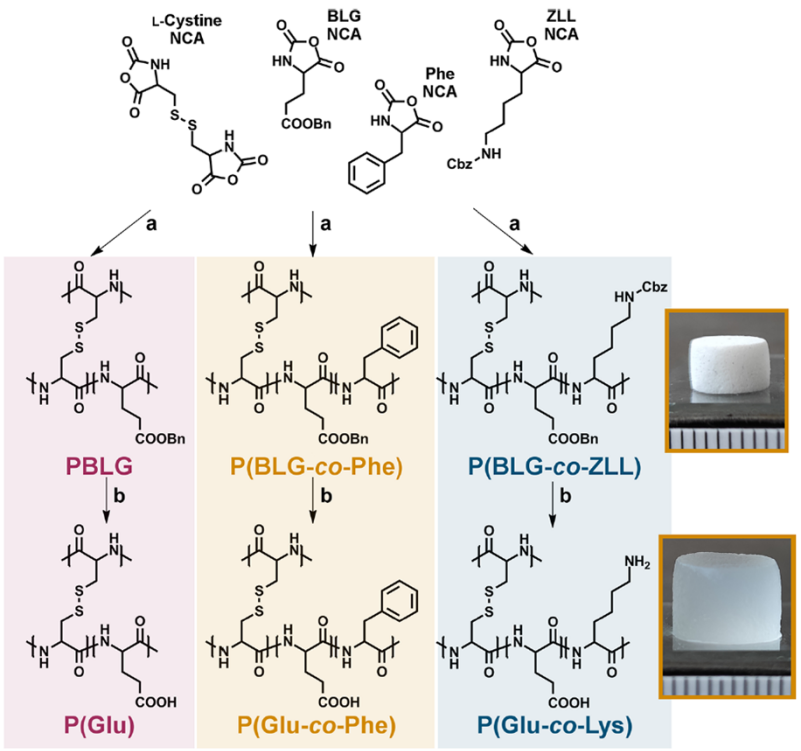

Figure 1. Schematic representation of the preparation of macroporous polypeptide hydrogels by (a) ROP of NCA in the continuous phase of HIPE, catalyzed with DIPEA and (b) followed by deprotection of the organogels in HBr/TFA. The photographs on the right show dry P(BLG-co-Phe, top) and swollen P(Glu-co-Phe, bottom) at pH 7.5 (scale interval 1 mm).

Onder 2021, Preparation of synthetic polypeptide–polyHIPE hydrogels with stimuli-responsive behavior

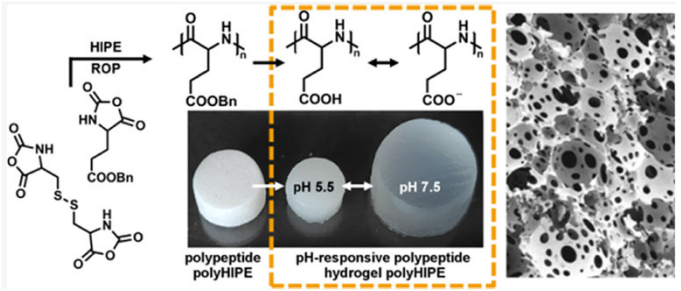

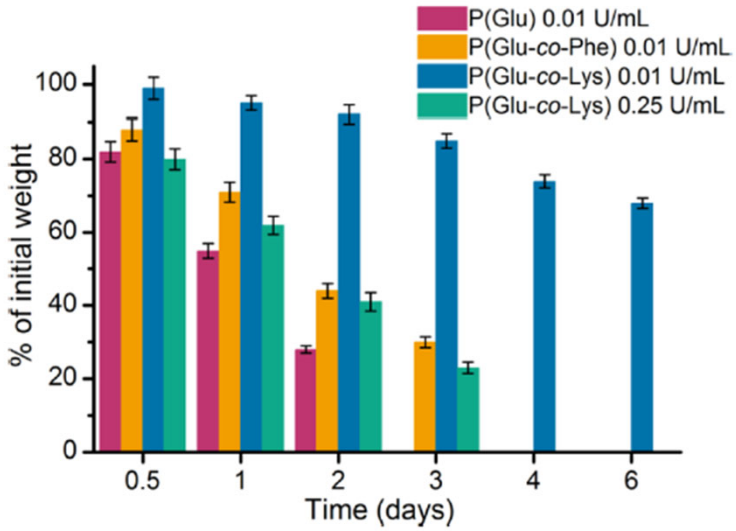

Figure 5. Enzymatic degradation profiles of P(Glu), P(Glu-co-Phe), and P(Glu-co-Lys) hydrogels in 0.01 U/mL protease type XIV solutions at pH 7.5 and 37 °C. P(Glu-co-Lys) hydrogels were also degraded in 0.25 U/mL protease type XIV solution under the same conditions. For each sample, average values of three specimens with standard errors are shown.

Enzyme-responsive Hydrogel Nanoparticles

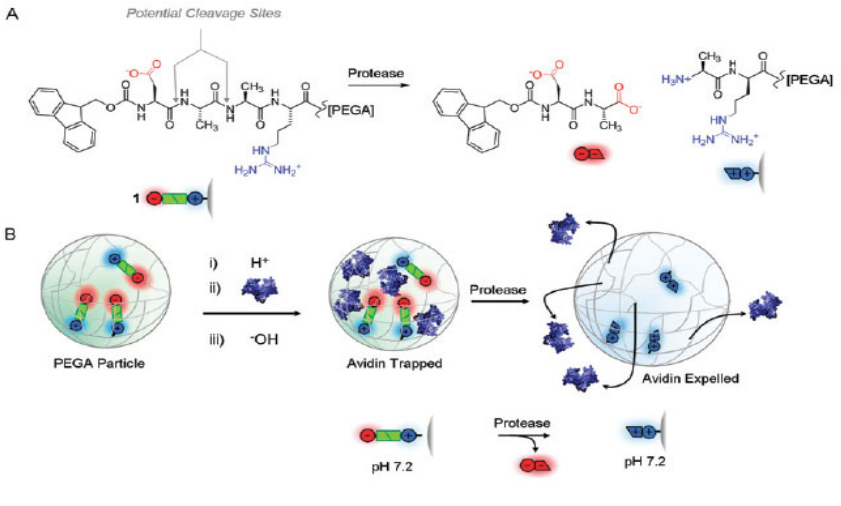

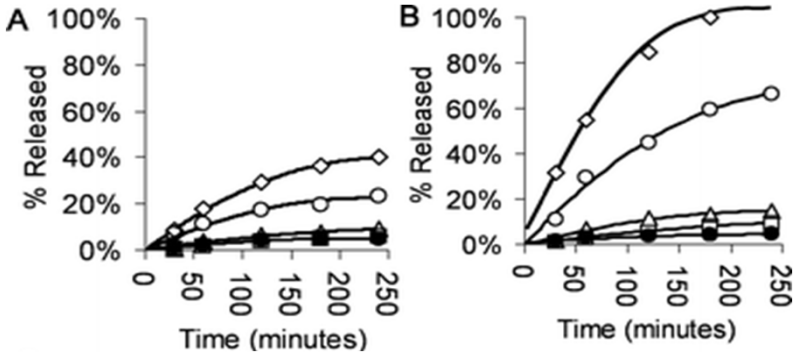

Albumin release Avidin release

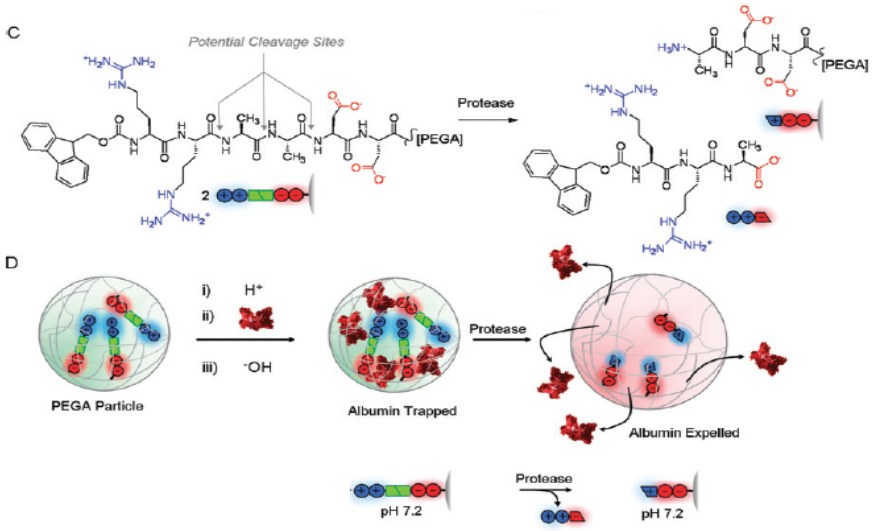

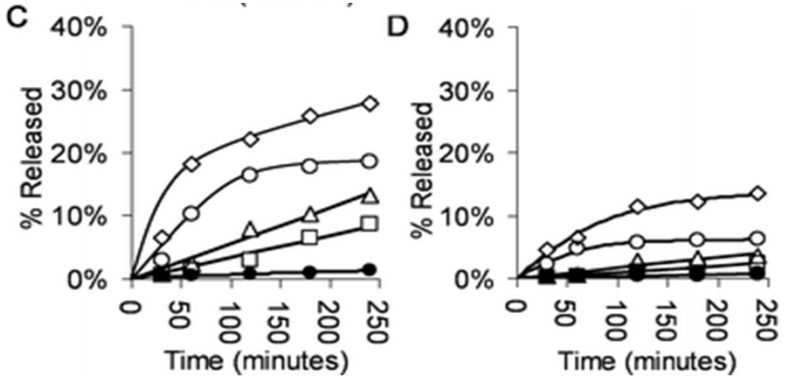

Albumin release Avidin release

Thornton. et al. *Soft Matt 4: 821,* 2008

Hypoxia-responsive Structures

Hypoxia-Activatable Nanosystems

Hypoxia-activated prodrugs (HAPs), on the other hand, represent a different strategy to deal with the hypoxic tumor microenvironment, turning this problem of hypoxia into a therapeutic target. Now, 11 types of HAPs have entered the clinical trial stage.96 HAPs are also known as bioreductive prodrugs. Under normoxic conditions, their dormant state will not cause toxic side effects to healthy organs, while in hypoxic regions, HAPs are activated by reductive metabolism and selectively kill hypoxic tumor cells. This is because, in hypoxic tumor cells, the unstable, oxygen-sensitive one-electron reduced HAP intermediates cannot be reversibly oxidized back to parent form as in normoxic conditions. Typical bioreductive drugs include quinones, N-oxides, and nitrocompounds. However, the current mainstream HAPs lack modification sites and do not need extra caging modification. Compared with other types of stimulus-activated prodrugs, the category of HAPs is still on a small scale, and many chemotherapy drugs that have been proven effective have

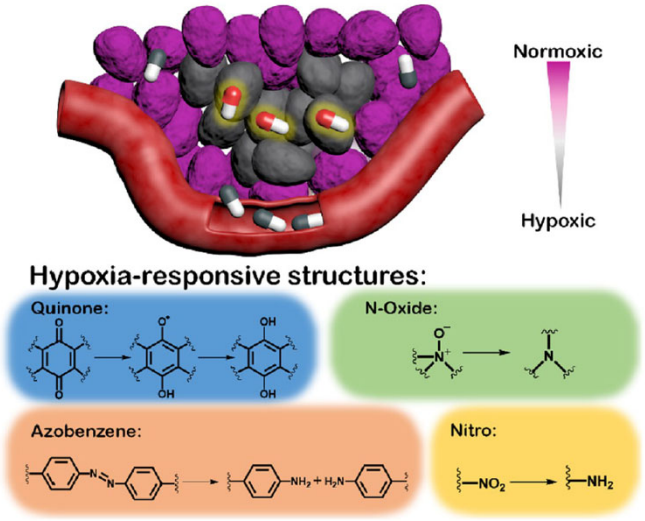

Scheme 4. Schematic illustration of hypoxia responsive prodrugs activated in hypoxic tumor regions and hypoxia-responsive structures for prodrug design.

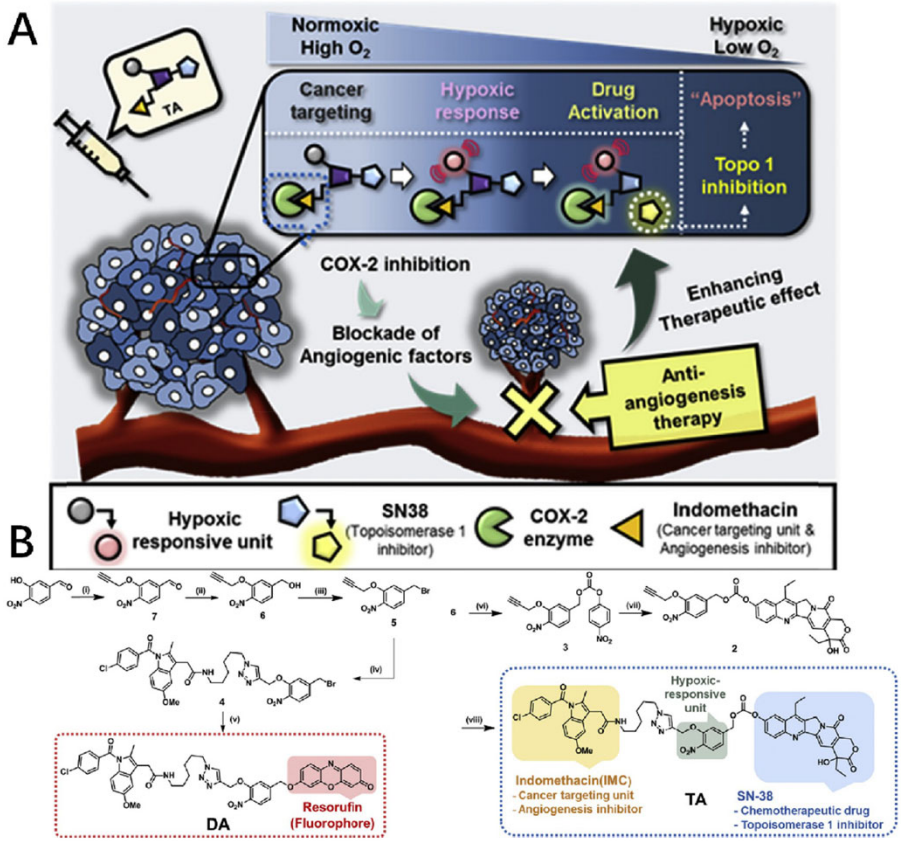

Figure 17. Hypoxia-responsive nitrobenzyl group used for prodrug design: (A) Theranostic prodrug system containing IND as tumor targeting moiety, angiogenesis inhibitor SN-38 as anticancer chemotherapy drug, and resorufin as diagnostic unit was activated in hypoxic tumor microenvironment, which was intensified by suppressing angiogenesis. (B) Synthetic route of nitrobenzyl containing diagnostic unit and therapeutic unit.

Ding 2022, Emerging strategies in stimuli-responsive prodrug nanosystems for cancer therapy

Self-Healing Polymers

Self Healing Plastics

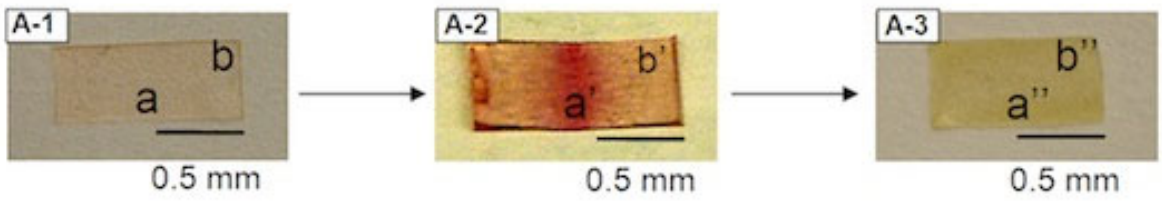

Cell phones, tablets, cars and even weapons systems that can heal themselves when scratched or cracked are no longer confined to science fiction. During the American Chemistry Society's annual conference on Monday, University of Southern Mississippi Professor Marek Urban demonstrated the new material and discussed numerous potential applications. When scratched or cracked, the new plastic responds on a molecular level and regenerates to repair itself without leaving any signs of damage. Similar developments in the past have made use of embedded capsules with repair material that would fill scratches when a plastic is cracked, but Urban's method repairs broken bonds when an outside stimulus is applied. In the case, sunlight alone can do the trick. "Our new plastic tries to mimic nature, issuing a red signal when damaged and then renewing itself when exposed to visible light, temperature or pH changes,"
Our material is what's called a thermoplastic,"— which means no cross-links are formed during the creation of the plastic. In contrast, plastics that *do* form cross-links are called "thermosets." The key difference between the two, explains Urban, is that once a thermoset cures, its structure is basically set for life, which makes it less-than-optimal for self-healing applications. "Thermoplastics, however, you can heat and reshape however you want," Urban explains.
When we pressed Urban to share more details with us about the bleeding capabilities of his team's latest plastic, he politely declined to go into specifics on the science, explaining that it would have to remain under wraps until a later date.

Nissan recently announced they were creating the world's first self-healing iPhone case that uses their "Scratch Shield" paint originally designed for cars.

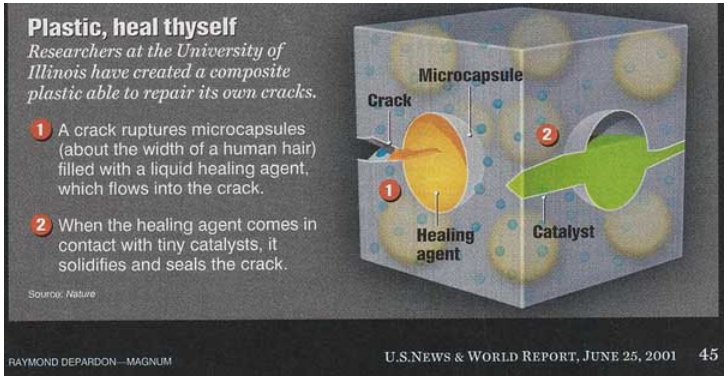

http://www.bgr.com/2012/03/29/scientists-create-self-healing-plastic-the-holy-grail-of-material-science/
http://io9.com/5897475/new-bleeding-healing-plastic-will-be-used-on-airplanes-not-androids

Self Healing Finish

Scratch Shield: Nissan Introduces World's First Self-Healing iPhone Case
Serkan Toto@serkantoto / 6:08 AM EST•January 17, 2012

An iPhone case from Nissan? As you can imagine, it would make no sense for the automaker to develop an ordinary case, and the so-called Nissan Scratch Shield iPhone Case is actually special. According to the company, it's the world's first "self-healing" iPhone cover: in other words, it quickly fixes (fine) scratches by itself.

Nissan says they used their self-healing paint finish originally developed for vehicles for the case, which is made from light weight ABS plastic. Scratch Shield as a paint technology has been used in various Nissan cars since 2005, before Nissan teamed up with the University of Tokyo and Japan-based Advanced Softmaterials [JP] to create the case.

Nissan explains:

The outer 'paint' is made from polyrotaxane, which means that when damage occurs to the coating in the form of a fine scratch, the chemical structure is able to react to change back to its original shape and fill the gap – 'healing' the blemish.

The company distributed a number of prototype iPhone cases to journalists and "customers" and might commercialize the product later this year. Mobile carrier Docomo is already offering the NEC N-03B, a feature phone using Scratch Shield, on the Japanese market.

https://techcrunch.com/2012/01/17/nissan-scratch-shield/

Acrylonitrile butadiene styrene (ABS)

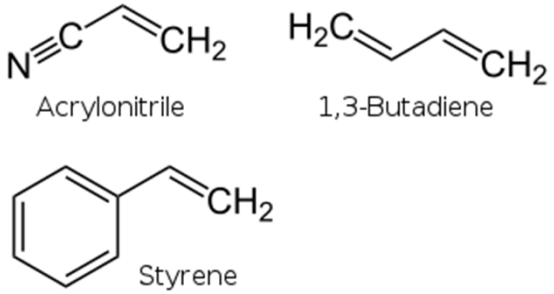

Slide-Ring Material is basically formed with a nanosize "necklace" made from molecules. This is referred to as "polyrotaxane" and is comprised of three materials: the linear polymer "polyethyleneglycol (PEG)", the cyclic molecule "cyclodextrin (CD)" and the stopper molecule "adamantane". Polyrotaxane was first composed at the laboratory of Prof. Akira Harada at Osaka University in 1990. In the field of chemistry, the complex of molecules like polyrotaxane is called a "supermolecule".

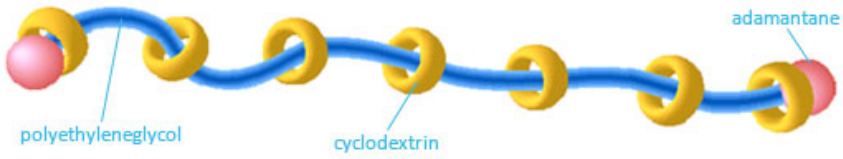

https://www.asmi.jp/en/tech/

Self-Healing Hydrogels

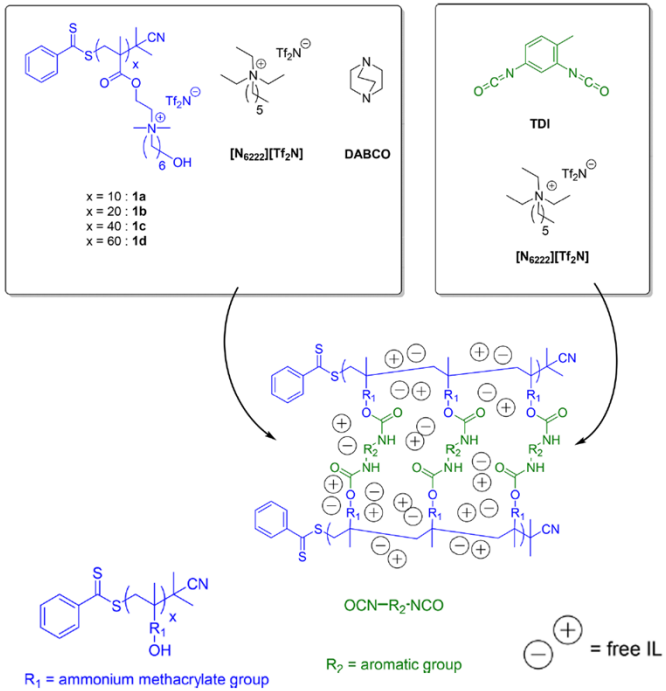

Scheme 1. Structures of curable coating components and resulting cross-linked polyurethane network composite coatings.

ABSTRACT: A peelable gel coating based on a curable ammonium-alcohol ionic liquid (IL) prepolymer has been developed for the decontamination of toxic industrial chemicals (TICs) from porous substrates. The physical properties of these coatings can be tuned by controlling the prepolymer molecular weight (prepared by RAFT polymerization) and by altering the formulation of the initial coating mixture. The initially applied (uncured) solutions can be applied onto porous wood and ceramic substrates with minimal soak-in, and these films cure quickly in situ under ambient conditions. These coatings were tested in a series of assays meant to demonstrate their effectiveness as TIC vapor barriers and materials that absorb liquid TICs from the aforementioned substrates. The coatings were found to suppress ~80% of the vapor released by a TIC simulant (odichlorobenzene) from these substrates and to extract up to 85% of the mass of the originally applied simulant that soaked into these substrates.

Mori 2018, Curable ionic liquid prepolymer-based ion gel coating system

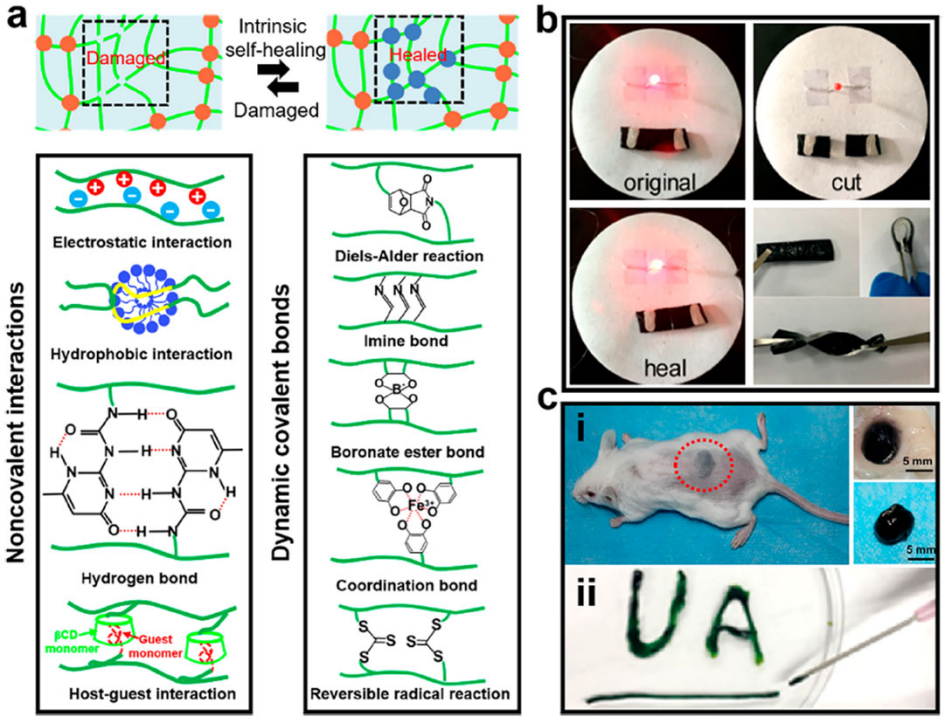

Figure 4. Self-healing and injectable conductive hydrogels. (a) Schematic illustration and mechanism diagram of fabricating intrinsic self-healing conductive hydrogels. (b) Self-healing conductive hydrogel based on transferring CNT film into a repairable carrageenan/PAAm hydrogel. (c) Injectable self-healing conductive hydrogels. The upper panel (i) shows the subcutaneous injection of a Dex-AT/CECS conductive hydrogel. The lower panel (ii) shows an injectable PANI/PSS-UPy conductive hydrogel that can pass through a needle and be molded into different shapes.

Fu 2020, Functional conductive hydrogels for bioelectronics

Self Healing Thermosets

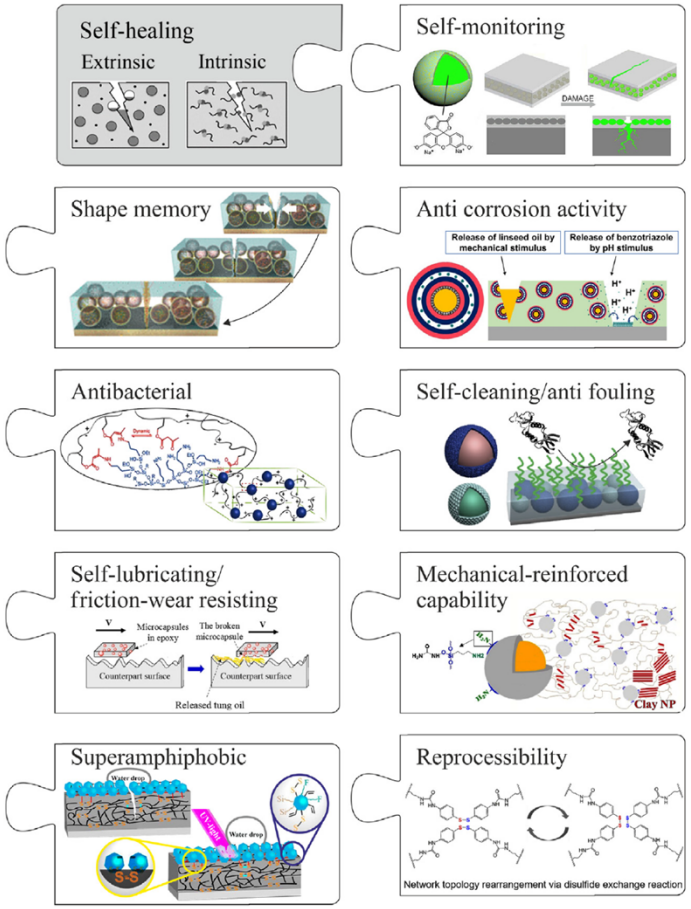

Kutuzova 2022, Self-healing thermosets

FIGURE 22.1 Multifunctional self-healing thermoset systems in composite coating and matrix composite applications [6]: self-healing ability in combination with corrosion protection [40], mechanical reinforcement [50], self-monitoring [51], self-cleaning and superamphiphobic [39,53], self-lubricating [72], antibacterial [73] properties, shape memory [64], and reprocessability [68]. *Modified after Zhang Y, Yuan L, Guan Q, Liang G, Gu A. Developing self-healable and antibacterial polyacrylate coatings with high mechanical strength through crosslinking by multi-amine hyperbranched polysiloxane viadynamic vinylogous urethane. J Mater Chem A 2017;5(32):16889–97. Available from: https://doi.org/10.1039/C7TA04141A; Huang Y, Deng L, Ju P, Huang L, Qian H, Zhang D, et al. Tripleaction self-healing protective coatings based on shape memory polymers containing dual-function microspheres. ACS Appl Mater Interfaces 2018;10 (27):23369–79. Available from: https://doi.org/10.1021/acsami.8b06985; Zhao D, Du Z, Liu S, Wu Y, Guan T, Sun Q, et al. UV light curable self-healing superamphiphobic coatings by photo-promoted disulfide exchange reaction. ACS Appl Polym Mater 2019;1(11):2951–60. Available from: https://doi.org/10.1021/acsapm.9b00656; Chen J-H, Hu D-D, Li Y-D, Meng F, Zhu J, Zeng J-B. Castor oil derived poly(urethane urea) networks with reprocessibility and enhanced mechanical properties. Polymer 2018;143:79–86. Available from: https://doi.org/10.1016/j.polymer.2018.04.013 [68].*

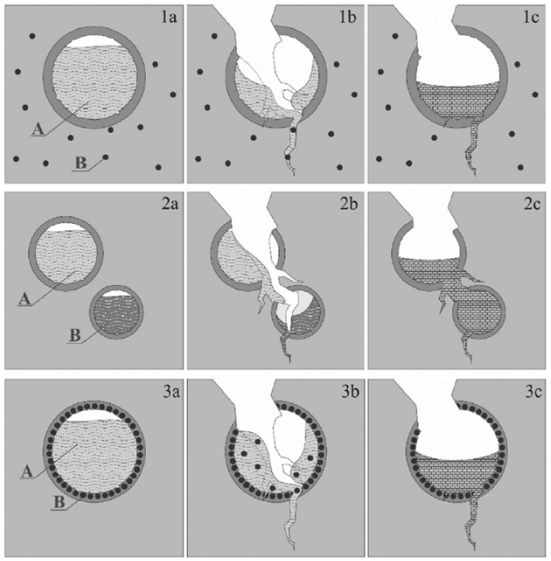

FIGURE 22.19 Self-healing approach based on rupture-release microcapsules: (1) monocapsule or capsule-catalyst systems; (2) dual-capsule system; (3) all-in-one capsule system.

A fundamental problem in the use of materials in general is the loss of their functionality during practical application. This loss of functionality may be due to continuous wear and tear of the materials during their use or to abrupt damage caused by the sudden impact of harmful events such as impact, shock, or pull. This material failure leads to an undesirable collapse in mechanical strength and can cause further consequential damage. An essential strategy to improve the long-term stability of materials under application conditions is the implementation of self-healing properties in the material.

PVA-Boric Acid Gel

Scheme 1. Reactions of BDBA with Hydroxyl Groups on *x*PVAc Form Mono- (Yellow) and Diesterified (Red) Boronate Species, of which Only the Diesterified Species Lead to Intra- and Interchain Crosslinks between Polymer Chains (Blue)

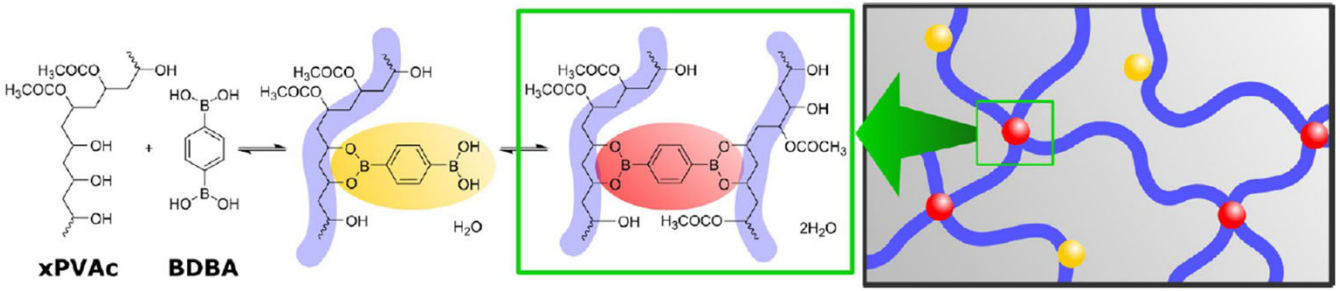

Soft, peelable organogels from 40% hydrolyzed poly(vinyl acetate) (40PVAc) and benzene-1,4-diboronic acid (BDBA).

Figure 1. Gels of 6 wt % 40PVAc/0.3 wt % BDBA in methanol, DMSO, and THF (left to right) 7 days after preparation.

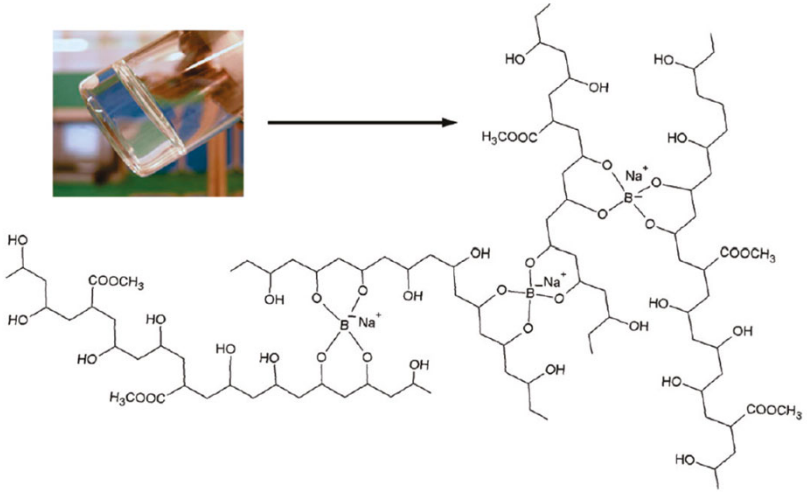

Scheme 1. Representation of the structure of the PVAc network induced by borate cross-links and (top left) an example of a cross-linked aqueous dispersion.

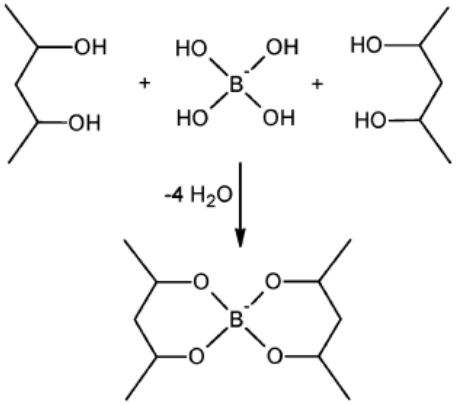

"Peelable" Gels. Hydrogels employing two component gellants, poly(vinyl alcohol) and borate as a crosslinker (PVA-B) have been investigated extensively. The ester cross-links are reversible, so a steady-state concentration of them is established. Initially formed gels "age", allowing conformations of the polymer chains and locations of cross-links to change. Depending upon the length (i.e., average molecular weight) of the PVA chains, the concentrations of PVA and borate ion, temperature, and pH of the aqueous part, the gels can be very stiff or quite malleable.

Duncan 2017, Soft, peelable organogels from partially hydrolyzed poly(vinyl acetate
Natali 2011, Structural and mechanical properties of "peelable" organoaqueous dispersion
Carretti 2009, New frontiers in materials science for art conservation: Responsive gels and beyond.

Self Healing, Highly Compressible Soft Polymer Network

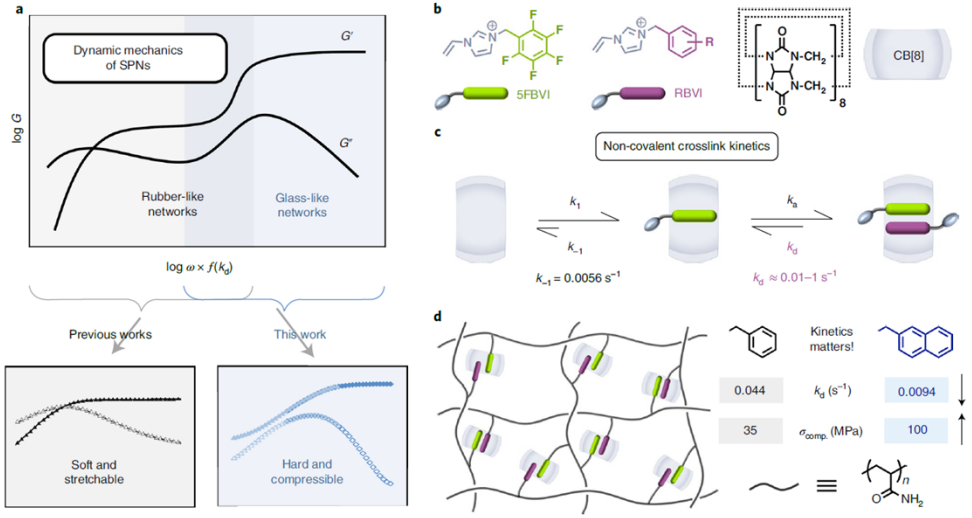

Fig. 1 | Design of glass-like SPNs. a, Schematic overview of the frequency (ω)-dependent dynamic mechanics of SPNs (top) including two real data sets of a reported SPN (left, grey)[20] and this report (right, blue). **b**, Molecular structures of perfluorophenyl (5FBVI), substituted phenyl (RBVI) guests and the host macrocycle (cucurbit[8]uril, CB[8]). **c**, Ternary complexation equilibrium of host-enhanced polar–π interactions including first and second association and their related kinetic parameters (k_1, first-step association constant; k_{-1}, first-step dissociation constant). **d**, Supramolecular polyacrylamide networks crosslinked by the above interactions and two RBVI guests that exhibit slow-dissociative kinetics and high compressive strengths ($\sigma_{comp.}$).

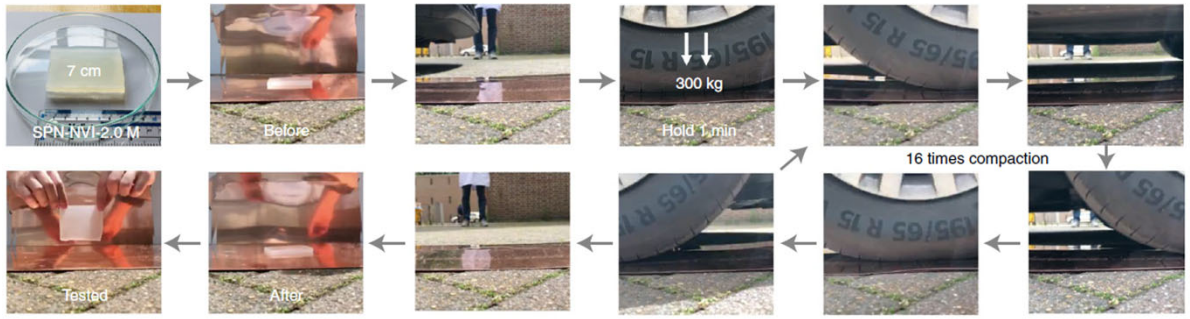

Photographs of a car-compression test carried out by compressing a 70 (L) × 50 (W) × 6 (T) mm cuboid specimen with a 1,200 kg four-wheel car for 1 min followed by 16 consecutive effects.

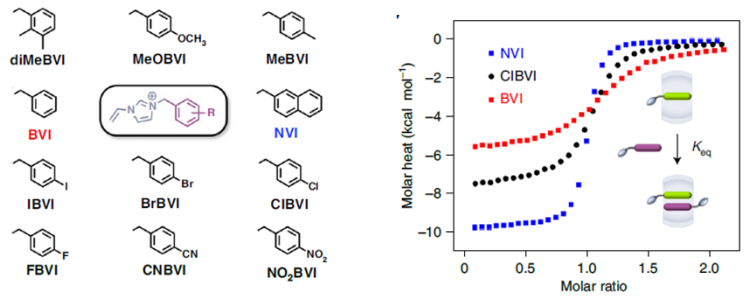

Fig. 2 | Thermodynamic and kinetic properties of slow-dissociative non-covalent crosslinks. **a**, Molecular structures for all RBVI second guests. **b**, Three typical ITC plots obtained by titration of NVI, ClBVI and BVI (5 mM) into 5FBVI-CB[8] (0.5 mM), respectively.

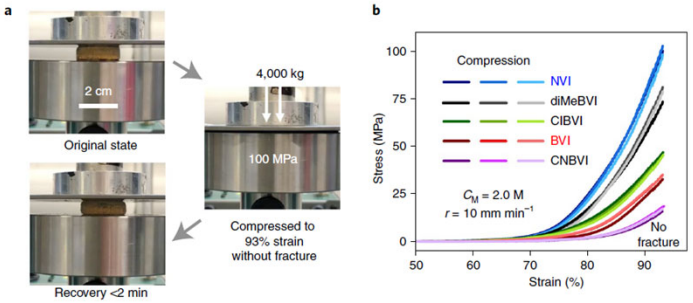

Fig. 4 | Evaluation of compressive properties of glass-like SPNs. **a**, Photographs of a typical compressive test including uniaxial compression and self-recovery of a cylindrical specimen (22 mm D × 7 mm H). **b**, Compressive stress–strain curves for four SPNs based on 5FBVI-CB[8] and NVI (blaue), diMeBVI (black), ClBVI (green), BVI (red) or CNBVI (purple) crosslinks.

Huang 2021, Highly compressible glass-like supramolecular polymer networks

Self Healing Polymers

Self-healing materials open new prospects for more sustainable technologies with improved material performance and devices' longevity.

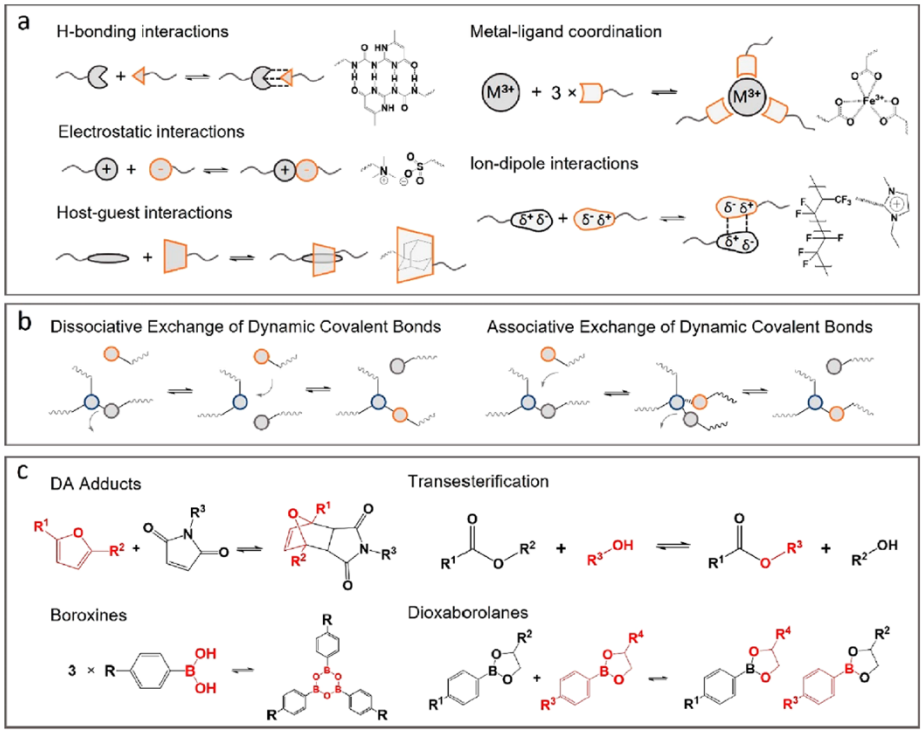

Figure 3. Illustrations of the different dynamic bonds. (a) noncovalent bonds; (b,c) dynamic covalent bonds

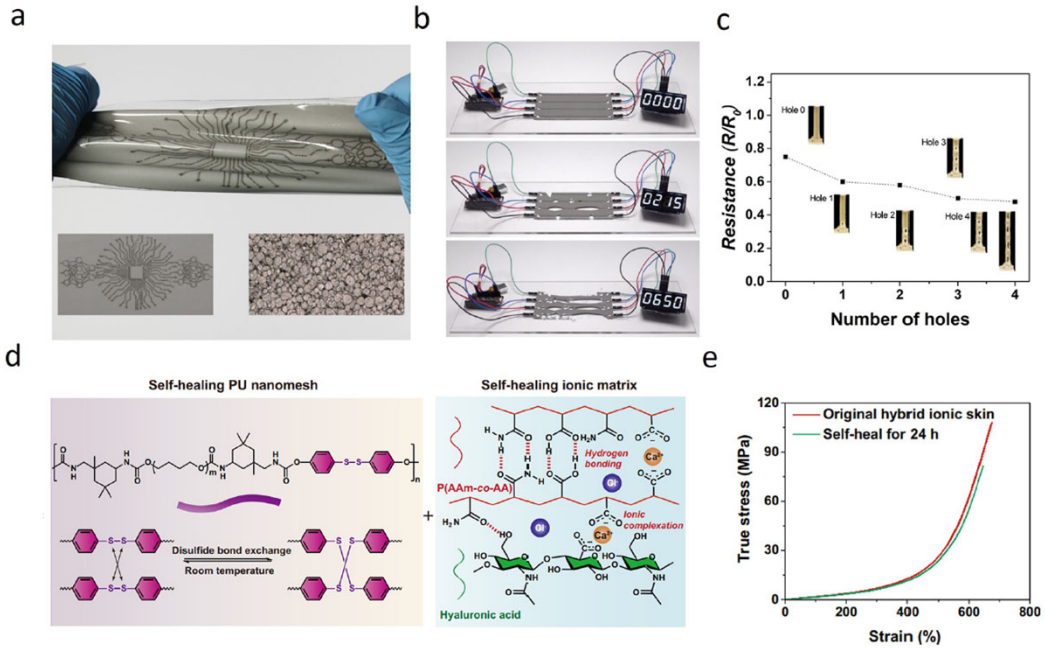

Figure 20. Self-healing polymer for strechable electronics applications. (a) Liquid metal elastomer composite being stretched and twisted with an intricate design of electrically conductive traces. (b) Example of the reconfigurable material (ϕ = 50%) transmitting dc power after severe damage was induced. (c) Photos of hole-punch test during tension; no loss in electrical conductivity was observed after stretch. (d) Schematic illustrations of the hybrid structure and respective self-healing mechanisms of PU nanomesh scaffold and ionic matrix. (e) True stress− strain curves of the original and self-healed hybrid ionic skins.

Li 2022, Intrinsically self-healing polymers- From mechanistic insight to current challenges

Vitrimers

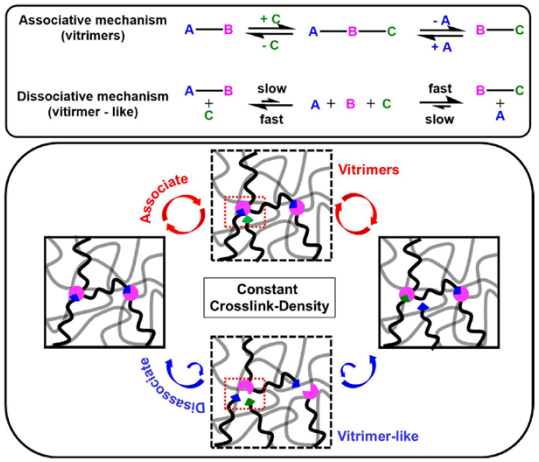

Scheme and image illustration of vitrimers and vitrimer-like materials. The crosslink density of these materials is almost constant at different temperature

Covalent Adaptable Networks (CANs) are polymeric materials with covalent crosslinks which become reversibly dynamic when a specific stimuli such as heat, catalyst, light, or pH is applied. In the absence of the corresponding stimuli, their cross-linked structure can impart to them thermoset-like properties such as increased strength and durability.

Vitrimers are a new class of CANs. In contrast to CANs, the crosslinks of these vitrimers are associative in nature, with their crosslinks being broken only when new bonds are formed. As a result, the crosslink density of associative CANs can be considered almost constant regardless of external stimuli.

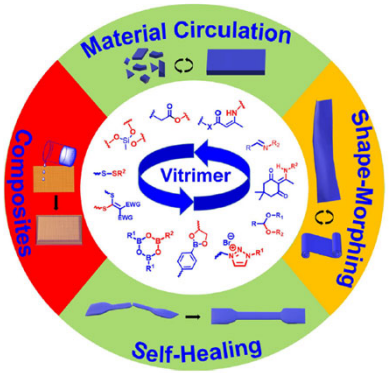

Schematic illustration of dynamic covalent bonds used in vitrimeric materials and their applications.

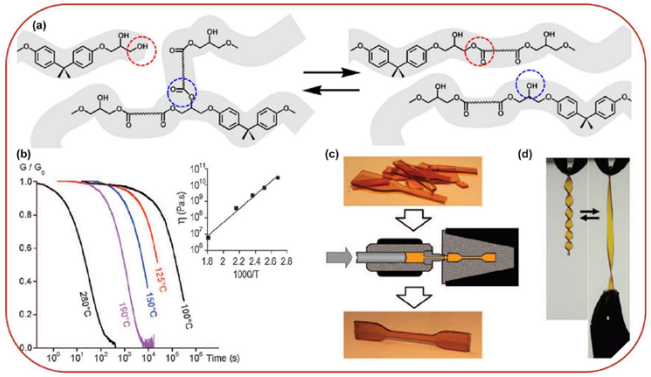

(a) Illustration of transesterification in hydroxyl-ester networks. (b) Normalized stress relaxation at different temperatures. The inset shows the temperature variation of zero-shear viscosity. (c) Reprocessing the broken pieces in an injection machine to recover its initial aspect and properties. (d) Reshaping the sample into a fusilli-shape.

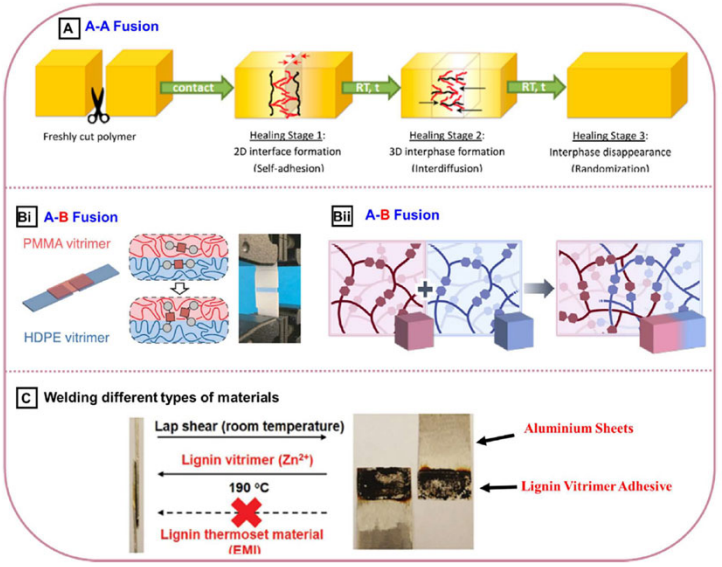

Schematic illustration of (a) A–A fusion, (b) A–B fusion, and (c) welding different types of materials using vitrimers.

Zheng 2021, Vitrimers- Current research trends andtheir emerging applications

Vitrimers

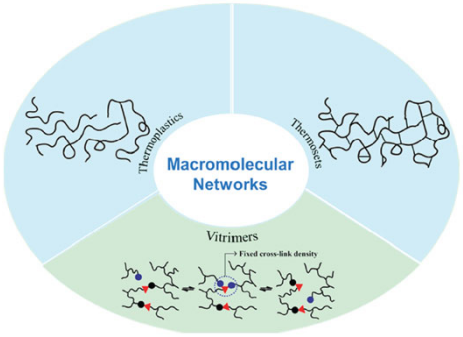

Figure 1. The macromolecular networks of thermoplastics, thermosets and vitrimers. Zhang 2022, Recycling strategies for vitrimers

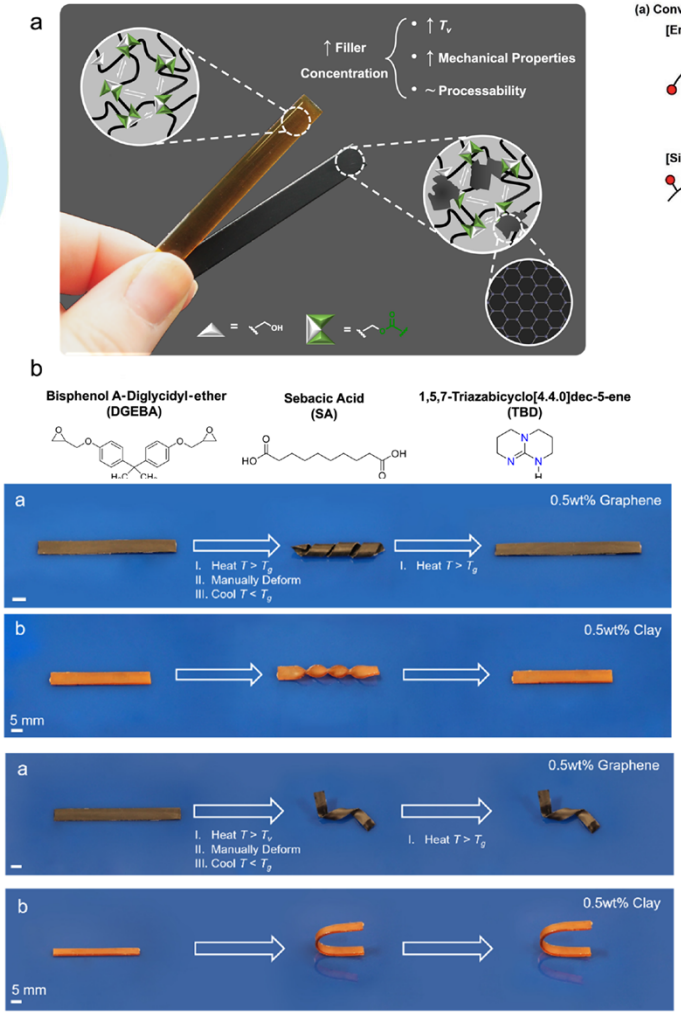

Hubbard 2022, Vitrimer vomposites- Understanding the role of filler in vitrimer applicability

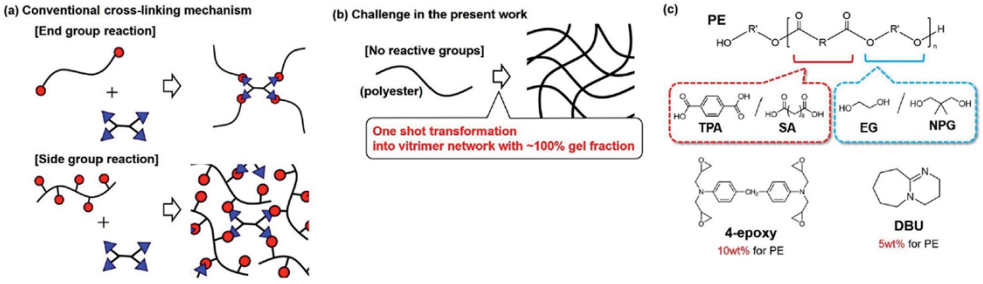

Fig. 1 Schematic representation of (a) conventional cross-linking mechanisms, (b) the challenge in the present work, and (c) components of the present vitrimer preparation.

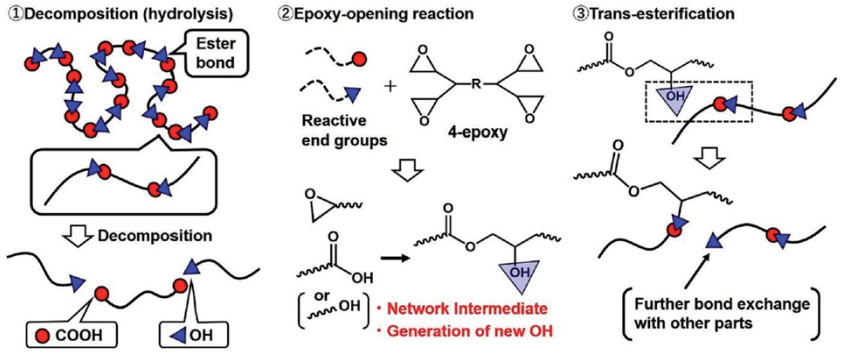

Fig. 3 Probable cross-linking mechanism derived from the experimental results.

Kimura 2022, One-shot transformation of ordinary polyesters into vitrimers- decomposition triggered cross-linking and assistance of dynamic covalent bonds

Smarter but Not Smart Enough

Getting Smarter

- Smarter materials:
  - proteins, peptides, DNAs, hybrid materials, affordable degradable materials
- Smarter response:
  - multiple stimuli-sensitivity, new stimuli, fast-responsive
- Smarter function:
  - cell-free enzyme synthesis, microfabrication, extracellular matrix, bioseparation, actuation, sensor

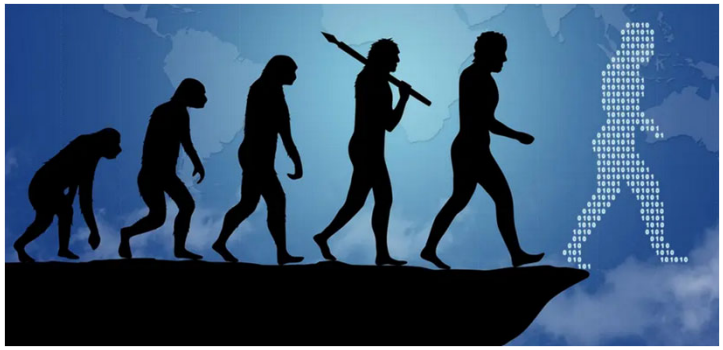

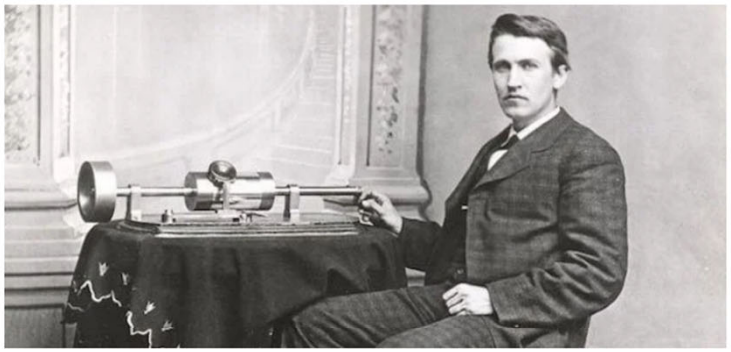

National Park Service, Thomas Edison National Historical Park

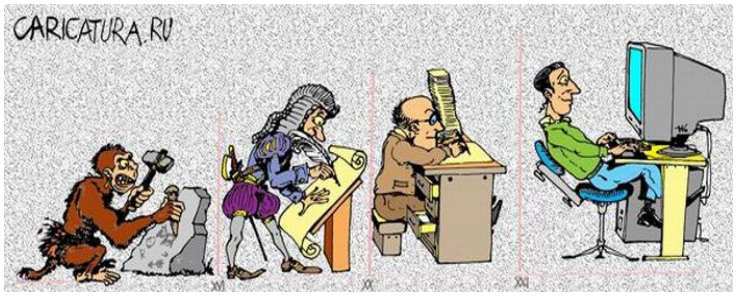

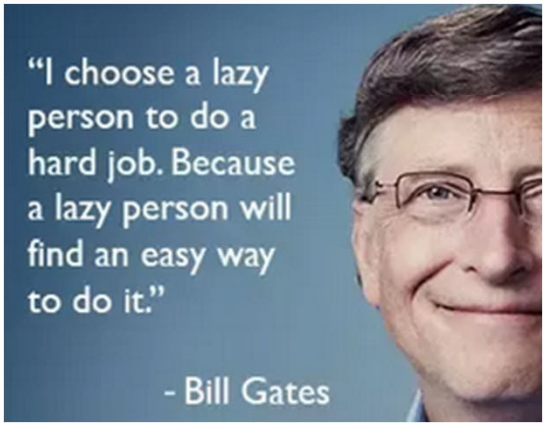

Current	Future

Material development:
Smart hydrogels with high IQ

Target application:
Understand physiological requirements

Find applications:

Mismatch between material properties and application

Clinical success:

Faster translation to clinical formulations

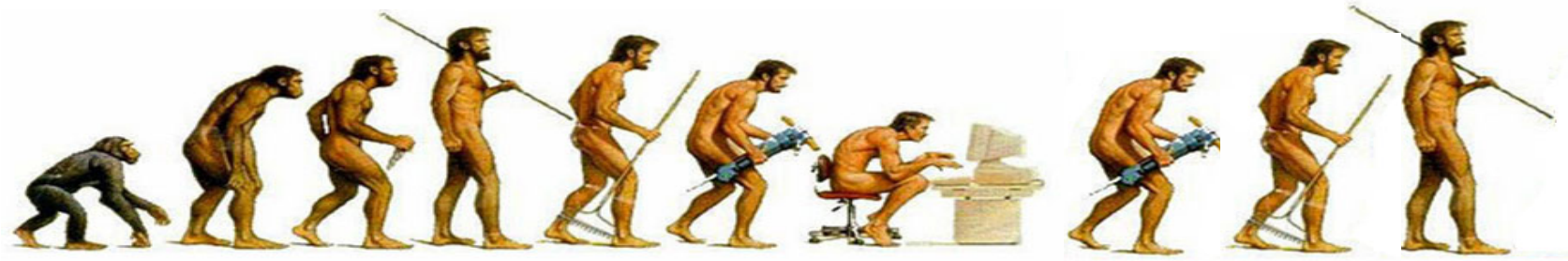

Getting Smaller

Faster

'Galaxy' of Stimuli-responsive Polymers

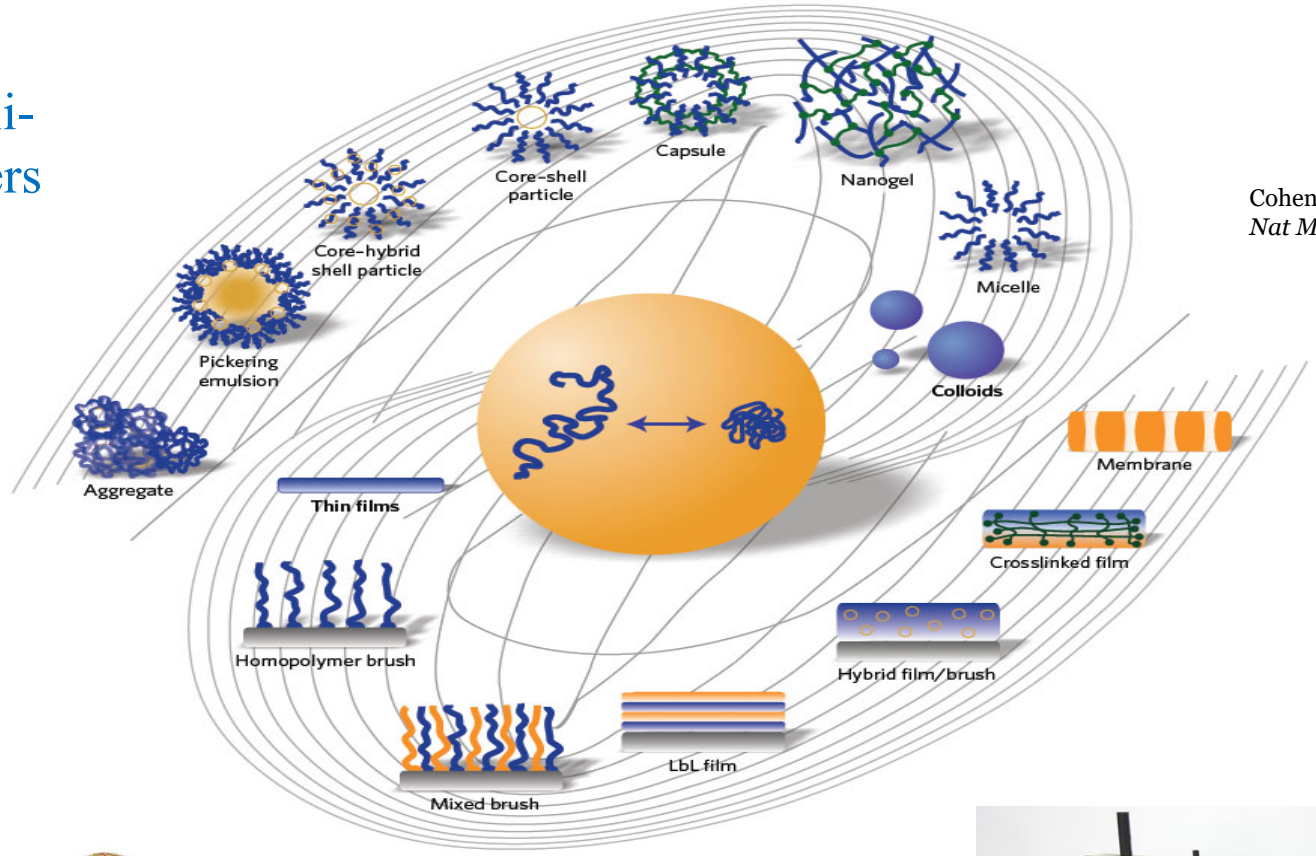

Cohen Stuart, et al.
Nat Mater 9: 101, 2010

Getting Smarter

REVIEW ARTICLE OPEN

Smart nanoparticles for cancer therapy

Leming Sun[1,2], Hongmei Liu[1], Yanqi Ye[3], Yang Lei[2], Rehmat Islam[2], Sumin Tan[1], Rongsheng Tong[1], Yang-Bao Miao[4]✉ and Lulu Cai[1]✉

Smart nanoparticles, which can respond to biological cues or be guided by them, are emerging as a promising drug delivery platform for precise cancer treatment. The field of oncology, nanotechnology, and biomedicine has witnessed rapid progress, leading to innovative developments in smart nanoparticles for safer and more effective cancer therapy. In this review, we will highlight recent advancements in smart nanoparticles, including polymeric nanoparticles, dendrimers, micelles, liposomes, protein nanoparticles, cell membrane nanoparticles, mesoporous silica nanoparticles, gold nanoparticles, iron oxide nanoparticles, quantum dots, carbon nanotubes, black phosphorus, MOF nanoparticles, and others. We will focus on their classification, structures, synthesis, and intelligent features. These smart nanoparticles possess the ability to respond to various external and internal stimuli, such as enzymes, pH, temperature, optics, and magnetism, making them intelligent systems. Additionally, this review will explore the latest studies on tumor targeting by functionalizing the surfaces of smart nanoparticles with tumor-specific ligands like antibodies, peptides, transferrin, and folic acid. We will also summarize different types of drug delivery options, including small molecules, peptides, proteins, nucleic acids, and even living cells, for their potential use in cancer therapy. While the potential of smart nanoparticles is promising, we will also acknowledge the challenges and clinical prospects associated with their use. Finally, we will propose a blueprint that involves the use of artificial intelligence-powered nanoparticles in cancer treatment applications. By harnessing the potential of smart nanoparticles, this review aims to usher in a new era of precise and personalized cancer therapy, providing patients with individualized treatment options.

Signal Transduction and Targeted Therapy (2023)8:418 ; https://doi.org/10.1038/s41392-023-01642-x

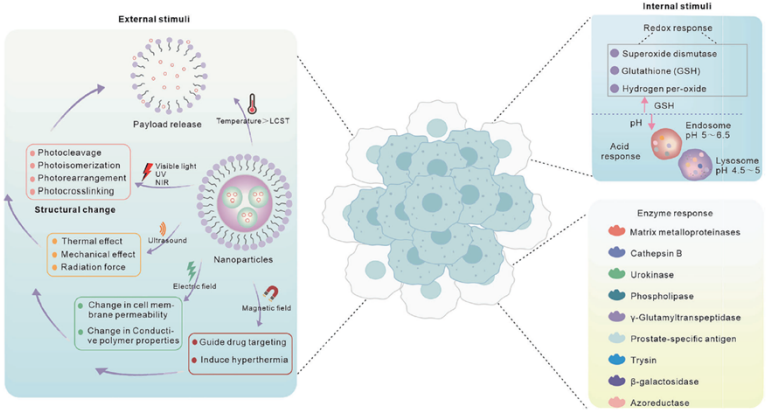

Sun 2023, Smart nanoparticles for cancer therapy

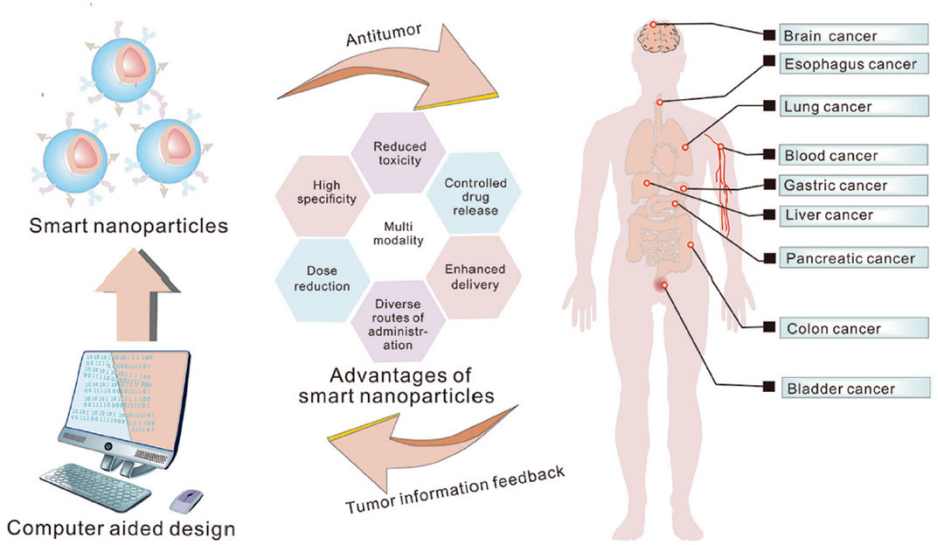

Fig. 1 Schematic illustration of smart nanoparticles for cancer treatment

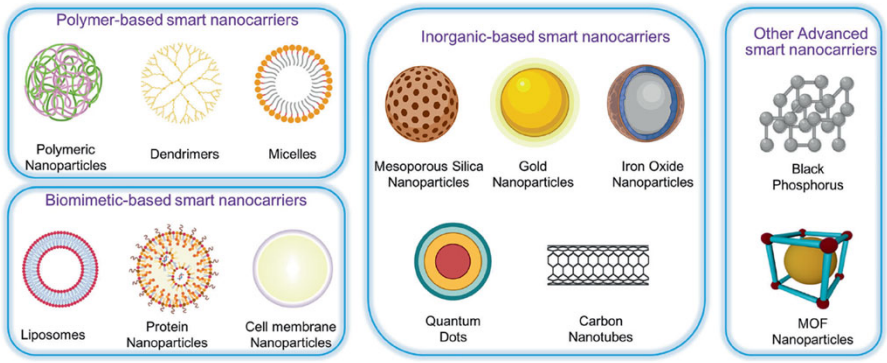

Fig. 2 Nanocarriers for smart nanoparticles

Mimicking Biosystems

Biomimetics

"Study of Materials, Structures, and Processes designed through eons of evolution of life to inspire and improve the engineering & design of artificial materials, man-made structures & processes." (Marc J. Madou, *Fundamentals of Microfabrication. The science of Miniaturization*. 2nd Edition. CRC Press. 2002).

Artificial materials that function as biological entities do.

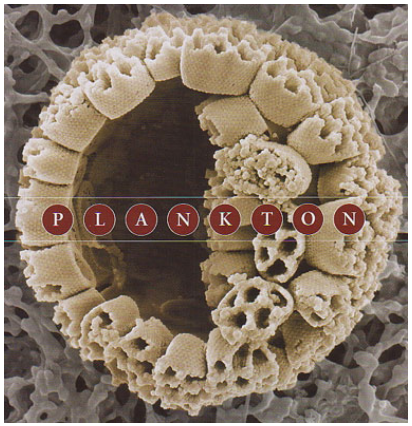

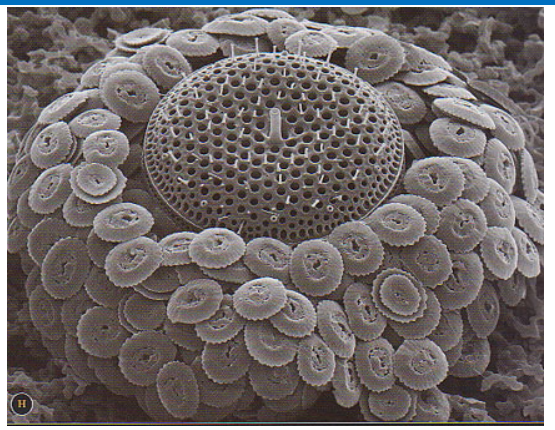

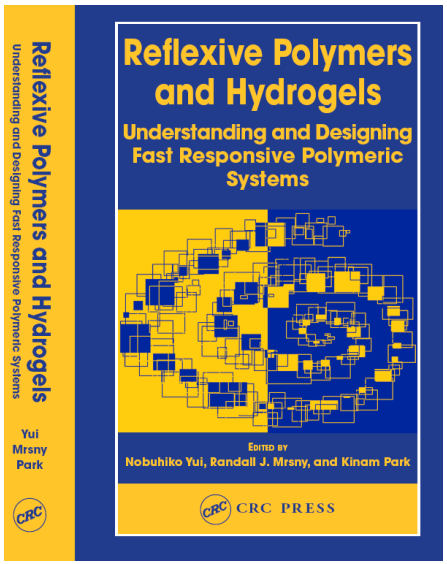

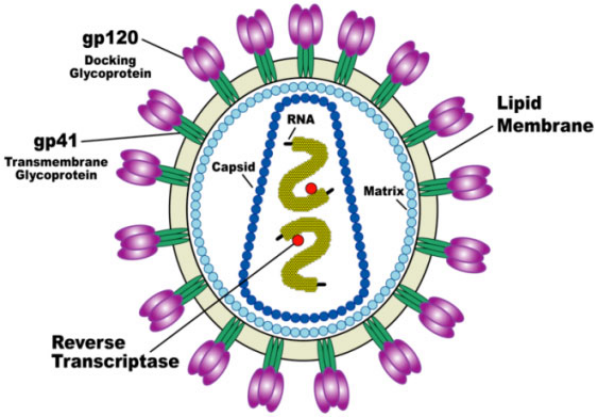

Natural Systems	Synthetic Systems
Efficacy, Simplicity (Bottom-up)	Diffusion, Selectivity (Top-down)
⇩	⇩
Survival	Miniaturization
⇩	⇩
Biological Need	Clinical Efficacy

The Invisible Gorilla Experiment

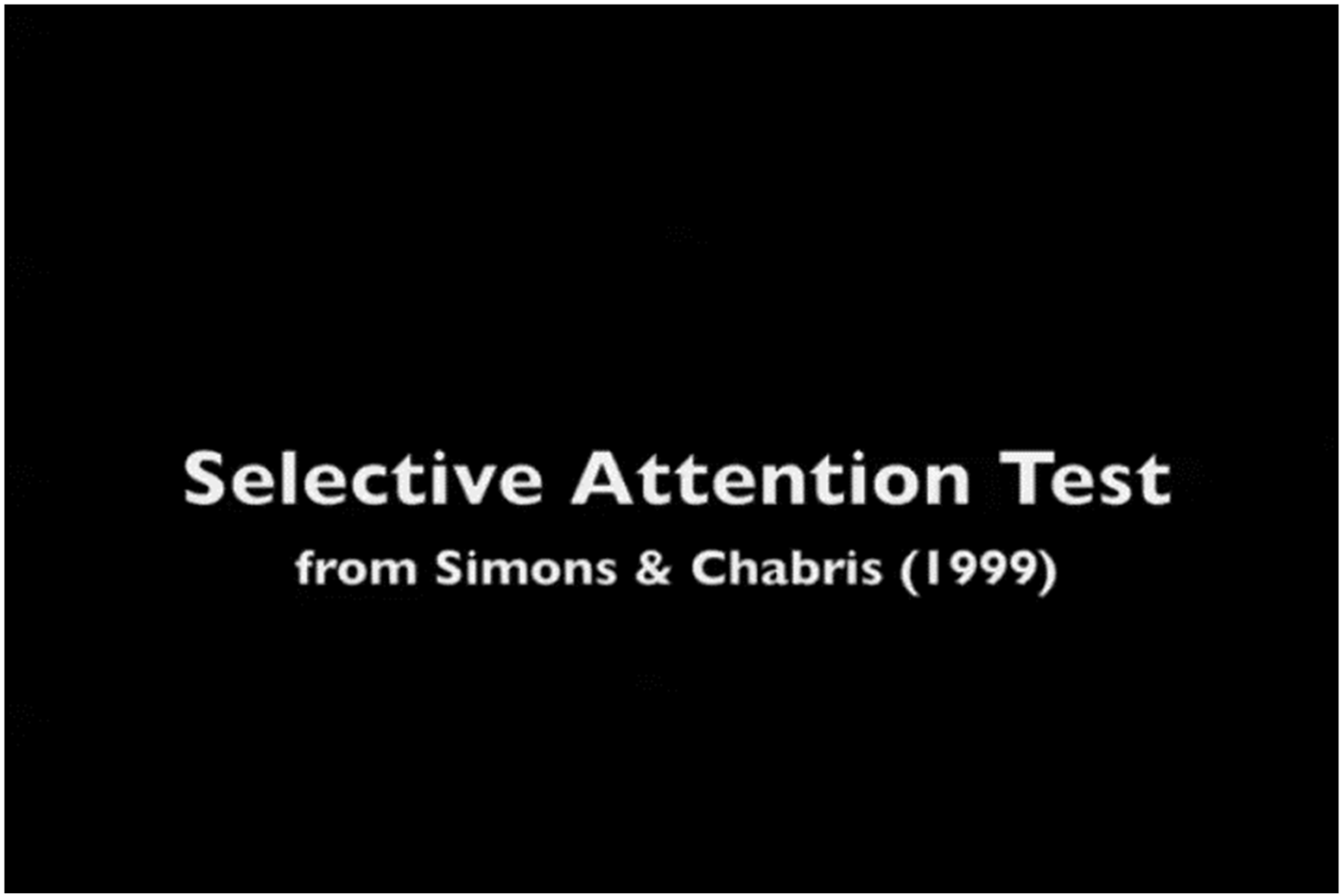

https://www.youtube.com/watch?v=vJG698U2Mvo

The Monkey Business Illusion

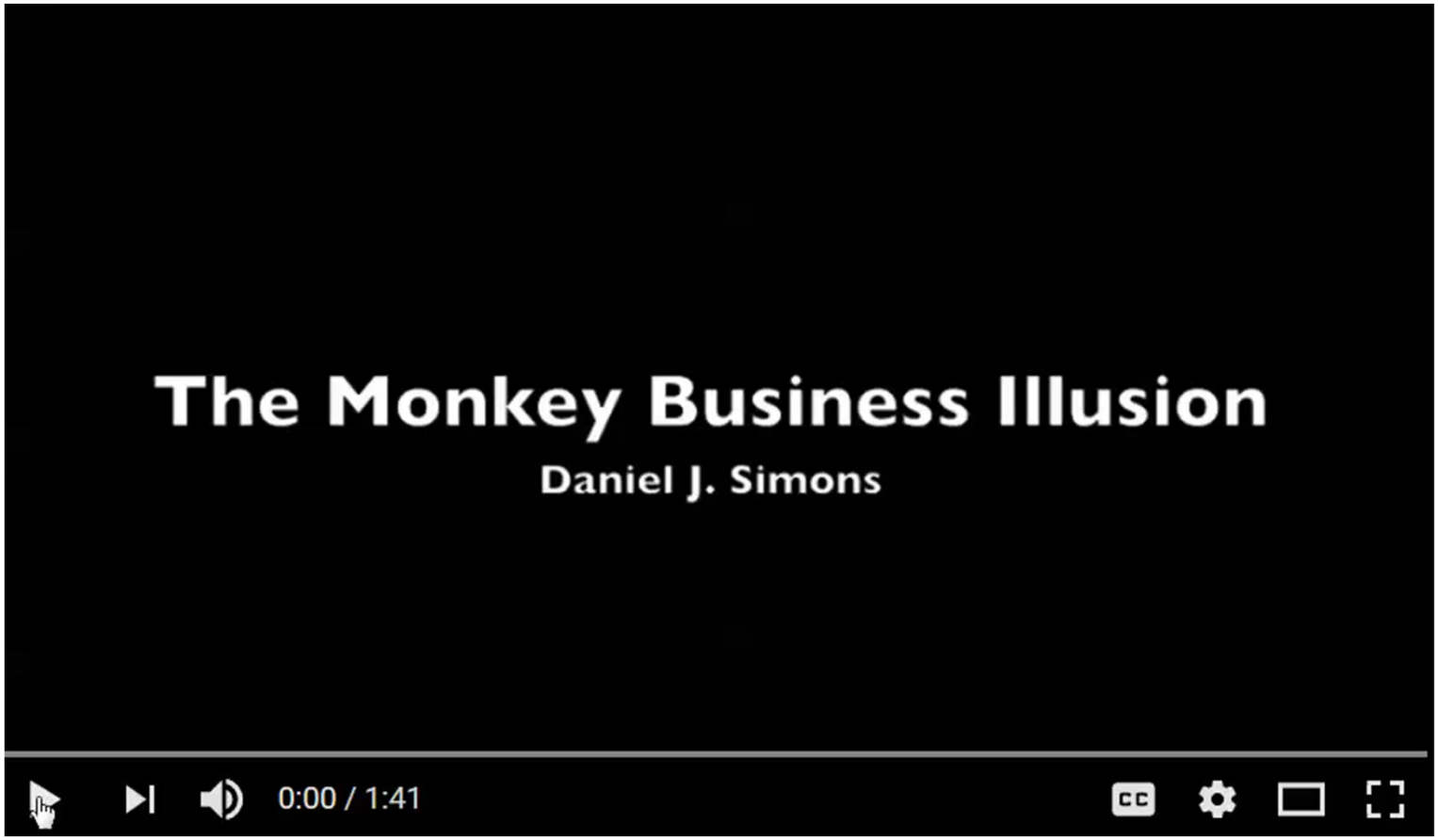

Theinvisiblegorilla.com

The Invisible Gorilla Experiment

Selective Attention Test (from Simons & Chabris, 1999)

Instructions: Count how many times the players wearing white pass the basketball.

How many passes did you count?

But did you see the gorilla?!

https://www.youtube.com/watch?v=vJG698U2Mvo

The Monkey Business Illusion

Count how many times the players wearing white pass the ball.

Theinvisiblegorilla.com

Did you spot the gorilla?

For people who haven't seen or heard about a video like this before, about half miss the gorilla.

If you knew about the gorilla, you probably saw it. But did you notice the curtain changing color or the player on the black team leaving the game?

Only 17% of those who were familiar with the original gorilla video noticed one or both of the other unexpected events. Some 29% of those who were unfamiliar with the original gorilla video spotted one of the other events

When you're looking for a gorilla, you often miss other unexpected events.

Knowing that unexpected events might occur doesn't prevent you from missing unexpected events

Self Made Man

Bobbie Carlyle's vision of Self Made Man is a man carving himself out of stone, carving his character, carving his future.

Each research field needs to carve itself out of any hype, carve its character, and carve its future through clear thinking.